LBL-28052

Lawrence Berkeley Laboratory

UNIVERSITY OF CALIFORNIA

Materials & Chemical Sciences Division

Reactivity of Coordinatively Unsaturated Organometallic Species in the Gas Phase and in Solution

E.P. Wasserman
(Ph.D. Thesis)

October 1989

LOAN COPY
Circulates
for 2 weeks
Bldg. 50 Library.
LBL-28052
Copy 2

Prepared for the U.S. Department of Energy under Contract Number DE-AC03-76SF00098.

DISCLAIMER

This document was prepared as an account of work sponsored by the United States Government. While this document is believed to contain correct information, neither the United States Government nor any agency thereof, nor the Regents of the University of California, nor any of their employees, makes any warranty, express or implied, or assumes any legal responsibility for the accuracy, completeness, or usefulness of any information, apparatus, product, or process disclosed, or represents that its use would not infringe privately owned rights. Reference herein to any specific commercial product, process, or service by its trade name, trademark, manufacturer, or otherwise, does not necessarily constitute or imply its endorsement, recommendation, or favoring by the United States Government or any agency thereof, or the Regents of the University of California. The views and opinions of authors expressed herein do not necessarily state or reflect those of the United States Government or any agency thereof or the Regents of the University of California.

LBL-28052

Reactivity of Coordinatively Unsaturated Organometallic Species in the Gas Phase and in Solution

Eric Paul Wasserman

Ph.D. Thesis

October 1989

Lawrence Berkeley Laboratory

and

Department of Chemistry

University of California

Berkeley, California 94720

This work was supported by the Director, Office of Energy Research, Office of Basic Energy Sciences, Chemical Sciences Division, of the U.S. Department of Energy under contract no. DE-AC03-76SF00098.

Abstract

Chapter 1. Our application of the technique of infrared flash-kinetic spectroscopy to organometallic chemistry is placed in the context of recent work. The advantages and drawbacks of the CO-laser-based system used in these experiments relative to other infrared detection sources are weighed.

Chapter 2. The details of the CO laser transient IR spectrometer are given. We focus on the operation of the CO laser, a homebuilt instrument. The means of photolysis, detection, and data analysis are also described. We offer some advice on optimization of transient signal quality.

Chapter 3. The room-temperature flash-kinetic spectroscopy of $CpCo(CO)_2$ in the gas phase and in organic solution is investigated. The primary observed photoproduct is the monocarbonyl CpCo(CO). In the gas phase, this species reacts with two-electron donor molecules such as CO and C_2H_4 with rate constants within about an order of magnitude of gas-kinetic. Reaction with nitrogen is also observed, although with a much slower rate constant. In cyclohexane solution, the monocarbonyl reacts with $P(n\text{-Bu})_3$ and MeCN at nearly diffusion-controlled rates. In cyclohexane doped with small amounts of benzene or THF, reaction with phosphine is slowed drastically. Benzene- and THF-solvated monocarbonyl species are spectroscopically observed. The decay of the benzene solvate in the presence of phosphine is examined as a function of phosphine and benzene solvates, yielding insight into the mechanism of ligand substitution. The primary pathway for decay of the benzene solvate is believed to involve prior dissociation of benzene, followed by reaction of ligand with a cyclohexane-solvated monocarbonyl.

Chapter 4. We examine the gas-phase flash-kinetic spectroscopy of $CpRh(CO)_2$. Again, the primary observed photoproduct is a monocarbonyl, CpRh(CO). This molecule is highly reactive, combining with CO at a frequency close to the collision rate. This coordinatively unsaturated species also reacts with H_2 and alkanes at nearly gas-kinetic rates, from which we obtain the oxidative addition products. The cross-sections for

reaction with alkanes increases according to the following trend: $CH_4 < C_2H_6 < CMe_4 < c\text{-}C_6H_{12}$. No substantial isotope effect is seen in the reactions of CpRh(CO) with H_2 (D_2) or with CH_4 (CD_4). A qualitative scheme is presented to account for these observations. It postulates the formation of an initial collision complex between alkane and monocarbonyl that has an "agostic"-type interaction.

Chapter 5. The photochemistry of $Cp^*Rh(CO)_2$ in liquid krypton is probed. Reaction between an initially-formed monocarbonyl intermediate and the alkanes cyclohexane and neopentane is noted, yielding C-H activation products. We find no reaction of this monocarbonyl with methane under similar conditions. While reaction of the monocarbonyl with CO appears to have no significant activation barrier, this is not true for its reactions with alkanes. From a variable-temperature study of the alkane concentration dependence of the reaction, we find a simple bimolecular scheme for the C-H insertion reaction to be inadequate. The merits of various mechanisms are discussed. We find our results are best explained by a reaction scheme in which both alkane- and krypton-solvated monocarbonyl species participate. In this mechanism, a pre-equilibrium between krypton and alkane solvates is quickly established following photolysis. The alkane solvate can be considered a σ-complex, in which all C-H bonds are essentially intact. This species can then undergo an intramolecular C-H insertion. The rates for these processes have been measured at several different temperatures, yielding activation parameters for the C-H activation step.

Acknowledgments

I have had the privilege and good fortune to work under two outstanding scientists at Berkeley, Brad Moore and Bob Bergman. To them I owe whatever scientific discipline and true objectivity I now possess. Bob was especially good at teasing the limits of the possible. He tried to get at the heart of the problems I wrestled with as a student, and never shied away from challenging an assumption. Brad, whom I got to know somewhat better, served as much as a model for living, as a model researcher. Though burdened with ever-mounting bureaucratic responsibilities, he still found time to guide and to teach, doing both with not a hint of condenscension toward a student with little physical training. He made me feel, as he did with all of the group members, a part of his family, and rewarded us with his trust and his Russian River pears. His and Bob's patience with my project were great (and greatly tried).

I have enjoyed collaborations with three very talented chemists. Dr. Page Stoutland helped turn the rickety CO laser into a wonder of automation. He also helped me acquire some facility with handling sensitive compounds. Dr. Mike Sponsler, with his incredibly wide-ranging chemical understanding, helped in experiments on metal radicals (not detailed in this dissertation). Dr. Bruce Weiller imparted his enthusiasm and insights into the C-H activation projects, and must take much of the credit for the liquid krypton results. He worked tirelessly in getting a difficult system to work (the lKr cell), and designed a second, improved cell. Professor George Pimentel deserves and has received far more important tributes. Without his generosity and understanding, the experiments in liquified inert gases would not have been possible. I would like to thank as well the NSF for a graduate fellowship.

To the Bergman group members, I owe thanks for helping me do synthetic and analytic tasks, as well as an apology for not getting to know them better. My classmates Liz Burkhardt, Jeff Chang, and Mary Trost made me feel at home among the stills. Tom

Foo deserves credit for straightening out my golf swing, and for making the effort to decode my group meetings. As for the Moorons, they too merit thanks for putting up with an unintelligible seminar or two, though it was Cp rings, not laser gratings, that put them to sleep. Dave Darwin, a loyal friend and true, was always ready to help when I reached an impasse in my experiment, and even taped the Mets when I forgot they were on. To Tom Butenhoff, sparkling captain of the wretched Moorons Softball Team, I owe an appreciation of hitting the cut-off man. As with his athletic performance, his science was marked with grace and incredible care. Will Polik made me realize why I wasn't a computer scientist with his airtight and effortless programming. To those from whom I stole the occasional 'scope or crescent wrench, including Yili Guo, Ramon Alvarez, and Charles Pibel, I offer my gratitude. Their semi-intentional version of the Marshall Plan was indispensable. I consider myself lucky to have worked among the Moorons, a group with a vague yet powerful aura of Birkenstocks and fine wine.

No acknowledgment would be complete without thanks to the legions of workers in the machine, electronics, and glass shops. Most of my designs were made after long consultations with them, taking advantage of their experience and intuition.

I would like to thank my parents, Claudia and Bob. They were always willing to rationalize my whims and support me through years in which I seemed to be stuck in suspended animation a continent away. It is a tribute to their love and the happiness of my childhood that I took so long to grow up. Finally, any thanks to Jane, my loving companion and friend, would be inadequate. I cannot thank her for being part of my achievements and disappointments while in graduate school, for she was simply a good portion of my life.

Table of Contents

Chapter 1. General Introduction 1

Notes and References 6

Table 8

Chapter 2. Experimental Details

2.1 Overview 9

2.2 The CO Laser: a Brief Introduction 10

2.3 Operation of the Moore Group CO Laser 12

2.4 The XeCl Excimer Laser 15

2.5 Infrared Detection 16

2.6 Data Acquisition and Analysis 18

2.7 Notes on Signal-to-Noise Optimization 21

Notes and References 24

Table 26

Figures 27

Chapter 3. The Reactivity of (η^5-C_5H_5)Co(CO) in the Gas Phase and in Solution

3.1 Introduction 30

3.2 Experimental 32

3.3 Gas-Phase Photolysis of $CpCo(CO)_2$ 34

3.4 Solution-Phase Studies 40

3.5 Conclusions 47

Notes and References 49

Tables 51

Figures 56

Chapter 4. C-H Activation by Gas-Phase (η^5-C_5H_5)Rh(CO)

4.1 Introduction 70

4.2 Experimental 73

4.3 Results and Discussion

4.3.1 Photolysis of $CpRh(CO)_2$ in the Absence of Added Ligand 75

4.3.2 Reaction of **2** with CO 76

4.3.3 Reaction of **2** with X_2 ($X \equiv H, D$) 77

4.3.4 Reaction of **2** with Alkanes 78

4.3.5 Other Mechanistic Considerations 83

4.4 Conclusions 84

Notes and References 86

Tables 89

Figures 93

Chapter 5. The Reactivity of (η^5-C_5Me_5)Rh(CO) in Liquid Krypton: Oxidative Addition of Alkanes

5.1 Introduction 103

5.2 Experimental 105

5.3 Estimation of Reagent Concentration 107

5.4 Results

5.4.1 Photolysis in the Absence of Added Ligands 109

5.4.2 Photolysis in the Presence of CO 109

5.4.3 Photolysis in the Presence of Cyclohexane and Neopentane 110

5.4.4 Other Alkanes 112

5.4.5 Comparison with Results in Liquid Xenon 113

5.5 Discussion

5.5.1 Possible Mechanisms 114

5.5.2 Isotope Effects 120

5.5.3 Solvation by Kr and Alkanes 122

5.5.4 Reaction Path and Selectivity 123

5.6 Conclusions 125

Notes and References 127

Tables 131

Figures 132

Appendix 1 CO Laser Control and Data Acquisition Program 152

Appendix 2 Transient Spectrum Generation Program 183

Table of Figures

Chapter 2

2-1	Experimental schematic of the IR flash-kinetic spectrometer	27
2-2	Pulse delay generator	28
2-3	Electronics of solenoid control	29

Chapter 3

3-1	Schematic of the gas-flowing arrangement for the study of $CpCo(CO)_2$	56
3-2	Transient absorption trace taken at 2011 cm^{-1}	57
3-3	Transient absorption spectra from photolysis in the presence of CO	58
3-4	Rate constant for reaction with N_2 versus pp(N_2)	59
3-5	Transient absorption spectra for the reaction of CpCo(CO) with N_2	60
3-6	Rate constant for reaction with $CpCo(CO)_2$ versus pp($CpCo(CO)_2$)	61
3-7	Transient spectra from photolysis of $CpCo(CO)_2$ in cyclohexane	62
3-8	Transient spectra from photolysis of **1** in C_6H_6/*c*-C_6H_{12} mixture	63
3-9	Transient absorption trace showing behavior of benzene solvate	64
3-10	Transient spectra from photolysis of **1** in THF/*c*-C_6H_{12} mixture	65
3-11	Dependence of benzene solvate decay rate upon [C_6H_6] and [PR_3]	66
3-12	Dependence of $1/k_{obsd}$ upon [C_6H_6]	67
3-13	Dependence of k_{obsd}/[**1**] upon 1/[C_6H_6]	68
3-14	Transient absorption at 1977 cm^{-1} showing behavior of N_2 adduct	69

Chapter 4

4-1	Transient absorption traces showing reaction of CpRh(CO) with CMe_4	93
4-2	Transient spectra from photolysis of $CpRh(CO)_2$ in Ar	94
4-3	FTIR spectrum of $CpRh(CO)_2$ vapor	95

4-4	Transient spectra showing reaction of CpRh(CO) with CO	96
4-5	Transient spectra showing reaction of CpRh(CO) with H_2	97
4-6	Transient spectra showing reaction of CpRh(CO) with D_2	98
4-7	Dependence of CpRh(CO) decay rate upon pp(X_2) ($X \equiv H, D$)	99
4-8	Transient spectra showing reaction of CpRh(CO) with C_2H_6	100
4-9	Transient spectra showing reaction of CpRh(CO) with *c*-C_6H_{12}	101
4-10	Dependence of CpRh(CO) decay rate upon pp(CX_4) ($X \equiv H, D$)	102

Chapter 5

5-1	Schematic of the experiment	134
5-2	Plot of ln(k_{obs}) versus [CO]	135
5-3	Transient traces showing reaction of monocarbonyl with cyclohexane	136
5-4	Transient spectra showing reaction of monocarbonyl with cyclohexane	137
5-5	FTIR difference spectrum showing reaction of **2** with cyclohexane	138
5-6	Dependence of kobs upon [*c*-C_6H_{12}] and temperature	139
5-7	Dependence of kobs upon [CMe_4] and temperature	141
5-8	Dependence of kobs upon [*c*-C_6D_{12}] and temperature	143
5-9	Dependence of kobs upon [$C(CD_3)_4$] and temperature	144
5-10	Plot of ln(k_2) versus 1/T for cyclohexane activation	145
5-11	Plot of ln(K) versus 1/T for cyclohexane activation	146
5-12	Plot of ln(k_2) versus 1/T for neopentane activation	147
5-13	Plot of ln(K) versus 1/T for neopentane activation	148
5-14	Plot of ln(k_2^H/k_2^D) versus 1/T	149
5-15	Reaction path diagram for alkane activation in liquid Kr	150
5-16	Reaction path diagram for C-H activation in mixed alkane solvent	151

Table of Tables

Chapter 1

1.1 A Comparison of the Characteristics of Some Infrared Sources 8

Chapter 2

2.1 CO Laser Transitions 26

Chapter 3

3.1 Rate Constants for Reaction of CpCo(CO) with Ligands in Gas Phase 51

3.2 Comparison of Results from Gas-Phase and Matrix Isolation Studies 52

3.3 Collected ν_{CO} from Solution-Phase Studies 53

3.4 Rate Constants for Reaction of Monocarbonyl with Ligands in Solution 54

3.5 Rate Constants for Reaction of Benzene Solvate with Phosphine 55

Chapter 4

4.1 Rate Constants for Reaction of Unsaturated Organometallics with CO 89

4.2 Carbonyl Stretching Frequencies 90

4.3 Rate Constants for Reactions of CpRh(CO) 91

4.4 Efficiency of Alkane Activation versus Alkane Properties 92

Chapter 5

5.1 Rate Constants from Linear fits to k_{obs} *vs.* [alkane] at low [alkane] 131

5.2 Reaction of Cp*Rh(CO) with Cyclohexane in Liquid Krypton 132

5.3 Reaction of Cp*Rh(CO) with Neopentane in Liquid Krypton 133

Though my heart pants and quivers to remember that I have been a student here these thirty years, O would I had never seen Wittenberg, never read book!

-Christopher Marlowe, *Doctor Faustus*

Chapter 1. General Introduction.

Molecules containing transition-metal atoms catalyze a wealth of reactions, from photosynthesis and oxidation of sugars in living cells to polymerization and hydrogenation in large-scale industrial chemistry. The keys to this range of activity are the variety of oxidation states and coordination numbers available to the metal center, and the number of geometries it permits the molecule to assume.[1] All inorganic catalysts are held together by a more or less stable framework of ligands, and have sites of coordination at the metal atom that can serve to immobilize reactant molecules. Inorganic species are unique in their ability to reversibly coordinate small, closed shell molecules, such as hydrogen,[2] nitrogen,[3] and oxygen.[4] The bonding schemes present in such complexes are often inadequately described by classical inorganic or organic theory, and challenge the imagination of the quantum chemist.[5] The very nature of inorganic and organometallic compounds blurs the distinction between "free" and "attached" ligands, for many molecular configurations are of nearly equal free energy. In our investigations of one small area of organometallic chemistry, we have seen an impressive number of molecules which can bind to the metal center and influence the course of reactions. Some, such as complexes with dinitrogen, are interesting metastable adducts, while others, such as π-complexes with benzene, participate in the reaction as intermediates, drastically affecting the rate at which the reaction occurs.

We have concentrated on the photochemistry of three molecules: $CpCo(CO)_2$, $CpRh(CO)_2$, and $Cp^*Rh(CO)_2$ ($Cp \equiv \eta^5\text{-}C_5H_5$; $Cp^* \equiv \eta^5\text{-}C_5(CH_3)_5$). These closely-related transition-metal compounds participate in some interesting reactions. The cobalt rhodium species $Cp^*M(CO)_2$[6,7] perform the alkyne cotrimerization reaction. Both rhodium-containing molecules appear to react with alkanes upon photolysis,[8] yielding products with Rh-C and Rh-H single bonds. This latter reaction, often called "C-H activation", could ultimately extend the range of industrial chemistry. It represents the first step in the homogeneous catalytic functionalization of saturated hydrocarbons, a process

which recently been recently demonstrated by Tanaka and others.[9] The potential of C-H activation lies in the possibility of selective conversion under mild conditions of unreactive hydrocarbons such as alkanes into species with direct uses in commercial organic chemistry. Processes involving the replacement of the hydrogen atom in a C-H bond with another atom or functional group are among the oldest and most basic of organic reactions, and include mercury sensitization, free-radical[10] or biradical[11] attack, and dehydrogenation reactions.[12] Alkanes have long been known to decompose on metal surfaces.[13] These alkane transformations lead to an array of different adducts for each alkane, however, due either to the high energy of the reactive intermediate (in the case of radicals) or to the multiplicity of different reactive sites (in the case of heterogeneous catalysts). By contrast, in the C-H activation of alkanes by $Cp^*(PMe_3)MH_2$ ($M \equiv Rh, Ir$), the relative reactivity of certain types of C-H bonds was found to be greater than that of others.[14]

We have begun an investigation into the nature of the reactive intermediate responsible for the photochemical oxidative addition of alkanes in the $Cp^{(*)}Rh(CO)_2$ system and the mechanism by which C-H activation proceeds. In a related study, we examine the mechanism of photochemical ligand substitution in $CpCo(CO)_2$. We employ the technique of time-resolved infrared flash-kinetic spectroscopy, using a CO laser as our infrared source. Flash-kinetic spectroscopy (FKS) is a method for examining the energy levels and concentration of a species too reactive to detect by conventional analytic techniques. A short excitation pulse, usually of ultraviolet light, creates a transient high density of reactive species from a mixture of compounds that includes a precursor. Between pulses, the system tends back to equilibrium[15] as the transient intermediate reacts with other molecules in the mixture. By altering the concentrations of other species, or by changing the temperature of the mixture, we obtain relationships which quantify the kinetics and thermodynamics of the chemical system. FKS is suited to the study of chemical reactions which occur on timescales slower than 10^{-8} seconds, the limit being set by the excitation pulse duration[16] (short-time). The short-time limit prevents us from

examining primary processes such as the actual dissociation step, electronic-state relaxation, or, in condensed phases, the dynamics of solvation of the intermediate. Recent advances in laser technology have widened the timescale range of photochemical experiments, allowing spectroscopic studies of these initial reactions on the picosecond and even femtosecond timescales.[17] We restrict ourselves in the experiments detailed in this dissertation to unimolecular and bimolecular reactions whose observed rate constants lie in the range 4×10^6 to 2×10^3 s^{-1}. This made possible the observation in real time of diffusion-controlled reactions both in the gas and solution phases.[18]

Infrared FKS, rather than UV-VIS FKS, was the method chosen for the study of these organometallic reactions. On the debit side, transient infrared spectroscopy generally suffers from lower signal-to-noise ratios, difficulties of IR light detection, and a more limited choice of light sources. Its advantages are few but profound. The information content of the infrared spectra of organometallic complexes exceeds that of UV-VIS spectra, which are usually broad and unstructured.[19] Because infrared bands are generally narrow,[20] one may more easily resolve one molecule from another. By choosing to study an area of the infrared spectrum for which frequency shifts and substituent effects are well-known, such as the organometallic carbonyl stretching region, one may speculate as well upon the electronic nature of species not previously observed. If more than one band appears in a characteristic region, both the number of ligands of a certain type as well as their geometry about the metal center may be elucidated.

One chooses the infrared source for the FKS experiment based on the infrared range of interest, desired resolution, and signal-to-noise criteria.[21] Several continuously tunable infrared lasers now exist, among them the diode laser, the F-center (color-center) laser, the optical parametric oscillator (OPO), and the difference-frequency laser (see Table 1.1). Other laser sources include the line-tunable CO and CO_2 gas lasers. Black-body radiation from a globar similar to the infrared source of a conventional FTIR spectrometer, in tandem with a dispersive frequency selector such as a monochromator, may also be

used. All of the sources except the OPO can be run continuous-wave, *i. e.*, they operate continuously as opposed to in pulses, although the CO and CO_2 lasers can be run pulsed. Of all the sources listed in Table 1.1, the diode laser has the brightest future in infrared FKS.[22] The range of the infrared spectrum now covered by diode lasers extends from the near-IR to about 350 cm^{-1}. It is continuously tunable, and has a very narrow bandwidth (< 0.01 cm^{-1}), allowing one to resolve complicated rotationally-resolved vibrational structure. On the other hand, each diode has a limited tuning range of approximately 20-100 cm^{-1}, and has gaps in this coverage. It is a weak light source (*ca.* 50 μW), and is very sensitive to RF noise, making it a difficult source for FKS. Much faster IR FKS systems have recently been developed by Hochstrasser and others[17c,d] based on a non-linear optical technique (IR up-conversion). This promises to be an important tool in the study of picosecond organometallic processes.

For our study, we used a CO laser as our means of detecting transient changes in concentration. We thereby took advantage of the huge infrared absorption cross-sections of organometallic carbonyl complexes.[23] The magnitude of these infrared intensities as well as the high laser power (2-10 mW) increases the S/N capability of the transient spectrometer. The limited resolution of the CO laser, determined by the spacings between laser transitions (±4 cm^{-1}), does not interfere for the most part in the spectroscopy of organometallic carbonyls, since in the gas phase, rotational structure is lost at room temperature,[24] while in solution, band structure is completely suppressed. For these reasons, the use of the CO laser in infrared FKS has gained widespread popularity.[25] Other workers have utilized the globar/monochromator technique[26] and, more recently, the diode laser.[27] These last two IR sources do have the advantage of being able to detect absorptions by vibrational ground-state carbon monoxide, and thus can reveal the distribution of energy among the various degrees of freedom of photodetached CO.[28]

In the following chapter, I discuss the details of the infrared FKS spectrometer, with special emphasis given to the actual operation of the CO laser and detection apparatus

for the specialist. I also give an account of the data acquisition system and the data analysis programs, as well as a brief report on common artifacts. In Chapter 3, I will describe the first application of our spectrometer, the study of the photochemistry of $CpCo(CO)_2$ in the gas phase and in cyclohexane solution. Of particular interest here is the effect of reversible donor-solvent binding upon the kinetics of the decay of the monocarbonyl CpCo(CO). Chapters 4 and 5 contain accounts of our studies of C-H activation by coordinatively unsaturated rhodium intermediates. In Chapter 4, I describe how CpRh(CO) produced from the gas-phase photolysis of $CpRh(CO)_2$ reacts with CO, hydrogen, and alkanes. The photochemistry of $Cp^*Rh(CO)_2$ in liquid krypton solutions receives attention in Chapter 5. In this final study we examine the C-H activation of cyclohexane and neopentane and discuss possible mechanisms for the reaction. The scheme which we now feel describes this process involves the intermediacy of two solvation complexes: one with a weak Rh-Kr bond, and one with a weak Rh-alkane bond in which the C-H bond is nearly intact.

Notes and References

[1]A good introduction to organometallic chemistry can be found in: Cotton, F. A.; Wilkinson, G. *Advanced Inorganic Chemistry: A Comprehensive Text*, 4th ed. NewYork: Wiley, 1980, pp. 619ff.

[2]Kubas, G. J. *Comments Inorg. Chem.* **1988**, *7*, 17.

[3](a) Henderson, R. A.; Leigh, G. J.; Pickett, C. J. *Adv. Inorg. Chem. Radiochem.* **1983**, *27*, 197. (b) Pelikan, P.; Boca, R. *Coord. Chem. Rev.* **1984**, *55*, 55.

[4]Gubelmann, M. H.; Williams, A. F. *Struct. Bonding* **1983**, *55*, 1.

[5]See, for example: Saillard, J.-Y.; Hoffmann, R. *J. Am. Chem. Soc.* **1984**, *106*, 2006.

[6]For a review, see: Vollhardt, K. P. C. *Acc. Chem. Res.* **1977**, *10*, 1.

[7]Abdulla, K.; Booth, B. L.; Stacey, C. *J. Organomet. Chem.* **1985**, *293*, 103.

[8]Rest, A. J.; Whitwell, I.; Graham, W. A. G.; Hoyano, J. K.; McMaster, A. D. *J. Chem. Soc., Dalton Trans.* **1987**, 1181.

[9](a) Sakakura, T.; Tanaka, M. *J. Chem. Soc., Chem. Commun.* **1987**, 758. (b) Nomura, K.; Saito, Y. *J. Chem. Soc., Chem. Commun.* **1988**, 161. (c) Tanaka, M.; *CHEMTECH*, Jan. 1989, 59.

[10]For a review of radical attack on hydrocarbons, see: *Free Radicals*, Vol. I. Ed. Kochi, J. K. New York: Wiley, 1973.

[11]For reaction of methylene with alkanes, see: Halberstadt, M. L.; McNesby, J. R. *J. Am. Chem. Soc.* **1967**, *89*, 3417.

[12]For recent work on the functionalization of alkanes, see: Activation and Functionalization of Alkanes. Ed. Hill, C. L. New York: Wiley, 1989.

[13]For reactions on clean metal single-crystal surfaces, see: Ehrlich, G. "Activated Chemisorption" in *Chemistry and Physics of Solid Surfaces VII*. Eds. Vanselow, R.; Howe, R. F. Berlin: Springer-Verlag, 1988, p. 21. For a review of supported rhodium activation catalysts, see: Schwartz, J. *Acc. Chem. Res.* **1985**, *18*, 302.

[14]Janowicz, A. H.; Periana, R. A.; Buchanan, J. M.; Kovac, C. A.; Stryker, J. M.; Wax, M. J.; Bergman, R. G. *Pure and Appl. Chem.* **1984**, *56*, 13.

[15]True equilibrium may not be attained, but rather a photostationary state in which photolytic as well as thermal interconversion of reactants and products occurs.

[16]Conventional photolysis lasers, such as excimer or Nd:YAG lasers, produce 10-20 ns light bursts, while flashlamps generally fire over a 1 μs period.

[17](a) Simon, J. D.; Peters, K. S. *Chem. Phys. Lett.* **1983**, *98*, 53. (b) Joly, A. G.; Nelson, K. A. *J. Phys. Chem.* **1989**, *93*, 2876. (c) Moore, J. N.; Hansen, P. A.; Hochstrasser, R. M. *Chem. Phys. Lett.* **1987**, *138*, 110. (d) Wang, L.; Zhu, X.; Spears, K. G. *J. Phys. Chem.* **1989**, *93*, 2.

[18]Reaction with solvent in condensed phase or with buffer gas in the gas phase could not be seen directly.

[19]This is not to denigrate the fine work in UV-visible FKS of organometallic compounds, of which there is too much to list. A few examples from the early flash-kinetic spectroscopy of metal carbonyls: (a) Bonneau, R.; Kelly, J. M. *J. Am. Chem. Soc.***1980**, *102*, 1220. (b) Kelly, J. M.; Long, C.; Bonneau, R. *J. Phys. Chem.* **1983**, *87*, 3344.

[20]Carbonyl stretching bands are *ca.* 25 cm^{-1} FWHM in the gas phase, 5-10 cm^{-1} in room-temperature organic solution, and *ca.* 4 cm^{-1} in liquid inert gases.

[21]For general texts on lasers and applications, see: (a) Demtroeder, W. *Laser Spectroscopy* Berlin: Springer-Verlag, 1982. (b) Chemical and Biochemical Applications of Lasers Ed.: Moore, C. B. New York: Academic Press, 1974.

[22]See: Darwin, D. C. *Ph. D. Thesis*, University of California, Berkeley, 1989.

[23]Kettle, S. F. A.; Paul, I. *Adv. Organomet. Chem.* **1972**, *10*, 199.

[24]Molecular beam studies of the rotational structure of metal carbonyl absorptions of have recently been published: (a) Takami, M. *Reza Kenkyu* **1985**, *13*, 325. (b) Davies, P. B.; Martin, N. A.; Nunes, M. D.; Pape, D. A.; Russell, D. K. *Chem. Phys. Lett.* **1989**, *156*, 553.

[25]See the following review: Poliakoff, M.; Weitz, E. *Adv. Organomet. Chem.* **1986**, *25*, 277.

[26](a) Hermann, H.; Grevels, F.-W.; Henne, A.; Schaffner, K. *J. Phys. Chem.* **1982**, *86*, 5151. (b) Weiller, B. H.; Grant, E. R. *J. Am. Chem. Soc.* **1987**, *109*, 1051.

[27]Holland, J. P.; Rosenfeld, R. N. *Chem. Phys. Lett.* **1988**, *145*, 481.

[28]Other methods that have been used to study population distributions of organometallic CO photoproducts are: (a) VUV fluorescence; see: Waller, I.; Hepburn, J. W. *J. Chem. Phys.* **1988**, *88*, 6658. (b) multiphoton ionization; see: Whetten, R. L.; Fu, K.-J.; Grant, E. R. *J. Chem. Phys.* **1983**, *79*, 4899.

Table 1.1. A Comparison of the Characteristics of Some Infrared Sources.

Source	Range (cm^{-1})	Resolution (cm^{-1})	Typ. Power (mW)[a]
diode laser[b]	350-2300	0.0003[c]	>0.1[d]
F-center laser[e]	3450-4000	0.2	240
difference-freq. laser[f]	2400-4500	0.0007	0.02
OPO[g]	2500-7000	<2	10[a]
CO laser[h]	1800-2080	4	3
CO_2 laser[i]	900-1100	1	1.5×10^4
globar[j]	(entire IR)	8[k]	0.005[k]

[a]In mW except for OPO power, which is in mJ $pulse^{-1}$. [b]Characteristics of series SP5615 lead-salt devices (Spectra-Physics, Laser Analytics Div., 1988). [c]Single-mode. [d]Multimode. [e]Mollenauer, L. F. *Laser Handbook*, Vol. 4, Eds. Stitch, M. L.; Bass, M. Amsterdam: North-Holland, 1985, p.143. [f]Characteristics of Moore-group $LiNbO_3$ difference-frequency laser pumped by ring-dye laser and Ar^+ laser. See: Petek, H.; Nesbitt, D. J.; Ogilby, P. R.; Moore, C. B. *J. Phys. Chem.* **1983**, *87*, 5367. [g]Byer, R. L. *Tunable Lasers and Applications* , Eds. Mooradian, A.; Jaeger, T.; Stokseth, P. Berlin: Springer-Verlag, 1976, p. 70. [h]See Chapter 2. [i]Describes line tunable laser in: Witteman, W. J. *The CO_2 Laser* , Berlin: Springer-Verlag, 1987, p. 108. [j]Reference 26b. [k]Resolution and power can be changed, improving one at the expense of the other, by changing the settings of the IR-dispersive optics.

Chapter 2. Experimental Details.

2.1 Overview. The CO laser flash-kinetic spectroscopy experiment consists of three major elements: the photolysis apparatus; the system for detecting transients formed by photolysis; and the cell in which the photochemistry takes place. Since the first two elements remain common to all the work described in this dissertation, they will be described in this chapter, whereas descriptions of the cells used will accompany the accounts of the experiments to which they belong. This chapter will also cover the means used to achieve reproducible, high signal-to-noise data, as well as the methods of data acquisition and analysis.

The optical arrangement which joined the elements of the transient spectrometer is shown in Figure 2-1. Gold- or aluminum-coated mirrors direct the infrared CO laser light toward the entrance of the photochemistry cell. A beamsplitter is placed in the IR beam path either before or after the cell and before the detector used to record transient absorptions. The beamsplitter was made of one of two uncoated substrates: (a) germanium, which splits off ca. 40% of the IR; (b) NaCl, which splits off ca. 10% of the IR. The portion of the beam which is split off by the beamsplitter (reference beam) passes through a tuning-fork chopper operating at 400 Hz, then is directed to a second IR detector which is used for relative CO laser power estimation. (The reference beam is generally not focussed on the element of the normalization detector unless the CO laser beam has travelled more than about 2 m.) The transmitted portion of the beam then impinges upon the transient infrared detector.

The photolysis beam, which was occasionally compressed in the horizontal dimension by a pair of BaF_2 lenses with focal lengths 25 and 75 cm, is reflected toward the cell by one or two coated quartz mirrors. A coated piece of sapphire acts to combine the IR and UV beams by reflecting the UV laser while transmitting the IR beam which is directed through the optic from its uncoated side. The two laser beams run coaxially through the

photolysis cell and are separated at the exit by a second dichroic optic. For this purpose, one of two partially reflective elements was used. A piece of CaF_2 coated for reflection of 308 nm light was used for most of the experiments described in Chapter 3, while, for all other experiments, a slab of NaCl which was sanded by fine (600 mesh) emery paper on one side served to remove the UV beam by diffusing it.

2.2. The CO Laser: a Brief Introduction. Lasing action in the vibrational transitions of carbon monoxide laser was first observed in 1964.[1] The CO laser has since evolved into an array of infrared sources with different characteristics suited for a wide range of uses. While the first[2] documented CO laser action involved a pulsed electric discharge excitation system, the continuous-wave (cw) laser soon followed.[3] The means of achieving vibrationally excited-state CO have been varied. While electric discharge is the most popular method of energy input, excitation can also be accomplished by shock-tube heating.[4] The energy of chemical reaction may also provide hot CO, such as in the CS_2-O_2 chemical laser.[5] CO lasers have been found[6] to emit in the near-ir as well, with $\Delta v = 2$, 3 in ground-state CO, and also in the UV[7].

Due to the wide range of lasers which can be called CO lasers, we will restrict the bulk of this introduction to the discussion of the CO laser of the type employed in our experiment. This laser is characterized by light emission in the P-branches of the vibrationally excited, electronically ground-state CO molecule, with $\Delta v = 1$ (equation 2.1).

$$CO(v = x, J = y) \longrightarrow CO(v = x - 1, J = y + 1) + h\nu \qquad (2.1)$$

Although R-branch lasing has been reported,[8] the P-branch laser is predominant. The reason for this lies in the fact that the same rotational population distribution describes CO(v = x) and CO(v = x - 1). As a consequence, population inversion in transitions

involving J' larger than the peak of the rotational population envelope may be more easily achieved if there is a net increase in J in the transition, rather than if J" < J'.

In order to produce the large populations of vibrationally "hot" CO, a DC electric discharge is created through the heart of the laser medium, which consists of a mixture of gases including CO. The excitation process is a complicated one, but proceeds through two major pathways. The electrons in the plasma created by the discharge may directly excite the CO (eq. 2.2), or they may first excite other species in the medium, such as nitrogen or helium (both popular bath gases), which then transfer some of their internal energy to CO upon collision with it (eqs. 2.3, 2.4).

$$CO + e^- \longrightarrow CO^* + e^- \qquad (2.2)$$

$$M + e^- \longrightarrow M^* + e^- \qquad (2.3)$$

$$CO + M^* \longrightarrow CO^* + M \qquad (2.4)$$

The nitrogen molecule, which is isoelectronic with CO, is an efficient conduit of energy derived from inelastic collision with an electron to the carbon monoxide vibrational manifold. This means of excitation is made possible by the closeness in energy of the vibrational levels of N_2 ($\omega_e = 2360\ cm^{-1}$) and of CO ($\omega_e = 2170\ cm^{-1}$).

The anharmonicity of the CO ground-state potential energy surface causes the vibrational spacings to decrease as the vibrational quantum number v increases. One effect of this is to increase the cross-section for vibrational energy transfer (V-V transfer) in which energy flows from a less-excited CO molecule to one with greater or equal v. The up-pumping of excited CO is facilitated by the fact that, in this process, shown in eq. 2.5 in which x > y, there is a net loss (though small) of vibrational energy in the two-molecule system due to anharmonicity.

$$CO(v=x) + CO(v=y) \longrightarrow CO(v=x+1) + CO(v=y-1) \qquad (2.5)$$

This excess energy can be readily accomodated in the other degrees of freedom of the system. The cross-sections for V-V transfer in the CO system are much larger than the cross-sections for V-T and V-R transfer.[9] Thus CO vibrational populations characteristic of exceedingly high temperatures are found in CO lasing mixtures, yet the rotational population distribution for CO remains close to that for room temperature.

A second, more obvious effect of the anharmonicity of the CO potential energy surface is to make the origins of each vibrational manifold shift to lower frequency with increasing vibrational quantum number. To control the wavelength range of the CO laser, one can therefore choose conditions which favor a vibrational excitation profile which will produce emission in the desired frequency region.

Since the amount of energy deposited into the CO laser medium is much greater than the energy emitted as radiation, the gas cell must be cooled. The method used to cool the laser tube depends upon the configuration of the CO laser itself. In general, the more effective the cooling method, the greater is the inversion of CO population in the lower vibrational states. In a flowing-gas system, one wants the cooling to be as effective as possible if high-frequency laser emission is desired. Thus, liquid nitrogen is often employed to cool the laser cell. If the gas mixture is static, as is often the case in commercial systems, a closed cycle of refrigerant such as water or methanol flows through a jacket which surrounds the outside of the laser tube. In a static-gas CO laser, it is nearly impossible to purge unexcited CO from the ends of the cell. Absorptions by CO at the ends of the cell limit the high-frequency range of the laser, usually to below 2020 cm^{-1}, so a low plasma temperature is less important.

2.3. Operation of the Moore Group CO Laser. The CO laser used in all the experiments detailed in this thesis has been described before, both by Houston *et al.*[10]and by Pauline Ho.[11] This version of the CO laser has its roots in the continuous-wave cooled

laser designed by Djeu *et al.*[12] The laser consists of a liquid-nitrogen-cooled pyrex tube of *ca.* 1 m length, fitted with acrylic window mounts at the ends. The mounts have been cut to Brewster's angle and support 1.5" diameter CaF_2 windows. Gases are flowed through a manifold made of 0.25" O.D. Cu tubing, through 0.375" O. D. polyflo tubing into four inlets on the cell: two at the windows (pure He) and two a few inches closer to the center. One vacuum port, centrally located, serves to remove the gases. Small, folded sheets of silver foil are placed in this exit line to catalytically decompose ozone generated in the laser discharge.

The gas mixture used depends on the set of lasing frequencies one desires (see below). The following mixture, however, is sufficient to achieve lasing from ~1820 - 2060 cm^{-1}: 2.5 Torr He, 3.5 Torr CO mixture (0.5% CO, 0.1% O_2, balance N_2), and < 0.1 Torr Xe. Table 2.1 displays the accessible CO laser frequencies[13] arranged according to the vibrational and rotational quantum numbers of the upper state. A DC electrical discharge through the cell creates the condition for vibrational excitation in CO. Breakdown occurs between two outer electrodes held at -10 to -14 kV and a central, grounded electrode. It is imperative that the laser not be run without a satisfactory connection between the gas-handling manifold and ground, as the discharge is often shunted through the gas delivery tubes in cases of non-optimal gas mixtures. The liquid N_2 level is sensed by a resistor placed in the cooling jacket. The sensor dictates the state of a solenoid on a gaseous N_2 line which pressurizes the volume above the liquid N_2 in a 50 l dewar, whose liquid outlet is connected to the laser jacket.

The optical cavity of the CO laser is created by a partially transmitting ZnSe optic (antireflective coating on the external side, 98% reflective at 4.7 μm on the other, with an inner radius of curvature of 5 m) and a grating blazed for 4.8 μm. Wavelength selection is made by rotation of the grating about an axis perpendicular to the optical axis. The grating is mounted in a stepper-motor-equipped rotation stage (Newport Research), whose movements are dictated by the Metrabyte Dash-8 interface board in the Fountain-XT PC

(see section 2.6 for details on the interfacing). An intracavity iris placed ~3 cm from the output coupler serves mainly to eliminate the competition between various transverse emission modes. One may observe this problem as a fast (<100 ns) oscillation in laser output. One also may control the power of the laser by varying the aperture of this iris.

The CO laser may be stabilized against fluctuations among the longitudinal lasing modes by a feedback loop from a detector which monitors a small portion of the laser output and a piezoelectric crystal in the output coupler mount designed to remove laser power instability on timescales slower than 400 Hz. This technique, given a full account by Ho[11], was not implemented. For operation of the laser at frequencies >2083 cm^{-1} (*i. e.*, emission from the v = 1 --> 0 manifold), the active stabilization is necessary.

A brief description of the agenda for operating the CO laser is in order. One switches on the lN_2 controller, hooks up the gaseous N_2 flow to the dewar inlet, and begins to cool the laser jacket. At the same time *ca.* 1 Torr He is flowed through the window ports of the cell, while *ca.*1.5 Torr proceeds through the center port. The power supply is then turned on and a voltage of 12.5 kV is applied. 0.5 Torr CO mixture is then slowly added to the discharge, which turns bright yellow. The slight flow of Xe is added, followed shortly by 2 Torr more CO mixture. If the last is added too rapidly, or the He flow to the windows is unbalanced, one of the sides of the discharge will be extinguished. In this event, the CO mixture is shut off, then slowly restored (with all other flows brought to proper ranges). The voltage applied across the electrodes is then dropped very slowly to 11.5 kV. At this point, the laser should function, giving IR output of 2-10 mW. The 50 l of lN_2 should cool the laser for 5-6 hrs.

As mentioned above, laser output consists of vibrational transitions in the electronic ground state of CO. The vibrational "temperature" of the CO can be influenced by several factors; these therefore greatly affect laser performance. The flow rate of gases is an important parameter, since it reflects the residence time of the CO medium in the discharge. Slower flows are less stable, both electrically and in laser power, but in general give a

denser array of available laser lines. Faster flows extend the lasing range on the high frequency end. The applied voltage should by kept close to the shut-off point for good performance, especially if high-frequency operation is desired. The Xe flow is helpful in stabilizing the laser electrically, but though it lowers the required electrode voltage for breakdown of the gas mixture, it greatly raises the conductivity of the plasma, allowing more current to be passed thus raising the CO vibrational temperature. Increasing the pressure of CO mixture has two significant effects on laser output: (1) it increases laser power on most lines (2) it reduces the lasing efficiency on the high-frequency lines (> 2030 cm^{-1}).

2.4. The XeCl Excimer Laser. A Lambda-Physik model EMG-103 excimer laser was used to photolyze all sample mixtures. The excimer laser takes advantage of the existence of a bound upper state of the Xe + $Cl^{\bullet}$ system. This complex (called an "exciplex"), formed from the electric-discharge excitation of a mixture of Xe and HCl, emits a broad range of frequencies as it relaxes down into the unbound ground state of the two-atom system. In laser operation, this emission is strongly peaked at 308 nm. The electric discharge is pulsed, so high peak powers of UV emission can be achieved within the short duration of excitation, which is about 20 ns long.

The excimer laser was generally filled with the following mixture of gases: 100 mbar 5% HCl/He; 80 mbar Xe; ca. 1500 mbar Ne; ca. 700 mbar He. Using this mixture, laser powers between 60 and 90 mJ $pulse^{-1}$ were commonly achieved. He and Ne are more or less interchangeable (although higher powers were achieved with high-Ne fills); the total pressure must never exceed 2650 mbar, however. The gas mixture would have to be replaced after approximately 10^7 shots or about two weeks after the fill, whichever came first. Cooling water must be supplied to the laser to avoid triggering the high-temperature interrupt. Power supply voltage was kept at 31 kV, since the laser increases in power with

increasing voltage but also becomes less stable and more prone to misfiring above this voltage.

The laser, made in 1983, was refurbished by the manufacturer in 1988. In its rehabilitation, the laser was cleaned and its ionization pins and high-voltage capacitors were replaced. Because a less costly variety of capacitor was chosen, pulse repetition rates >100 Hz are not possible. This had no effect on our experiments, since we used repetition rates of 2-10 Hz. Since its refurbishment, the leak rate is <10 mbar/day, which is well within its specifications.

In our experiments, the laser was generally triggered by an internal clock. A Synch-Out pulse precedes by about 2 ms the electric pulse to the thyratron which shunts the charge stored in the high-voltage capacitors into the laser cell. Alternately, one can use an external trigger pulse which has been converted into the proper voltages and input impedance (50 Ω) to initiate laser firing. The Metrabyte A/D board has been configured to emit pulses at any desired frequency between 2 and 70 Hz. The electronics involved in pulse amplification are shown schematically in Figure 2-2. After amplification and inversion of logical parity, these pulses can trigger the excimer. This scheme was rarely used, however.

It is not recommended to leave the high voltage across the laser capacitors even for short periods of time without allowing the build-up charge to discharge. Therefore, the laser was allowed to fire at 2-10 Hz even when the laser light was not need for photochemistry. In order to block the light, a black-anodized aluminum shutter was placed before the laser. One lowered the shutter by activating a solenoid controlled by the computer data acquisition program as will be described in section 2.6.

2.5. Infrared detection. For detection of transient changes of infrared transmission in the sample upon photolysis, one of two detectors was used. The first was a liquid nitrogen-cooled InSb detector; the second, a liquid helium-cooled doped germanium

detector. The InSb detector was only used during the gas-phase experiments using $CpCo(CO)_2$ (see Chapter 3), since the Ge:Cu detector was found to perform better as will be described in section 2.7. The same infrared filter was used for both detectors, a bandpass filter which bears the Moore filter catalogue designation L-4086-4. This filter transmits more than 10% of light in the range 2452-1470 cm^{-1} and more than 70% between 2100 and 1800 cm^{-1}, and was mounted cold in the case of the Ge:Cu detector (*i. e.*, in contact with the 4K dewar) to reduce the 300K blackbody radiation incident upon the detector element.

The InSb detector (Santa Barbara Research) is by nature an intrinsic detector, meaning that the absorptions in the infrared which cause electric changes in the material are due to states in the bulk, not to impurity states such as in the copper-doped Ge detector, which is of the extrinsic type. The detector used is photovoltaic, so one monitors infrared power striking the element by the voltage across the element. No bias voltage was applied to the detector. The output from the lN_2-cooled detector proceeds directly to a Perry model 497 fast amplifier (ca. 50 MHz) which has an output impedance of 50 Ω. The risetime of this detector is approximately 150 ns, as measured by the rise of its electric response to the fluorescence of a brick struck by the scattered output of a Nd:YAG laser. It was found that the response of the detector to changes in infrared power ceased to be linear when output voltages were more than about 0.2 V. The transient signals in this experiment, however, were rarely more than 20 mV, and are not influenced by saturation.

The other detector used, a homebuilt Ge:Cu photoconductive detector apparatus, demands more careful use.[14] The 3 × 10 mm element (Santa Barbara Research) is mounted on the end of a long liquid helium dewar, which is itself surrounded by a metal sleeve cooled to 77K. The detector has a fairly high sensitivity, with $D^* = 3.4 \times 10^9$ cm $Hz^{0.5}$ W^{-1}. The dewar itself must be evacuated for at least 4 h before cooling, or else lHe is not retained for a useful period. The inner and outer dewars of the detector must be pre-cooled with lN_2 prior to injection of lHe. The detector is biased (-45 V), and changes in

infrared power are manifested in changes in the resistance of the detector element. A capacitor (0.02 μF) couples these resistivity changes to a pre-amplifier and determines, along with a load resistor (12kΩ) the timescale of the detector, which was about 150 ns. The voltage output from the detector is amplified by a 0033-series preamplifier circuit (50 MHz bandwidth), which is supplied voltages of +6, -6, 0V by a pair of joined, rechargeable 6V gel-cell batteries (Power-One).

A pyroelectric detector was used to monitor the relative CO laser power. The detector unit (ELTEC, model 408) contains the 2 mm diameter element and an uncoated Ge window. The detector was operated unbiased, with a 9V battery. Its nominal D* is 7×10^7 cm $Hz^{0.5}$ W^{-1}.

2.6. Data Acquisition and Analysis. Transient signals from the Ge:Cu detector were collected and processed by a Tektronix 7912 AD transient digitizer, which includes two plug-in units: (a) a programmable amplifier, 7A16P and (b) a programmable timebase, 7B90P. Signal from the detector, often amplified by a factor of ten by a Keithley model 104 wideband amplifier, is fed into the first plug-in, which is terminated for 50 Ω and contains a 20 MHz bandwidth filter. The signals were also inverted in polarity so transient absorptions appear as positive excursions from the baseline, whereas transient bleaching leads to negative-going traces. The trigger input, also terminated for 50 Ω, received either the Synch Out pulse from the excimer laser, or the user-selected pulse train generated by the Metra-Byte A/D board. If this latter option was chosen, the pulse delay generator shown in Figure 2-2 was used to delay the computer pulses by 0.1 or 1 μs.

During routine operation, lasing wavelength is selected by the user from within the data acquisition program C.COM, a compiled Turbo Pascal 3.0 program which controls a National GPIB-IEEE interface board for communication with the Tektronix 7912 AD transient digitizer as well as a Metrabyte Dash-8 A/D board. Most of the software used to link the 7912 AD with the computer was developed by Polik[15]. The Dash-8 A/D sends out

binary pulses which direct a stepper motor interface (Oriel, model 17992) to step in one direction. The controller is set to one-half step increments. The CO laser wavelengths, having previously been calibrated against a monochromator (Spex, 0.75 m) which was in turn calibrated by a HeNe laser (632.8 nm), are stored as an array with corresponding step number "addresses" in the file LINEFILE.BNK which is read upon entering C.COM. Also accessed is a configuration file, START.CFG, which contains the present wavelength of the laser. This file is rewritten upon any program-initiated change in wavelength, and thus the setting of the laser grating is known in the event of a program crash. From the C.COM environment, one can select laser frequencies directly, laser tuning being accomplished by stepper motor turning of the grating by the expected number of steps in the direction desired, followed by a short tweaking routine. Because the axis of grating rotation is neither exactly parallel to the axis of the grating grooves nor precisely in the plane of the grating, some slight adjustments of the output coupler are often necessary when tuning from one line to another, especially if the frequencies lie more than ca. 80 cm^{-1} apart.

As mentioned in section 2.1, part of the IR beam is split off for CO laser power normalization. The split-off beam, chopped by a tuning-fork chopper run at 400 Hz, is directed to the element of a pyroelectric detector, before which occasionally is placed a CaF_2 lens (used in cases in which the beam had travelled more than 2 m). The unamplified output of this detector becomes the input for a lock-in amplifier (PAR, JB-5). The lock-in amplifier was set to take an external reference of level 0.1. The RC filter of the device was set to 0.1 s. The chopper reference output serves as the lock-in reference. Because the lock-in output is in the form of two single-ended outputs, one must subtract one from the other in a differential amplifier before reading a DC voltage proportional to the laser power. This amplifier output is then read by one of the A to D inputs of the Metrabyte A/D board, and is used to monitor laser power as the grating is scanned through lasing transitions, as

well as to record laser power during data acquisition for the purpose of trace normalization (see Appendix 1 for CO laser control program).

As an example of a transient absorption trace acquired by the transient digitizer, see Figure 3.2. In general, 8 to 512 photolysis shots were allowed to strike the sample, from which data was subtracted an equal number of traces acquired with the excimer shutter closed. The electronics which convert A/D board signals into voltages which can operate the shutter solenoid (as well as the flow solenoid used in the liquid-phase experiments of Chaper 3) are shown schematically in Figure 2-3. To extract from such data a rate constant which corresponds to either the disappearance or the production of a species, the digitized trace was fit by computer. The programs used to fit the traces were F2A.COM and F2B.COM, two compiled Turbo Pascal 3.0 programs[16] which employ an iterative, non-linear least-squares, three-parameter Marquardtian technique to fit the traces. Since pseudo-first-order conditions were the rule for these experiments, the traces were fit to first-order exponential functions. One uses F2A to fit traces showing exponential decay, while one fits rising functions with F2B. The functions used in the two programs were $y = a_1\exp(a_2x) + a_3$ for F2A, and $y = a_1(1-\exp(a_2x)) + a_3$ for F2B, where y represents transient absorption, x is $(t-t_0)$, and (a_1-a_3) stand for the fitting parameters. From the optimization of the fitting parameters, one obtains the decay rate, which in both cases is equal to $-a_2$.

For the acquisition of transient spectra, one may use the appropriate selection from the first C.COM menu (F10). In the automated spectrum acquisition mode, the CO laser is scanned from line to line through the user-defined spectrum range. At each laser line of power above that of the user-set threshold, a certain number of traces are acquired and the same number are subtracted. The average relative power as read by the lock-in amplifier is also stored as the title line for the 7912 AD data file upon storage. It is possible to abort data collection from within the spectrum-taking procedure by pressing the space-bar between the phases of data storage on hard disk and laser tuning to the next line. The data

files are of the following format. The title of the trace is always the first five digits of the CO laser line frequency as listed in LINEFILE.BNK, followed by the user-supplied "suffix" which is of the form XX.XXX. The first line of the file records the laser power during data acquisition. Then follow lines describing the transient digitizer timescale and voltage settings as well as the number of traces acquired and subtracted. Finally, the 512 digitized data points are listed.

One assembles the transient absorption spectra using another Turbo Pascal 3.0 program, EPWSPECT.PAS, which is listed in Appendix 2. After first assembling and storing a parameter file containing the frequencies, filenames, and powers of each data file, the program determines the $t = 0$ point with the aid of the user, who then selects the time increment between each spectrum. From each spectrum, an array of data points corresponding to the user-selected times after photolysis is then created for each trace. This array is then divided by the power of the CO laser line. Finally, the array is "zeroed" by the subtraction of the $t = 0$ data point value from each value in the array. This means that transient absorption at all frequencies is assumed to be zero at t_0. Then, the normalized, zeroed data values at every frequency corresponding to one specific time after photolysis are collected and stored in order of decreasing wavenumbers. Each time after photolysis thus becomes a spectrum data file which can be plotted as a function of frequency. In such a spectrum, transient absorptions appear as bands which deviate both above and below the baseline which represents zero transient absorption. Provision in the program is made for the subtraction of the values of a trace taken at any frequency from all traces. This is useful if, as was often the case (see below), an IR frequency-independent artifact such as a shock wave persists in all traces.

2.7. Notes on Signal-to-Noise Optimization. I will now briefly discuss the major artifacts which interfere in the analysis of the transient absorption data, as well as the methods which appear to maximize the signal-to-noise ratio.

Flash-kinetic spectroscopy involves the input of large amounts of energy into a mixture containing molecules which can undergo photo-induced chemical change. At 308 nm, the photon responsible for photolysis of the metal carbonyls studied in these experiments has much more energy than is required to break the metal-CO bond.[17] When one recognizes that quantum yields for photolysis are often substantially less than unity,[18] one sees that much energy is injected into the system which is not "productive" in the sense of producing the chemical species of interest. This energy becomes heat, which causes transient changes in the pressure and index of refraction of the medium. Such effects, which I will broadly call "shock waves", are most insidious.[19] They are often manifested in rolling oscillations with 1-10 μs period in the transient absorption traces. In order to minimize the component of shock wave in the traces, one must (a) assure a uniform photolysis-light flux over the cross-sectional aspect of the interrogating CO laser beam; (b) avoid concentrations of starting material which are optically dense at the photolysis wavelength; (c) achieve good overlap of the photolysis and detection beams throughout the cell; and (d) not focus the photolysis or detection beams too severely. In fact, the photolysis beam was not focussed down to a beam waist inside the cell, as this caused acute thermal lens effects. One important way in which the shock wave problem was lessened was in the use of a large-area detector, the Ge:Cu. Since the beam-walk caused by shock wave effects creates the artifacts in transient signals, the larger the area of the detector, the easier it is to prevent the beam from wandering off the detector element.

The photolysis source, the excimer laser, emits a tremendous amount of RF radiation lasting for roughly 1 μs after each discharge. It is therefore critical that all electronics involved in IR detection be properly shielded. Braided wire was placed around the BNC coaxial cable which fed the amplified detector signals from the detector output to the Keithley 104 amplifier or directly to the transient digitizer. So long as contact between the detector's amplifier ground to the ground of the transient digitizer was made, most (>90%) of the RF noise could be eliminated. The noise that remained, as well as the 7912

AD artifacts, was virtually eliminated by the subtracting data taken with the shutter closed from data with the shutter open (section 2.5). Other electrical artifacts included a regular stream of spikes of about 100 μs period which appear to originate in the Keithley amplifier. This effect was minimized when good contact was maintained between the braided coaxial shielding and the amplifier ground.

Notes and References

[1]A review of both the physics and the history of the development of the CO laser can be found in: Center, R. E. "High-Power, Efficient Electrically-Excited CO Lasers," *Laser Handbook*, ed. Stitch, M. L. Amsterdam: North-Holland, 1979, p. 89.

[2]Patel, C. K. N.; Kerl, R. J. *Appl. Phys. Lett.* **1964**, *5*, 81.

[3](a) Patel, C. K. N. *Phys. Rev.* **1965**, *141*, 71.; (b) Patel, C. K. N. *Appl. Phys. Lett.* **1965**, *7*, 246.

[4]McKenzie, R. L. *Appl. Phys. Lett.* **1970**, *17*, 462.

[5]Pollock, M. A. *Appl. Phys. Lett.* **1966**, *8*, 237.

[6](a) Sadie, F. G.; Bueger, P. A.; Malan, O. G. *J. Appl. Phys.* **1972**, *43*, 2906. (b) Bergman, R. C.; Rich, J. W. *Appl. Phys. Lett.* **1977**, *31*, 597.

[7]For the CO VUV laser, see: Hodgson, R. T.; *J. Chem. Phys.* **1971**, *55*, 5378. For the UV CO laser, see: Henry, A. *Compt. Rendu.* **1965**, *261*, 1495.

[8]R-branch lasing observed from the CO chemical laser: Gregg, D. W.; Thomas, S. J. *J. Appl. Phys.* **1968**, *39*, 4399.

[9]For a compilation of data on CO vibrational relazation by gases, see: Yardley, J. T. *Introduction to Molecular Energy Transfer*, New York: Academic Press, 1980, p. 84.

[10]Houston, P.; Moore, C. B. *J. Chem. Phys.* **1976**, *65*, 757.

[11]Ho, P. *Ph. D. Thesis*, University of California, Berkeley, 1981.

[12]Djeu, N. *Appl. Phys. Lett.* **1973**, *23*, 309.

[13]These frequencies were calculated using parameters from Roh, W. B.; Rao, K. N. *J. Mol. Spectrosc.* **1974**, *49*, 317.

[14]A more extensive discussion of the doped-germanium detectors in the Moore group may be found in: Young, L. *Ph. D. Thesis*, University of California, Berkeley, 1981; Finzi, J. *Ph. D. Thesis*, University of California, Berkeley, 1975, p. 62. For a general review of detector theory, see: *Optical and Infrared Detectors*, Ed. Keyes, R. J., New York: Springer-Verlag, 1980, Chapters 2, 4.

[15]Polik, W. F. *Ph. D. Thesis*, University of California, Berkeley, 1988.

[16]These programs are based upon the program FITDATA written by Polik. FITDATA allows the user to fit 7912 AD-format data files to any user-defined function which contains a limited number of fitting parameters.

[17]The M-CO bond energy is 25-40 kcal mol^{-1}, while the 308-nm light contains 93 kcal $einstein^{-1}$.

[18]This is especially common in condensed phases, where non-radiative de-excitation processes are facilitated.

[19]Shock waves are often used to detect small absorbances as a function of pulsed-laser frequency. This effect is the basis for both photoacoustic and thermal lens spectroscopies.

Table 2.1. Selected Ground-State P Branch Vibrational Transitions, in cm^{-1}. V', J' Represent Upper State Quantum Numbers. CO Laser Transitions Observed from Moore Laser in Boldface.

J'⇓\V'⇒	1	2	3	4	5	6	7
0		2113.0	2086.6	2060.3	2034.0	2007.9	1981.8
1	2135.6	2109.1	2082.8	2056.5	2030.3	2004.2	1978.1
2	2131.6	2105.3	2078.9	2052.7	2026.5	2000.4	1974.4
3	2127.7	2101.3	2075.1	2048.9	2022.7	1996.7	1970.7
4	2123.6	2097.4	2071.2	2045.0	2018.9	**1992.8**	**1966.9**
5	2119.7	2093.4	2067.2	**2041.1**	**2015.0**	**1989.0**	**1963.1**
6	2115.6	2089.4	**2063.2**	**2037.1**	**2011.1**	**1985.1**	**1959.2**
7	2111.5	**2085.3**	**2059.2**	**2033.1**	**2007.1**	**1981.2**	**1955.4**
8	2107.4	**2081.3**	**2055.2**	**2029.1**	**2003.2**	**1977.3**	**1951.5**
9	2103.3	**2077.1**	**2051.1**	**2025.1**	**1999.2**	**1973.3**	**1947.5**
10	2099.1	**2073.0**	**2047.0**	**2021.0**	**1995.1**	**1969.3**	**1943.5**
11	2094.9	2068.8	**2042.8**	2016.9	**1991.0**	**1965.2**	**1939.5**
12	2090.6	2064.6	2038.6	2012.7	**1986.9**	1961.2	**1935.5**
13	2086.3	2060.3	2034.4	2008.6	1982.8	1957.0	**1931.4**
14	2082.0	2056.1	2030.2	2004.3	1978.6	1952.9	1927.3

J'⇓\V'⇒	8	9	10	11	12	13	14
0	1955.8	1929.8	1903.9	1878.1	1852.4	1826.8	1801.2
1	1952.1	1926.2	1900.4	1874.6	1848.9	1823.3	1797.8
2	1948.4	1922.6	1896.8	1871.0	1845.4	1819.8	1794.4
3	1944.7	1918.9	1893.1	1867.4	1841.8	1816.3	1790.9
4	**1941.0**	**1915.2**	1889.5	**1863.8**	**1838.2**	1812.7	**1787.3**
5	**1937.2**	**1911.5**	**1885.8**	**1860.1**	**1834.6**	**1809.1**	**1783.8**
6	**1933.4**	**1907.7**	**1882.0**	**1856.4**	**1830.9**	**1805.5**	**1780.2**
7	**1929.6**	**1903.9**	**1878.3**	**1852.7**	**1827.2**	**1801.9**	**1776.5**
8	**1925.7**	**1900.0**	**1874.4**	**1848.9**	**1823.5**	**1798.2**	**1772.9**
9	**1921.8**	**1896.2**	**1870.6**	**1845.1**	**1819.7**	**1794.4**	**1769.2**
10	**1917.9**	**1892.3**	**1866.7**	**1841.3**	**1815.9**	1790.7	1765.5
11	**1913.9**	**1888.3**	1862.8	1837.4	1812.1	1786.9	1761.7
12	1909.9	1884.3	1858.9	1833.5	1808.2	1783.0	1757.9
13	1905.8	1880.3	1854.9	1829.6	1804.3	1779.2	1754.1
14	1901.8	1876.3	1850.9	1825.6	1800.4	1775.3	1750.2

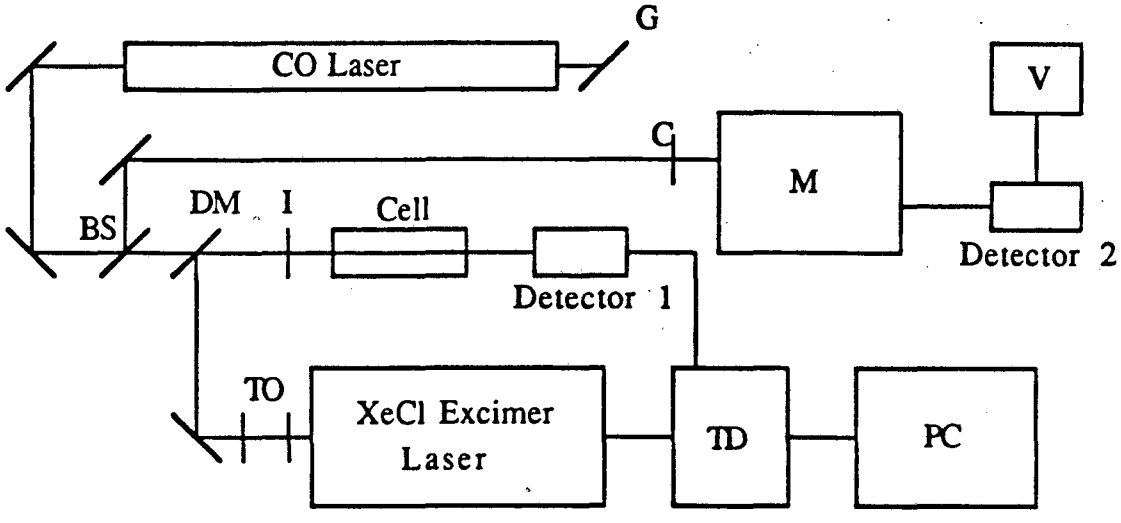

Figure 2-1. Experimental schematic of the IR flash-kinetic spectrometer.

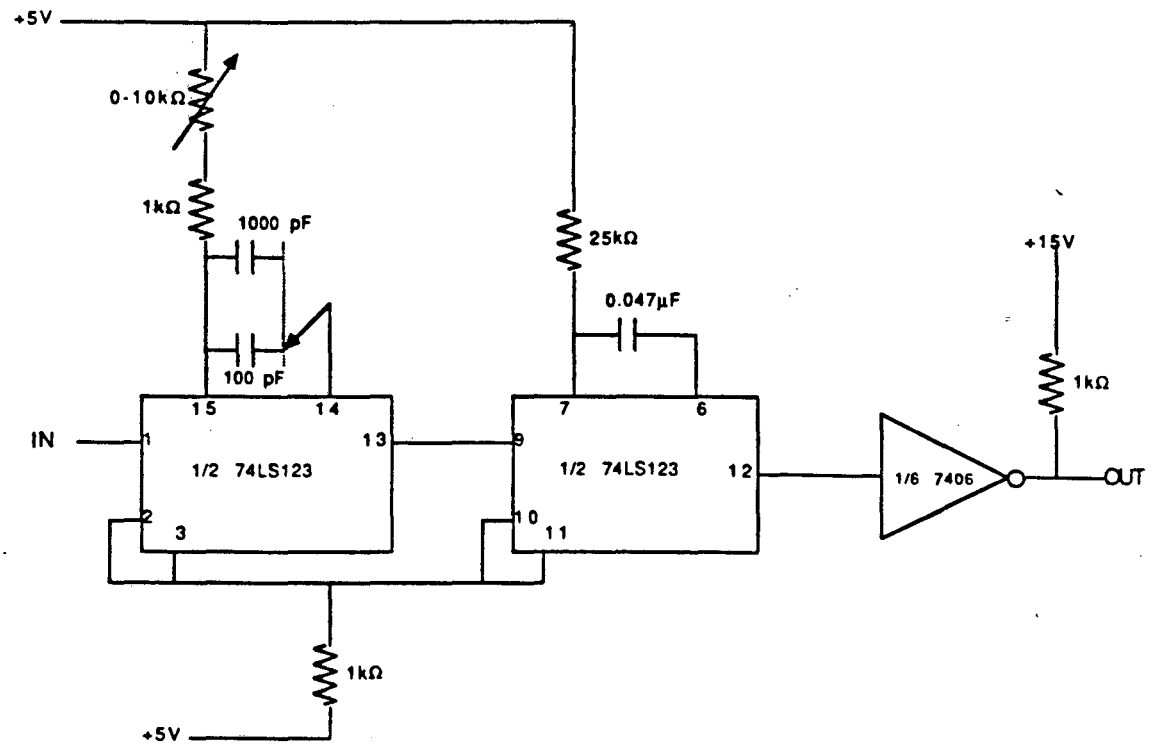

Figure 2-2. Pulse delay generator.

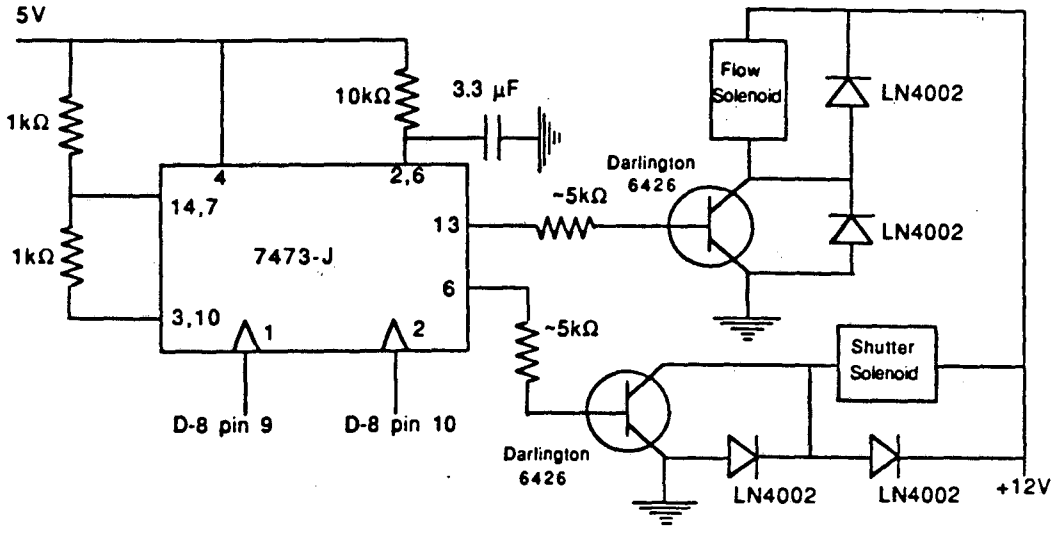

Figure 2-3. Electronics of solenoid control.

Chapter 3. The Reactivity of (η^5-C_5H_5)Co(CO) in the Gas Phase and in Solution

3.1. Introduction. The role played by solvent molecules in organometallic reactions is not well-understood. This is especially true for nonaqueous solutions, whose physical properties have received relatively little attention, given the enormous experimental literature on the effect of solvent on the reactivity and thermodynamics of organic molecules and of simple inorganic ions.[1] It is known, however, that varying the solvent has a profound effect on the reactivity of coordinatively unsaturated organometallic species.[2] Coordination of solvent has a substantial influence on the rate of carbonyl migratory insertion,[3a] one of the most well-studied organometallic transformations.[3b,c] In the case of octahedral WL_6 complexes,[3d] the presence of a solvent molecule effectively locks the pentacoordinate WL_5 photoproduct into distinguishable octahedral geometries, an interaction so strong as to lead Dobson *et al.* to coin the term "token ligand" for the occupant solvent molecule. The recent discovery of solvates of C-H activating fragments in ultracold matrices[4] has raised our curiosity about their role in solution-phase mechanisms, since the solvating hosts range from noble gas to potentially reactive matrices.

Within the past several years, the technique of flash photolysis, combined with fast detection of transient species, has led to significant contributions to the understanding of fundamental problems in organometallic chemistry.[5] In this work, an important unsaturated organometallic fragment, CpCo(CO) (Cp = η^5-C_5H_5), is studied in both gas and solution phases. The extent to which solvent occupation and stabilization of the open site affects its reactivity is determined for two-electron donor ligands.

$CpCo(CO)_2$ was settled on as a good starting point for our study for several reasons. A volatile (partial pressure at 300 K = 1.1 Torr), light-sensitive compound, it lends itself to gas- as well as liquid phase photochemical study. Not only is it a congener of the second- and third-row C-H activating compounds $Cp^{(*)}M(CO)_2$ (M= Rh, Ir; Cp* =

η^5-C_5Me_5)[6] but $CpCo(CO)_2$ is also an important catalyst precursor in its own right, for example, in alkyne trimerization.[7] Certain results indicate that closely related molecules may be precursors to H_2-activating fragments.[8] Finally, due to its availability, structural simplicity, and chemical significance, the compound has been the subject of much pertinent investigation, both experimental[9] and theoretical.[10]

In 1977, Lee and Brintzinger examined the photochemistry of $CpCo(CO)_2$ in toluene and petroleum ether at -78°C,[11] in an attempt to identify spectroscopically the intermediates in the alkyne cotrimerization reaction. Under these conditions, they claimed to have seen the monocarbonyl CpCo(CO) (from its carbonyl stretching frequency at 1970 cm^{-1}) as the first species formed upon photolysis. Subsequent reaction of this species yielded the dimers $Cp_2Co_2(CO)_3$ and $Cp_2Co_2(CO)_2$ or, in the presence of diphenyl alkynes, the monosubstituted carbonyl alkyne complex, CpCo(CO)(RCCR). These species then presumably lead into the trimerization pathway, the last via coordinationof a second alkyne and isomerization to a coordinated cyclopentadienone derivative. In most catalytic schemes for the cotrimerization reaction, the CpCo moiety remains intact and acts as the template upon which the linking of the alkynes is effected. Later, this group isolated[12] two partially purifiable, sublimable materials assigned the formulae $CpCo(C_6H_6)$ and $CpCo(C_6H_6)_2$ on the basis of mass spectral data alone, which supported the hypothesis of CpCo being the catalytic unit involved in this cyclization. The former adduct reacted with 2-butyne to produce a material showing a parent ion in the mass spectrum consistent with its assignment as $CpCo(C_6Me_6)$.

While Rest and co-workers did not detect CpCo(CO) following the photolysis of $CpCo(CO)_2$ in Ar and CH_4 matrices,[13] but rather the dinuclear species $Cp_2Co_2(\mu\text{-}CO)_2$, a later study[4] showed the monocarbonyls CpM(CO) (M = Rh, Ir) to be the direct products in the photolysis of the congeners of $CpCo(CO)_2$, $CpM(CO)_2$. Effects particular to the matrix environment may be responsible for the discrepancy between the photochemistry that Rest observed as opposed to that seen by Brintzinger. For examply, the cage effect which is of

importance in matrix chemistry may drastically reduce the yield of monocarbonyl by making it impossible for photogenerated CO to escape from the monocarbonyl and diffuse away. In a CO matrix, η^3-$CpCo(CO)_3$ is produced upon photolysis, lending credence to the associative mechanism first advanced by Wojcicki and Basolo.[14] When photolysis is performed on the dicarbonyl isolated in N_2 matrices, $CpCo(CO)(N_2)$ is the major product.

We undertook the study of $CpCo(CO)_2$ chemistry from two directions with somewhat different motivations. First, we examined the compound in the gas phase mainly in order to understand its facile ligand substitution processes. While most time-resolved photochemical studies on ligand addition processes at inorganic carbonyls show CO loss to be the first step,[15] a scheme involving primary ligand association followed by CO loss cannot be ruled out in this case *a priori* because of its undeniable applicability in the thermal substitution chemistry of both $CpCo(CO)_2$ as followed by CO exchange[14b] and also (indenyl)$Rh(CO)_2$ and related materials.[16] In repeating the photolysis of $CpCo(CO)_2$ in solution, we wished not only to ascertain whether CpCo(CO) is the primary photoproduct but also to establish the extent to which an incoming ligand molecule is impeded from attacking the open site on the organometallic fragment by one or more solvent molecules.

3.2. Experimental. The general scheme for the CO-laser transient IR spectrometer has been discussed at length in Chapter 2. Therefore, the experiment is briefly described.

For photolysis, an excimer laser (Lambda-Physik, EMG-103) was operated for XeCl* emission (308 nm). The beam, after telescoping and reflection, delivered about 5-10 mJ cm^{-2} $pulse^{-1}$ over an area of 2 cm^2. When the gas cell was in use, the 308 nm photolysis beam, directed into the cell by a dichroic mirror of coated sapphire, ran coaxially with the CO laser beam down the center of the cell. Repetition rates for the photolysis laser ranged from 2 to 20 Hz; pulse duration was ca. 20 ns. The photolysis beam diameter, which could be altered by changing the setting of an iris placed right in front of the IR cell,

ranged from 5 to 15 mm and completely contained the ir beam, whose diameter was 2-3 mm.

The gas cell is shown schematically in Figure 3-1. The gas cell, 107 cm path length and 2.5 cm inner diameter, was equipped with two capacitance manometers for pressure measurement. Measurement of the pressure of $CpCo(CO)_2$, when necessary, was made indirectly by monitoring the amplitude of the signals due to reflections from the photolysis beam reaching two silicon photodiodes placed before and after the gas cell and applying Beer's law, with the absorption cross-section at 308 nm ($\varepsilon_{10} \sim 1400$ l mol^{-1} cm^{-1}). The gas mixture was slowly flowed through the cell in the following manner. The buffer gas, either He Ar, or, for the N_2 reactions, N_2, was divided into three separate flows, regulated by needle valves. One streamed over the surface of the liquid $CpCo(CO)_2$ and thence into the cell through a central port. Another functioned as a bypass of this flow and proceeded directly to the center. Finally, a port at each end fo the cell allowed a stream of pure buffer bas to sweep over the inner surface of the CaF_2 windows, which were placed at Brewster's angle. Typical experimental conditions were 0.3 Torr $CpCo(CO)_2$ and 50 Torr Ar. Of the gases, N_2 (99.998%), Ar (99.995%), and He (99.995%) were supplied by Lawrence Berkeley Laboratory, while the CO (99.5%) and C2H4 (99.5%) were from Matheson. $CpCo(CO)_2$ was vacuum distilled before being placed in the gas cell apparatus. (The material decomposed slowly while under inert gas and shielded from light, but as the decomposition products are nonvolatile clusters, no subsequent purification was deemed necessary.)

For the liquid-phase experiments, a standard rectangular ir cell with CaF_2 windows (2 × 3.8 cm, one window drilled with holes top and bottom) separated by Teflon or lead gaskets of 1 or occasionally 0.5 mm thickness was used. Unless stated, solutions were purged of nitrogen by bubbling argon through them for roughtly 5 min before use. An overpressure of argon in a flask ontaining the solution forced it through Teflon delivery tubes into the cell, from which it left through more Teflon tubing. The flow rate of solution

varied, but it was typically 1 cm^3 s^{-1}. This flow rate, given the cross section of the ir beam (ca. 0.03 cm^2) and the photolysis repetition rates used, was found to be sufficient the ensure fresh sample for each photolysis shot. Solutions were prepared in a drybox under N_2. The concentration of $CpCo(CO)_2$ was typically $(0.3 - 1) \times 10^{-3}$ mol l^{-1} in cyclohexane. The cyclohexane, tetrahydrofuran (THF), and benzene were purchased from Fisher and were distilled from $LiAlH_4$ (C_6H_{12}) and Na/benzophenone (THF, C_6H_6). $P(n\text{-}C_4H_9)_3$ was obtained from Aldrich and was used without further purification. Acetonitrile was obtained from Merck adn distilled from CaH_2. $CpCo(CO)_2$ was vacuum distilled and stored under N_2 at reduced temperature.

3.3. Gas-Phase Photolysis of $CpCo(CO)_2$. Figure 3-2 shows transient absorption of 2011 cm^{-1} light following the photolysis of $CpCo(CO)_2$ in buffer gas (Ar), along with a superimposed fit to a first-order exponential decay. From a collection of such transient absorption traces taken through the CO laser frequency range, we construct transient absorption spectra (see Experimental). Figure 3-3 shows the transient absorption spectra observed 1 and 3 μs after the 308 nm photolysis of $CpCo(CO)_2$ (**1** in Scheme I) in ca. 45 Torr of He in the presence of 1 Torr CO. The negative relative absorptions centered at 1990 and 2040 cm^{-1} are due to the prompt depletion of **1** upon photolysis. A study of the variation of the amplitude of the positive transient observed at 2010 cm^{-1}, normalized for CO laser power, with photolysis laser power over a fluence range of 0.1-1 mJ cm^{-2} $pulse^{-1}$ indicates that a one-photon process is responsible for the production of this transient. Figure 3-3 shows that within 3 μs, the transient at 2010 cm^{-1} disappears, while a new positive transient near 1980 cm^{-1} grows in on the same timescale. At 2030 cm^{-1}, there is a somewhat smaller positive transient which forms promptly and does not decay on the 20 μs timescale of these spectra.

We feel confident in the identification of the 2010 cm^{-1} transient as the unsaturated species, CpCo(CO) (species **2** in Scheme I, drawn with a bent structure as indicated by the

calculations in Reference 10). The band is unique in the spectrum, as its kinetic behavior cannot be correlated with that of any other band down to 1900 cm^{-1}. The rate of disappearance of this species, obtained from the fit of the transient absorption to an exponential decay, grows linearly with the partial pressure of CO (varied from 0 to 5 Torr), a result consistent with simple ligand addition (Scheme I). A higher CO pressures (>1 Torr), the rate at which $CpCo(CO)_2$ grows back after photolysis is approximately that of the disappearance of the 2010 cm^{-1} transient. We have determined the residual rate of decay of the transient to de due to reaction of the monocarbonyl with starting material (see below). The product of this reaction shows a terminal CO absorption at 1980 cm^{-1}, and on this basis we postulate it to be the binuclear species $Cp_2Co_2(CO)_3$, denoted as **5**.

We have not been able to positively identify the species responsible for the transient absorption at 2030 cm^{-1}, though it is most likely monometallic, since it appears faster than does **5**, which is formed at a rate close to the hard-sphere collision frequency (see below). This feature is only seen in experiments in which CO was added. It is possible that this transient corresponds to the η^3-Cp product seen in the photolysis of $CpCo(CO)_2$ in CO matrices, $(\eta^3\text{-Cp})Co(CO)_3$, which has CO stretching vibrations at 2075 and 2018 cm^{-1}. Our CO laser range does not extend high enough in frequency to search for transient absorption at 2075 cm^{-1}, and thus this assignment remains a speculation.

This limitation also prevents us from examining the internal energy distribution of CO in low-lying vibrational states. In order to influence the reported spectra, the CO would have to be highly vibrationally excited ($v \geq 3$). We do not believe that such "hot" CO is responsible for any of the transient species involved in Scheme I, but may cause transient absorptions often noted at frequencies higher than 2060 cm^{-1}. These transient absorptions are in general large, are formed promptly upon photolysis, and do not decay within *ca.* 20 μs. However, much more rapid decay of these high-frequency transients may be induced by the replacement of the buffer gas with neopentane or propane. This supports as assignment of the transients to hot CO, since collisional quenching of

vibrational excitation in CO should be very inefficient for rare gas atoms, but much more feasible for large polyatomics. By way of comparison, Fletcher and Rosenfeld found[15c] CO generated from the photolysis of $Cr(CO)_6$ to be predominantly in the vibrational ground state.

In the gas phase, removal of energy is required during the formally bimolecular reaction CpCo(CO) + L = CpCo(CO)L, and it must be accounted for in any kinetic scheme. Since this reaction is exothermic, at least one buffer gas molecule must collide with the association complex [CpCo(CO)L]* in order to prevent the reverse reaction from occurring.[17] The amount of vibrational energy remaining in the monocarbonyl fragment after photolysis will certainly contribute as well to the nmber of effective collisions required to trap CpCo(CO)L as the ligand addition product. In our kinetic studies on the reactivity of the monocarbonyl **2**, we wanted to be sure that the excess energy from the ligand addition reaction, deriving from its exothermicity, would be removed rapidly by buffer gas. To determine this, we measured the rate constant for reaction of **2** with CO at four different argon pressures ranging from 4 to 95 Torr (Table 3.1). We saw a slight dependence of the rate upon buffer gas pressure, but the magnitude of this effect is not much greater than that of the uncertainty in the rate constant determination. Our kinetic studies were all performed with 20 Torr or more of buffer gas pressure, at which pressures product trapping should be complete.

The thermalized, coordinatively unsaturated species **2** (the 2010-cm^{-1} transient) reacts readily with good two-electron donors such as CO, following the pattern of $Cr(CO)_4$, $Fe(CO)_3$, and other complexes.[15] Table 3.2 shows the CO stretching absorptions we observe for the products formed from reaction with C_2H_4 and N_2 (species **3** and **4**, respectively) as well as those determined from matrix isolation work or other sources; the rates of reaction can be found in Table 3.1. While CO and C_2H_4 react with the monocarbonyl at rearly the diffusion-limited rate, N_2 forms a stable complex with **2** much less readily (Figure 3-4). In fact, nitrogen pressures had to be raised so high to observe

changes in monocarbonyl lifetime that argon gas pressure was correspondingly lowered so that total pressure was kept constant, in order to forestall significant alteration in the bulk properties of the sample mixture. That such a molecule (4) is formed at all at room temperature and in the gas phase is of interest, for while the dinitrogen complex was detected in matrix studies,[13] it had not previously been seen in other media. Figure 3-5 shows the appearance of the dinitrogen product CO stretch at ca. 2005 cm^{-1} in a bath of pure nitrogen at about 90 Torr. Note that the CO stretch is shifted to slightly lower frequency in the dinitrogen and ethylene complexes from the monocarbonyl, indicating greater electron density on the metal center, part of which is donated into the π^* orbital of the CO ligand.

Scheme I

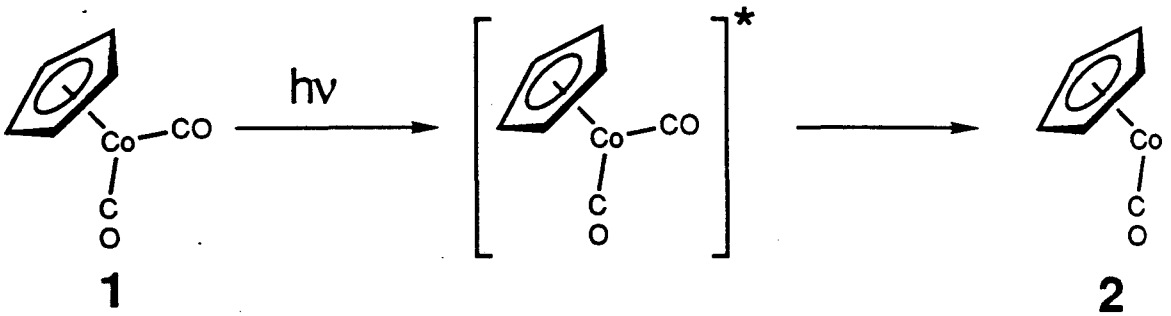

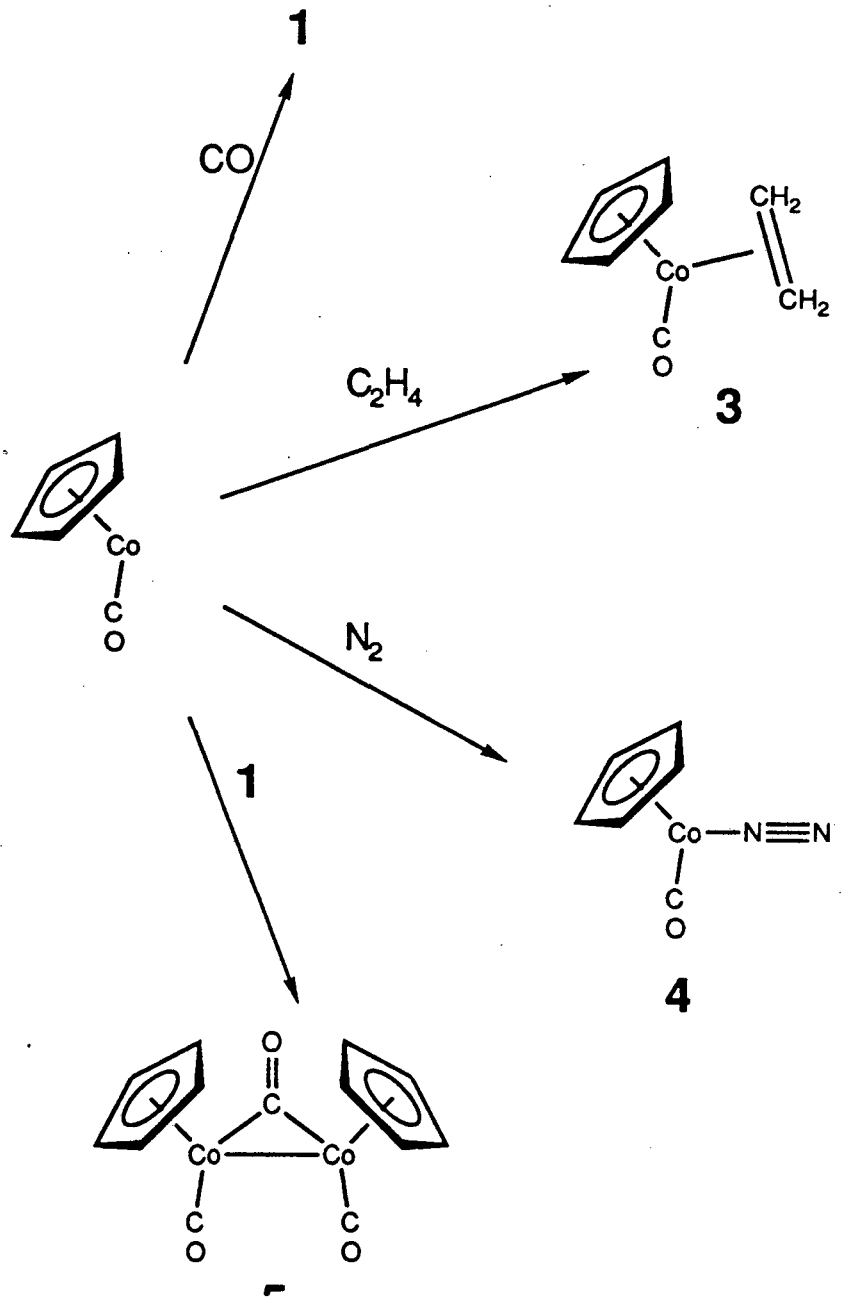

As mentioned above, in the absence of added ligand, CpCo(CO) decays by attack on the starting complex **1**. In order to obtain a rate constant for this process, the partial pressure of **1** must be known. (Since rarely more than 5% of the starting material in the photolysis bean was consumed per shot, the pseudo-first-order approximation was employed.) The technique used to deliver the gaseous mixture of **1** in buffer gas into the gas cell and the flowing arrangement of the cell made it necessary to measure this quantity indirectly (see section 3.2 for details). The uncertainties involved in the conversion of UV absorption of the gas sample into concentration of **1**, for example, due to the error in estimation of the true path length of the sample caused by buffer gas flow on the windows, account therefore for the greater part of the error bar reported for the rate constant for the reaction of the monocarbonyl with the unphotolyzed dicarbonyl. The method appeared to work well, however, to the extent that the inverse lifetime of the monocarbonyl is proportional to this derived $CpCo(CO)_2$ partial pressure (Figure 3-6). The rate constant for this dimerization reaction as well as those for reaction of **2** with CO and C_2H_4 is close to gas kinetic. This is indicative of small barriers to reaction and is consistent with similar studies on the reactivity of $Cr(CO)_4$[18].

Previous studies[15] of the UV photochemistry of metal carbonyls in the gas phase have shown that dissociation of more than one CO moiety predominates. We cannot eliminate the possibility that some CpCo is formed upon photolysis of $CpCo(CO)_2$, since this fragment is not detectable with our technique. However, the fact that the transient which we assign to CpCo(CO) appears promptly after photolysis (even in the absence of added CO) indicates that it is formed from a unimolecular process, since the concentration of photoproduct CO would be too small to account for its formation by recombination. Also, the rate constant for the reaction of CpCo(CO) with CO (Table 3.1) is close to gas kinetic in magnitude, and the decay of CpCo(CO) absorption is accurately fit by a single exponential from the end of the photolysis pulse (within our temporal resolution). This means that no significant amount of CpCo(CO) is derived from CpCo, since the latter must

react first with CO. We presume that the high number of low-frequency modes attributable to the C_5H_5 ring lowers the RRKM rate for CpCo(CO) dissociation to the point where collisions with buffer-gas molecules remove enough energy to trap the monocarbonyl.

3.4. Solution-Phase Studies. Photolysis (308 nm) of **1** in cyclohexane solution leads to the appearance of a positive transient at 1990 cm^{-1} (Figure 3-7). We have postulated this transient to be the monocarbonyl weakly solvated by cyclohexane. The change in medium from gas to liquid affects both the shape and frequency of the transient absorptions, making them narrower (as the wide P and R branches found in the gas phase disappear) and shifting them to lower energy by as much as 20 cm^{-1} (Table 3.3). The monocarbonyl solvate absorption disappears as major new absorption grows in at 1965 cm^{-1} (not readily seen in the spectrum because of its overlap with the negative transient due to starting material destruction at 1970 cm^{-1}),[18] along with a smaller absorption at 1945 cm^{-1}, which has not yet been identified. The 1965-cm^{-1} absorption corresponds to the tricarbonyl dimer adduct seen in the gas phase at 1980 cm^{-1}. If the cyclohexane solvate is produced in the presence of tri-*n*-butylphosphine, a new positive transient at 1925 cm^{-1} grows in at the same rate as that of monocarbonyl decay. This species appears to be the phosphine addition product, CpCo(CO)(P(*n*-Bu)$_3$), by the similarity between its CO stretching frequency and that of the triisopropylphosphine analogue (Table 3.3). In the presence of acetonitrile, a species which absorbs at 1940 cm^{-1} is formed, which we presume to be the acetonitrile complex, CpCo(CO)(CH_3CN). The dependence of the inverse of the decay time of the monocarbonyl upon ligand concentration yields k_2, the bimolecular rate constant for reaction with ligand. The extreme reactivity of the alkane-solvated monocarbonyl toward these two ligands may be seen in Table 3.4.

Because the monocarbonyl reacts so rapidly with starting material in solution, it was necessary to use dilute concentrations of **1** and, therefore, long (>0.5 mm) cell path lengths to achieve good signal-to-noise ratios. This situation led to one major problem: it

became impossible to study photolysis in neat solutions of tetrahydrofuran (THF) or benzene, since in cells of this thickness these solvents either absorb all the infrared probe light or absorb enough ultraviolet photolysis light to cause solvent heating, which produces shock waves and transient changes in absorption due to changes in the refractive index of the solvent. Therefore, in order to study the reactions of monocarbonyl species complexed by donor solvents, we doped cyclohexane solutions with those solvents to relatively high concentrations (ca. 0.2 mol l^{-1}) and then varied the ligand concentration. In such cases, the kinetic scheme is more complicated, since there are two types of solvent competing for the open site on the organometallic fragment. The photolysis of **1** in one such solution doped with benzene is shown in Figure 3-8. The benzene solvate is formed rapidly and constitues the major transient species present in solution after the initial photolysis pulse. A small remnant of the cyclohexane solvate is observed at 1990 cm^{-1}, while the positive transient lying at 1977 cm^{-1} represents the benzene solvate. A typical decay trace with shock-wave noise subtracted out for the benzene solvate is shown in Figure 3-9. The benzene solvate is most likely an η^2 side-bound species, by analogy with previously observed benzene complexes.[19] Figure 3-10 shows the transient spectrum of **1** photolyzed in cyclohexane solution in the presence of THF. The THF-solvated monocarbonyl appears at 1952 cm^{-1} and decreases in intensity concurrent with the rise of the 1965-cm^{-1} absorption due to dimer.

Scheme II

$$CpCo(CO)_2 \xrightarrow[CyH]{h\nu} CpCo(CO)(CyH) + CO$$

$$CpCo(CO)(CyH) + S \longrightarrow CpCo(CO)(S) + CyH$$

Indirect

$$CpCo(CO)(S) + CyH \underset{k_{-1}}{\overset{k_1}{\rightleftharpoons}} CpCo(CO)(CyH) + S \qquad (K \equiv \frac{k_1}{k_{-1}})$$

$$CpCo(CO)(CyH) + L \xrightarrow{k_2} CpCo(CO)(L) + CyH$$

$$CpCo(CO)(CyH) + CpCo(CO)_2 \xrightarrow{k_3} Cp_2Co_2(CO)_3 + CyH$$

$$CpCo(CO)(CyH) + N_2 \xrightarrow{k_6} CpCo(CO)(N_2) + CyH$$

Direct

$$CpCo(CO)(S) + L \xrightarrow{k_4} CpCo(CO)(L) + S$$

$$CpCo(CO)(S) + CpCo(CO)_2 \xrightarrow{k_5} Cp_2Co_2(CO)_3 + S$$

$$CpCo(CO)(S) + N_2 \xrightarrow{k_7} CpCo(CO)(N_2) + S$$

(L ≡ P(*n*-Bu)$_3$, CH_3CN; S ≡ C_6H_6; CyH ≡ cyclohexane)

The concentration of benzene in cyclohexane was varied in order to understand the mechanism of phosphine substitution into CpCo(CO)(S), S = C_6H_6. If the paths from donor-solvent solvate to phosphine adduct and to tricarbonyl dimer lead through an unstable unsaturated species (Indirect mechanism of Scheme II), then assumption of a steady-state concentration in this unsaturated intermediate leads to the following rate law for loss of the benzene solvate

$$\text{rate} = \frac{-d[\text{CpCo(CO)(S)}]}{dt} = k_{obsd}[\text{CpCo(CO)(S)}] \qquad (1)$$

where, at concentrations of CyH, S, L, and **1** kept high enough so that they do not change appreciably during a run,

$$k_{obsd} = \left(\frac{k_1k_2[\text{CyH}][\text{L}] + k_1k_3[\text{CyH}][\mathbf{1}]}{k_{-1}[\text{S}] + k_2[\text{L}] + k_3[\mathbf{1}]}\right) \qquad (2)$$

The first term in the numerator arises from the reaction of the donor-solvent solvate with ligand, while the second term represents the contribution of the dimerization reaction of the solvate with **1**; the kinetics of dimerization will be discussed later. Let us also define a quantity k'_{obsd}

$$k'_{obsd} = \frac{\partial(k_{obsd})}{\partial([\text{L}])} = \frac{k_1k_{-1}k_2[\text{S}][\text{CyH}]}{(k_{-1}[\text{S}] + k_2[\text{L}] + k_3[\mathbf{1}])^2}. \qquad (3)$$

which will become useful in later discussion.

Should the direct mechanism for ligand attack hold, however, the observed pseudo-first-order rate constant, k_{obsd}, would only be dependent upon the concentrations of L and **1** (Direct mechanism). If we assume that there will be components of both mechanisms for benzene solvate decay, then (2) and (3) become

$$k_{obsd} = \left(\frac{k_1k_2[CyH][L] + k_1k_3[CyH][\mathbf{1}]}{k_{-1}[S] + k_2[L] + k_3[1]}\right) + k_4[L] + k_5[\mathbf{1}] \qquad (4)$$

$$k'_{obsd} = \frac{k_1k_{-1}k_2[S][CyH]}{(k_{-1}[S] + k_2[L] + k_3[1])^2} + k4. \qquad (5)$$

At each different benzene concentration, the pseudo-first-order rate constants for decay fo the solvate in the presence of increasing amounts of phosphine were measured, and some of the results are shown in Figure 3-11. It is clear that the slopes of these lines, which represent values of k'_{obsd}, decrease with increasing $[C_6H_6]$; the values of these slopes can be seen in Table 3.5. This fact in itself is indicative of an indirect mechanism for the destruction of the benzene solvate. Also, note for Figure 3-11 that at no concentration of donor solvent was there significant curvature, which might indicate saturation kinetics, in the reciprocal lifetime versus ligand concentration plot. This strongly suggests that, given the expression for k_{obsd} in (4), $k_2[L] << (k_{-1}[S] + k_3[\mathbf{1}])$. There appears to be a linear relationship between $1/k'_{obsd}$ for benzene solvate destruction and $[C_6H_6]$ (Figure 3-12) which has an intercept at the origin. From this fact and an examination of (5), we conclude that $k_{-1}[S]$ is the dominant term in the denominator of (2) under the conditions of this experiment and also that k_4 is small, so that (4) and (5) reduce to

$$k_{obsd} = (k_1k_2[CyH][L] + k_1k_3[CyH][\mathbf{1}])/k_{-1}[S] + k_5[\mathbf{1}] \qquad (6)$$

$$k'_{obsd} = k_2K[CyH]/[S]. \qquad (7)$$

Equation 7 illustrates the inverse dependence of the slopes of k_{obsd} versus [L] plots upon [S], the effect seen in Figure 3-12. From the inverse slope in Figure 3-12, we find $k_2K = (7 \pm 1) \times 10^5$ l mol^{-1} s^{-1}.

We have already determined k_2 independently for phosphine (Table 3.4). If we assume the intermediate in the decay of the benzene solvate is the same cyclohexane solvate as that which reacts with phosphine in the absence of benzene, the $K = (2.3 \pm 0.5) \times 10^{-4}$.

Three points should be made here. First, the term "cyclohexane solvate" used to refer to the reactive intermediate in this discussion does not imply a detailed knowledge of the structure or even of the exact stoichiometry of this species. In fact, the degree of bonding of cyclohexane molecule(s) in the transition state between the "cyclohexane solvate" and the ligand-substituted adduct remains undetermined. Second, the fact that no saturation in the rate was observed as phosphine concentration was increased implies that k_{-1} is at least of the same order of magnitude as k_2 and is possibly even larger, since even at the highest [L]/[S] ratios (about 0.2) no significant deviation from linearity was noted. This reflects the highly reactive nature of the unsaturated metal center, which reacts with any two-electron donor at about the rate of diffusion. Attempts to check this by measuring k_{-1} independently were unsuccessful, partly because the reaction of the donor-solvent solvates with **1** precluded and significant build-up of these solvates at very low concentrations of S. Finally, we must admit the possibility of a competing direct bimolecular reaction between ligand and donor-solvent solvate which might prove important at very high [S]. If this were true for the case of benzene as donor solvent, then we would expect to see a leveling off of $1/k'_{obsd}$ as [S] increases. It is clear from Figure 3-12 that $1/k'_{obsd}$ is at least 6×10^{-8} mol l^{-1} s in the limit of very large [S], and thus we can derive an upper bound for k_4 of 1.7×10^7 l mol^{-1} s^{-1}.

The following kinetic analysis was applied to the benzene solvate decay data in order to extract the rate constant for reaction fo the cyclohexane solvate with the starting material, $CpCo(CO)_2$. The decay of the benzene-solvated monocarbonyl in the absence of

ligand was assumed to be entirely due to this process. From our analysis of the kinetics of reaction with ligand, $k_{-1}[S] >> k3[\mathbf{1}]$; so from (4), the intercept of the line through each plot of the inverse lifetime of the benzene solvate versus phosphine concentration (see Figure 3-11) then represents $k_3[\mathbf{1}]K[CyH]/[S] + k_5[\mathbf{1}]$. The values of these intercepts are shown in Table V. If we then plot $k_{obsd}/[\mathbf{1}]$ against 1/[S], we should obtain a straight line whose slope is $k_3K[CyH]$ and whose intercept at 1/[S] = 0 is k_5. The validity of our assumptions is supported by the linearity of this plot (Figure 3-13), which gives $k_3 = (3.6 \pm 0.7) \times 10^9$ l mol^{-1} s^{-1} and $k_5 = (3.8 \pm 0.6) \times 10^7$ l mol^{-1} s^{-1}.

If argon is not bubbled through the solutions prior to their use in the experiments, a long-lived ($t > 10^{-4}$ s) absorption at *ca.* 1980 cm^{-1} is observed which forms apparently within the risetime of the detector and at the expense of the monocarbonyl. This transient we believe to be the dinitrogen adduct, corresponding to the species seen in the gas phase at 2005 cm^{-1}, since the solutions were prepared under a nitrogen atmosphere.

Figure 3-14 shows transient absorption traces taken at 1977 cm^{-1} with two solutions which had not been purged of nitrogen and had identical benzene and $CpCo(CO)_2$ concentrations. No phosphine was added to the first solution; its concentration in the second was 4.0×10^{-3} mol l^{-1}. At this frequency, both the benzene and nitrogen adducts can be monitored, whereas at 1973 and 1981 cm^{-1} only the benzene solvate and the nitrogen adduct, respectively, absorb. The benzene solvate absorption can be seen in both traces as a fast early spike, while the nitrogen adduct appears as a large baseline offset, since its decay time is much greater. It is interesting to note that the increase in phosphine concentration appears to affect the yield of nitrogen adduct and not appreciably its rate of decay, for this implies that the adduct is relatively stable to ligand attack and is, in fact, more stable in this regard than the benzene solvate.

If we add reactions of nitrogen with both cyclohexane and benzene solvates (Scheme II), then the expression for the observed rate constant for benzene solvate loss is

$$k_{obsd} = \left\{\frac{k_1[CyH](k_2[L] + k_3[1] + k_6[N_2])}{k_{-1}[S] + k_2[L] + k_3[1] + k_6[N_2]}\right\} + k_4[L] + k_5[1] + k_7[N_2]. \quad (8)$$

If the benzene solvate decay rate is then plotted against the concentration of phosphine, the intercept of the line through the data at [L] = 0 mol l^{-1} should be as follows:

$$k_{obsd}([L] = 0) = \left(\frac{k_1k_3[CyH][1] + k_1k_6[CyH][N_2]}{k_{-1}[S] + k_3[1] + k_6[N_2]}\right) + k_5[1] + k_7[N_2]. \quad (9)$$

We then made the assumption that $k_{-1}[S] >> (k_3[1] + k_6[N_2])$, based on our experiments with phosphine. Thus

$$k_{obsd}([L] = 0) = \left(K \times \frac{[CyH]}{[S]}\right)(k_3[1] + k_6[N_2]) + k_7[N_2]. \quad (10)$$

We estimate the nitrogen conctration in cyclohexane at 293 K to be 7.0×10^{-3} mol l^{-1}.[20] By comparing values of $k_{obsd}([L] = 0)$ obtained at [S] = 0.11 mol l^{-1} and at [S] = 0.022 mol l^{-1}, we find the contribution of $k_7[N_2]$ to be negligible; $k_7 < 10^7$ l mol^{-1} s^{-1}. A rough value for k_6 of 4×10^8 l mol^{-1} s^{-1} is obtained. A similar estimate for k_6 is found from the decrease in N_2 adduct formed upon addition of phosphine (Figure 3-14).

3.5. Conclusions. By comparing the reactivity of the photoproducts of $CpCo(CO)_2$ produced in gas and solution phases, we have attempted to bridge the gap between the gas-phase-based and solution-based knowledge of organometallic photochemistry. CpCo(CO), whether naked (as in the gas phase) or weakly complexed by alkane, is an extremely reactive species which can be trapped by two-electron donor ligands. The liquid-phase reaction of the cyclohexane solvate with nitrogen is somewhat slower than that for reaction

with phosphine or acetonitrile. This is similar to the pattern seen in the gas phase, although in the latter medium this effect is more marked. Also, we note that the dimerization reaction is nearly the fastest bimolecular process observed in both media. The reactivity of CpCo(CO)(CyH) seems in general to be high in comparison with those of other complexes recently studied, such as $CpMn(CO)_2(S)$[21] and $W(CO)_4(L)(S)$[3], where S represents an alkane solvent molecule.

The fact that the rate constant for direct reaction of the benzene solvate with **1** is greater than that for its reaction with phosphine is particularly intriguing and is demonstrative of the high Lewis basicity of **1**. It also raises the following question: why are dimerization reactions not more important in preparative synthetic procedures in which the concentrations of organometallic precursor and reactant ligand are similar? While the answer to this question is dependent on the exact chemical system and reaction conditions and is therfore entirely outside the scope of this thesis, we suggest that the instability of the initially-formed dimers, such as $Cp_2Co_2(CO)_3$, in the presence of ligands over time leads indirectly to the production of ligand substitution products.

The solution-phase studies render insight into questions of solvent participation in ligand substitution, since they begin to quantify the differences in solvent-open-site donding among solvent types. Along these lines, Wrighton and co-workers have recently observed large variations in the reactivity of unsaturated organometallic species in low-temperature hydrocarbon solvents.[22] Our work has shown that the equilibrium constant for donor solvent versus cyclohexane solvation strongly favors benzene association at 293 K. In fact, we may crudely estimate that the metal-solvent bond of the benzene solvate is 5 kcal mol^{-1} stronger than that of the cyclohexane solvate. The dominance of the indirect, dissociative pathway for benzene solvate decay is in keeping with the reactivity observed by Asali *et al.*[23] for the cis-(pip)(L)$W(CO)_4$ system, in which there exists a similar equilibrium between chlorobenzene and cyclohexane solvation of $(L)W(CO)_4$.

Notes and References

[1]Some research on physical properties of nonelectrolyte solutions has been collected in *Physical Chemistry of Organic Solvent Systems*; Covington, A. K.; Dickinson, T., Eds.; London: Plenum Press, 1973.

[2]See, for example: (a) Belt, S. T.; Haddleston, D. M.; Perutz, R. N.; Smith, B. P. H.; Dixon, A. J. *J. Chem. Soc., Chem. Commun.* **1987**, 1347. (b) Church, S. P.; Grevels, F.-W.; Herrmann, H.; Schaffner, K. *Inorg. Chem.* **1985**, *24*, 418. (c) Church, S. P.; Grevels, F.-W.; Herrmann, H.; Kelly, J. M.; Klotzbuecher, W. E.; Schaffner, K. *J. Chem. Soc., Chem. Commun.* **1985**, 594. (d) Giordano, P. J.; Wrighton, M. S. *Inorg. Chem.* **1977**, *16*, 166.

[3] (a) Wax, M. J.; Bergman, R. G.; *J. Am. Chem. Soc.* **1981**, *103*, 7028. (b) Kuhlman, E. J.; Alexander, J. J. *Coord. Chem. Rev.* **1980**, *33*, 195. (c) Alexander, J. J. *The Chemistry of the Metal-Carbon Bond*; Hartley, F. R., Ed.; Wiley: New York, 1985; Vol. 2, Chapter 5. (d) Dobson, G. R.; Hodges, P. M.; Healy, M. A.; Poliakoff, M.; Turner, J. J.; Firth, S.; Asali, K. J. *J. Am Chem. Soc.* **1987**, *109*, 4218.

[4]Rest, A. J.; Whitwell, I.; Graham, W. A. G.; Hoyano, J. K.; McMaster, A. D. *J. Chem. Soc., Dalton Trans.* **1987**, 1181.

[5]For an excellent review on the progress in this area, cf.: Poliakoff, M.; Weitz, E. *Advances in Organometallic Chemistry*, Stone, F. G. A., Ed.; Academic Press: New York, 1986; Vol. 25, p. 277.

[6]Hoyano, J. K.; Graham, W. A. G. *J. Am. Chem. Soc.* **1982**, *104*, 3723.

[7]Vollhardt, K. P. C. *Acc. Chem. Res.* **1977**, *10(1)*, 1.

[8]Janowicz, A.; Bergman, R. G. *J. Am. Chem. Soc.* **1981**, *103*, 2488.

[9] (a) For a review, see: Basolo, F. *Coord. Chem. Rev.* **1982**, *43*, 7 (b) V ollhardt, K. P. C.; Bercaw, J. E.; Bergman, R. G. *J. Organomet. Chem.* **1975**, *97*, 283.
[10]Hofmann, P.; Padmanabhan, M. *Organometallics* **1983**, *2*, 1273.

[11] (a) Lee, W.-S.; Brintzinger, H. H. *J. Organomet. Chem.* **1975**, *97*, 283.

[12]Lee, W.-S.; Koola, J. D.; Brintzinger, H. H. *J. Organomet. Chem.***1981**, *206*, C4.

[13]Crichton, O.; Rest, A. J.; Taylor, D. *J. J. Chem. Soc., Dalton Trans.* **1980**, 167.

[14] (a) Wojcicki, A.; Basolo, F. *J. Inorg. Nucl. Chem.* **1961**, *17*, 77. (b) Schuster-Woldan, H.-G.; Basolo, F. *J. Am. Chem. Soc.* **1966**, *88*, 1657.

[15]Selected examples: (a) Seder, T. A.; Church, S. P.; Weitz, E. *J. Am. Chem. Soc.* **1986**, *108*, 4721. (b) Seder, T. A.; Ouderkirk, A. J.; Weitz, E. *J. Chem. Phys.* **1986**, *85*, 1977. (c) Fletcher, T. R.; Rosenfeld, R. N. *J. Am Chem. Soc.* **1985**, *107*, 2203.

---

[16]Rerek, M. E.; Basolo, F. *J. Am. Chem. Soc.* **1984**, *106*, 5908.

[17]Fletcher, T. R.; Rosenfeld, R. N. *J. Am. Chem. Soc.* **1986**, *108*, 1686.

[18]At the time the gas-phase experiments were done, our CO laser could not operate below 1860 cm^{-1}. Therefore, we could not probe for bridging carbonyl absorptions. In solution, we have observed as absorption at 1812 cm^{-1} which we believe is due to the bridging CO of $Cp_2Co_2(CO)_3$, while no other transient absorptions were observed in the 1790-1825-cm^{-1} region. We speculate that the dicarbonyl dimer $Cp_2Co_2(CO)_2$, which should also absorb in this region (see Reference 11a), is produced from the photolysis of the tricarbonyl dimer in previous preparative studies. Cf: Anderson, F. R.; Wrighton, M. S. *Inorg. Chem.* **1986**, *25*, 112.

[19]For example, see: Brauer, D. J.; Krüger, C. *Inorg. Chem.* **1977**, *16*, 884.

[20]Dymond, J. H. *J. Phys. Chem.* **1967**, *71*, 1829.

[21]Creaven, B. S.; Dixon, A. J.; Kelly, J. M.; Long, C.; Poliakoff, M. *Organometallics* **1987**, *6*, 2600.

[22]Hill, R. H.; Wrighton, M. S. *Organometallics* **1987**, *6*, 632.

[23]Asali, K. J.; Basson, S. S.; Tucker, J. S.; Hester, B. C.; Cortes, J. E.; Awad, H. H.; Dobson, G. R. *J. Am. Chem. Soc.* **1987**, *109*, 5386.

Table 3.1. Rate Constants for the Reaction of CpCo(CO) with Ligands in the Gas Phase

ligand	rate constant[a] (cm^3 $molecule^{-1}$ s^{-1})
CO (4 Torr Ar)	$(2.2 \pm 0.4) \times 10^{-11}$
CO (9 Torr Ar)	$(2.4 \pm 0.5) \times 10^{-11}$
CO (36 Torr Ar)	$(2.7 \pm 0.6) \times 10^{-11}$
CO (95 Torr Ar)	$(3.3 \pm 0.6) \times 10^{-11}$
C_2H_4	$(2.3 \pm 0.4) \times 10^{-11}$
N_2	$(1.0 \pm 0.2) \times 10^{-13}$
$CpCo(CO)_2$	$(2 \pm 1) \times 10^{-10}$

[a]Uncertainties are 95% confidence limits. To convert rate constants to units of mol l^{-1} s^{-1}, multiply values by 6.022×10^{20}.

Table 3.2. Comparison of Gas-Phase Work[a] and Relevant Matrix Studies

compound	ν (cm^{-1}) gas	matrix[b]
$CpCo(CO)_2$	2045, 1985	2032.1, 1971.9
$CpCo(CO)$	2010	
$Cp_2Co_2(CO)_3$	1980	
$CpCo(CO)(C_2H_4)$	2005	
$CpCo(CO)(N_2)$	2005	1981.9
$(\eta^3\text{-}Cp)Co(CO)_3$		2075, 2018

[a]For this work, spectral peaks can be known to within ± 4 cm^{-1}. [b]Reference 13.

Table 3.3. Collected CO Stretching Frequencies (in cm^{-1}) from Solution-Phase Studies[a]

compound	ν, this work	ν, literature
$CpCo(CO)_2$	2030, 1969	
$CpCo(CO)(C_6H_{12})$	1990	
$CpCo(CO)(C_6H6)$	1977	
"CpCo(CO)"		1955[b]
CpCo(CO)(THF)	1952	
$CpCo(CO)(CH_3CN)$	1940	
$CpCo(CO)(C_2H_4)$		1974[c]
$CpCo(CO)(P(n\text{-}C_4H_9)_3)$	1925	
$CpCo(CO)(P(i\text{-}Pr)_3)$		1925[d]
$Cp_2Co_2(CO)_3$	1965, 1812	1965, 1814[e]

[a]The solvent is cyclohexane unless indicated otherwise. [b]Reference 11a. Solvent: toluene. [c]Theopold, K. H.; Bergman, R. G. *J. Am. Chem. Soc.* **1983**, *105*, 464. Solvent: C_6D_6. [d]Hoffman, L.; Werner, H. *J. Organomet. Chem.* **1985**, *289*, 141. Solvent: pentane. [e]Reference 9b. Solvent: methylcyclohexane.

Table 3.4. Rate Constants for the Reaction of CpCo(CO)•••*c*-C_6H_{12} with Ligands (L)

L	k'_{obsd}, l mol^{-1} s^{-1}
$P(n\text{-}C_4H_9)_3$	$(2.9 \pm 0.4) \times 10^9$
CH_3CN	$(5.0 \pm 0.4) \times 10^9$
$CpCo(CO)_2$[a]	$(3.6 \pm 0.7) \times 10^9$
N_2[a]	*ca.* 4×10^8

[a]Determined indirectly (see text).

Table 3.5. Rate Constants for the Reaction of $CpCo(CO)\cdots C_6H_6$ with $P(n\text{-}C_4H_9)_3$ and Values of the Intercepts Taken from their Determination

[S], mol l^{-1}	[1], 10^{-4} mol l^{-1}	k'_{obsd}, 10^7 l mol^{-1} s^{-1}	intercept, 10^5 s^{-1}
0.0078	8.1	41 ± 17	8 ± 2
0.016	5.3	22 ± 4	2.7 ± 0.1
0.056	6.2	10 ± 4	1.2 ± 0.2
0.14	5.8	5.1 ± 1.1	0.55 ± 0.11
0.22	6.0	3.4 ± 0.2	0.45 ± 0.04
0.33	4.6	1.74 ± 0.05	0.31 ± 0.07
0.53	5.9	1.8 ± 0.5	0.26 ± 0.06

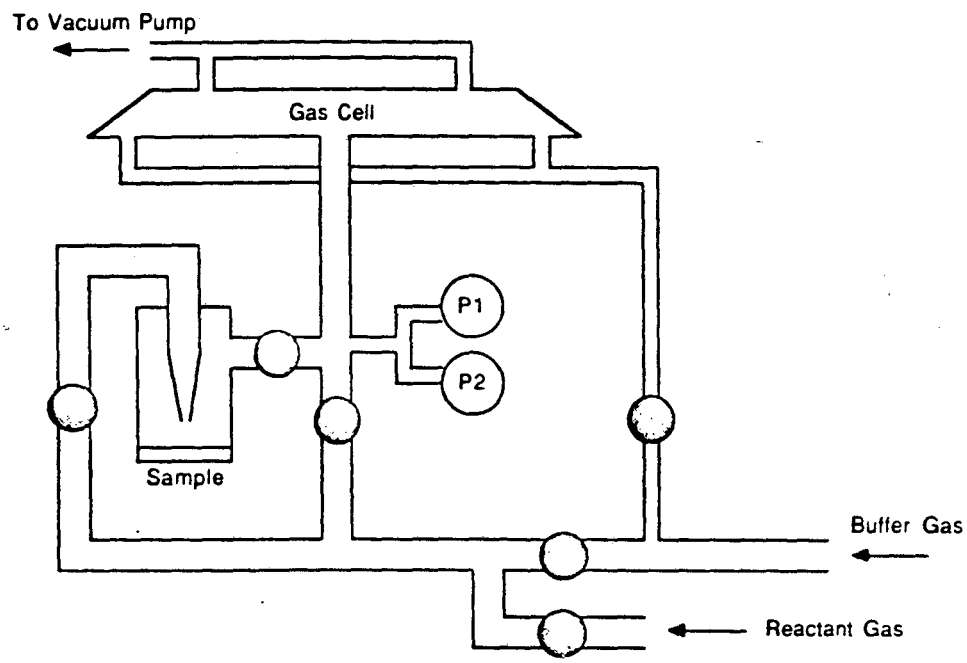

Figure 3-1. Schematic of the gas-flowing arrangement for the study of $CpCo(CO)_2$ in the gas phase. Shaded circles represent valves.

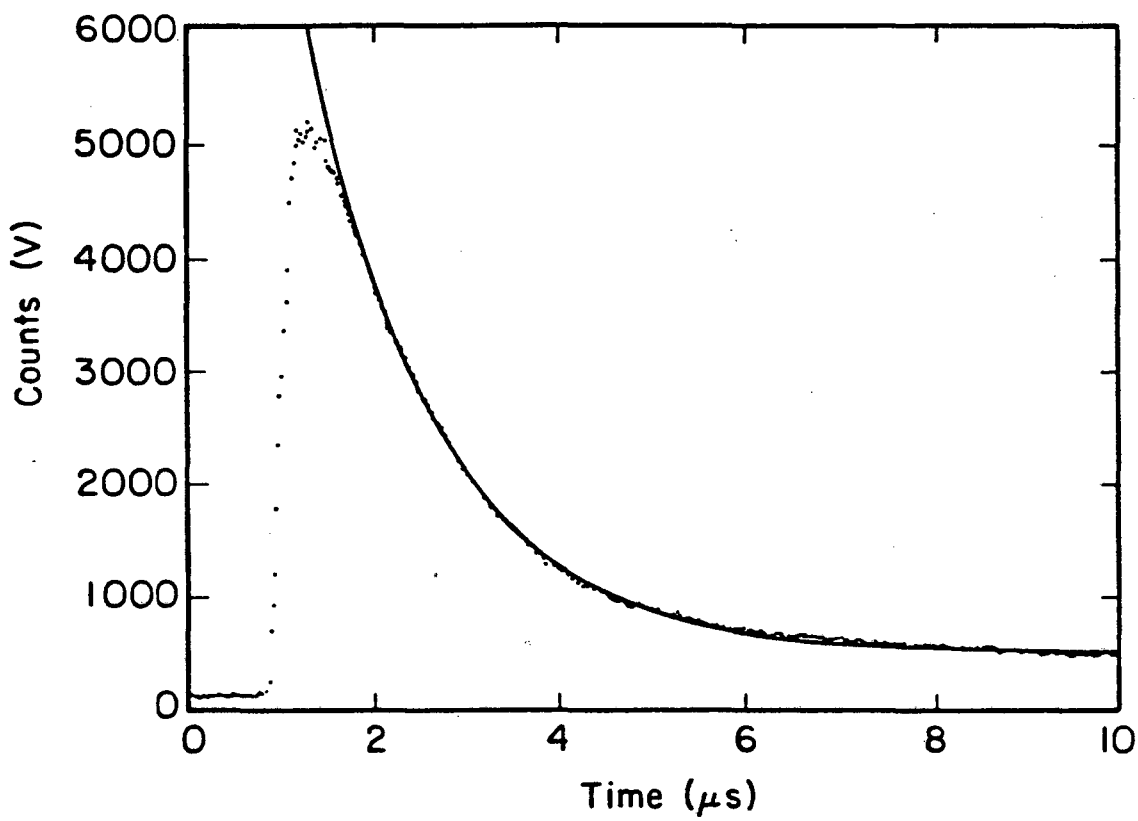

Figure 3-2. Transient absorption at 2011 cm^{-1} following the 308 nm photolysis of a mixture of *ca.* 100 mTorr $CpCo(CO)_2$ in 80 Torr Ar and an exponential fit of the decay section corresponding to $k_{obsd} = (7.2 \pm 0.1) \times 10^5\ s^{-1}$.

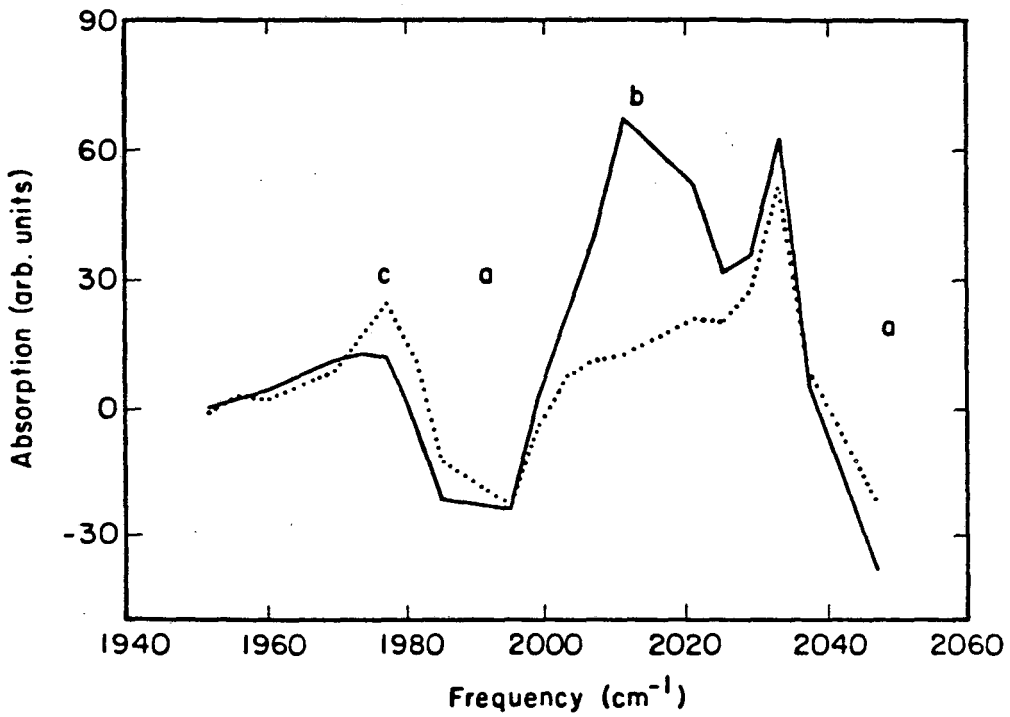

Figure 3-3. Transient absorption spectrum for the 308 nm photolysis of $CpCo(CO)_2$ in 45 Torr He with 1 Torr CO, 1 (solid line) and 3 μs (dotted) after photolysis: a, $CpCo(CO)_2$; b, CpCo(CO); c, $Cp_2Co_2(CO)_3$.

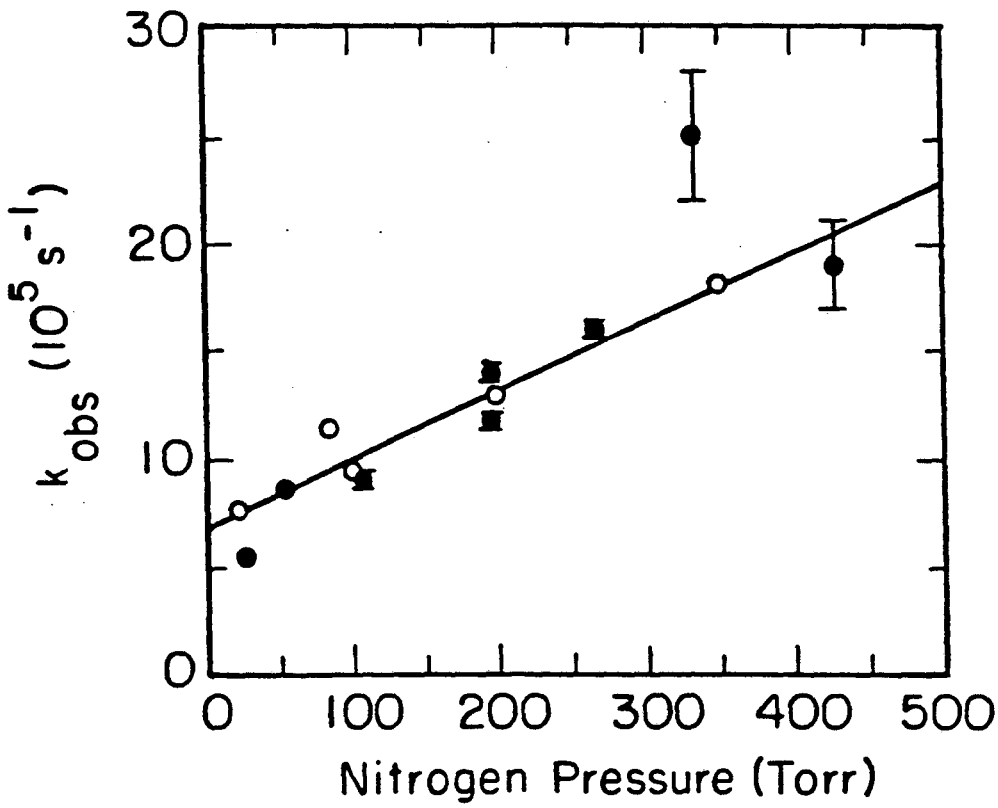

Figure 3-4. Dependence of the inverse of the decay time of the monocarbonyl transient upon the partial pressure of nitrogen, under both static (shaded circles) and flowing cell (open circles) conditions.

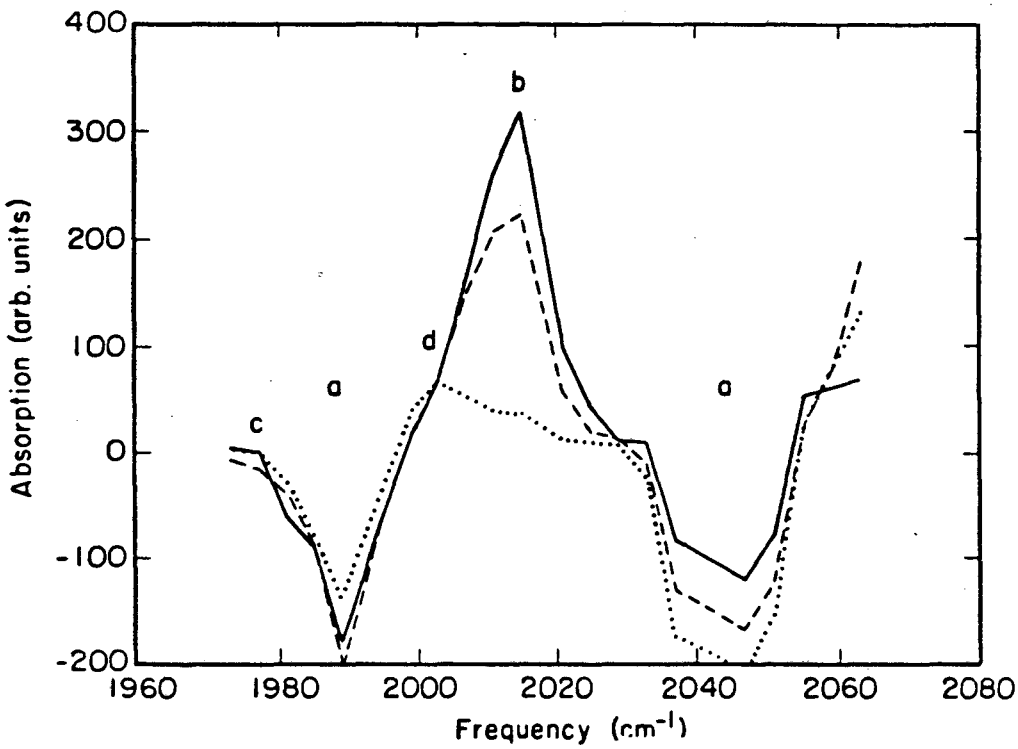

Figure 3-5. Transient spectra obtained 0.4 (solid line), 1.2 (dashed), and 7.6 μs (dotted) after 308 nm photolysis of $CpCo(CO)_2$ in ca. 90 Torr N_2: a, $CpCo(CO)_2$; b, $CpCo(CO)$; c, $Cp_2Co_2(CO)_3$; d, $CpCo(CO)(N_2)$.

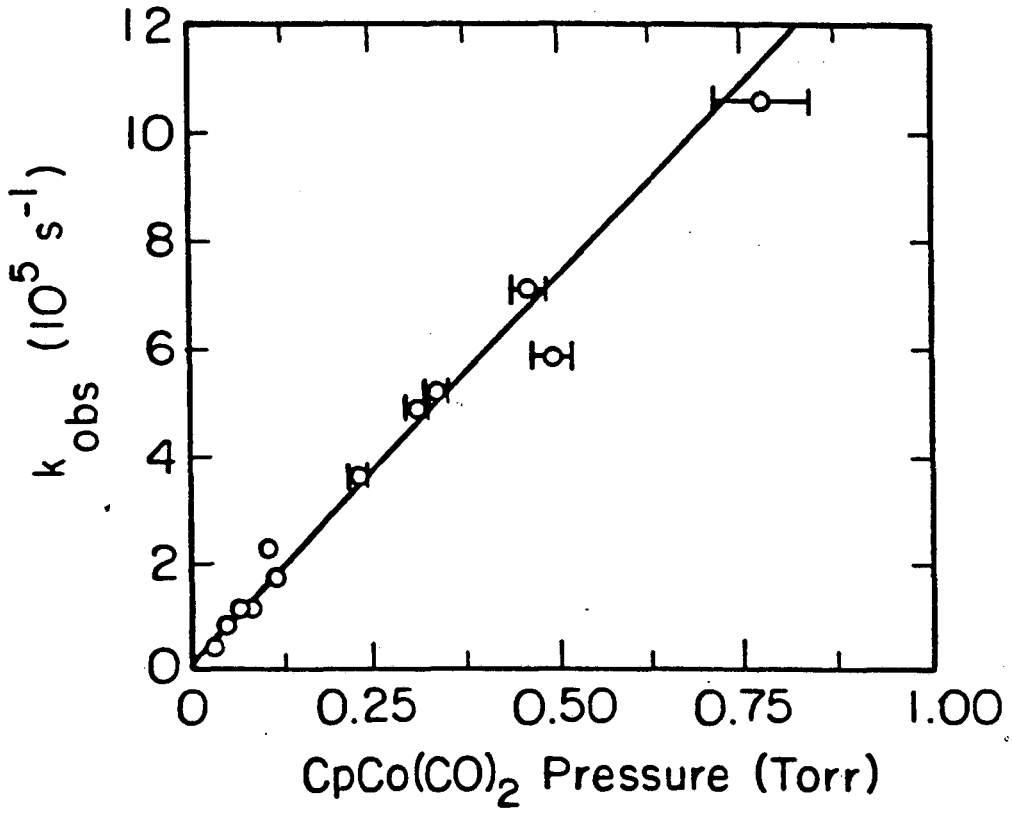

Figure 3-6. Dependence of the inverse of the decay time of the monocarbonyl absorption upon the partial pressure of $CpCo(CO)_2$.

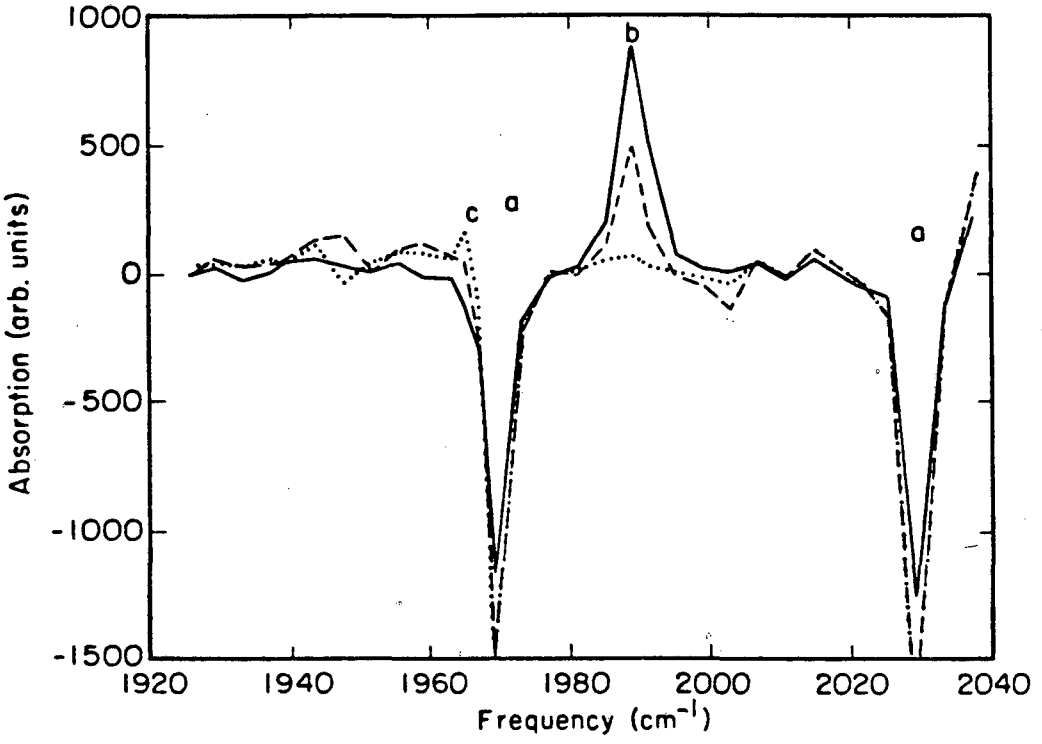

Figure 3-7. Transient spectra obtained 0.25 (solid line), 0.75 (dashed), and 1.5 μs (dotted) after the 308 nm photolysis of a 2.9×10^{-4} mol l^{-1} solution of $CpCo(CO)_2$ in cyclohexane: a, $CpCo(CO)_2$; b, $CpCo(CO)(c\text{-}C_6H_{12})$; c, $Cp_2Co_2(CO)_3$.

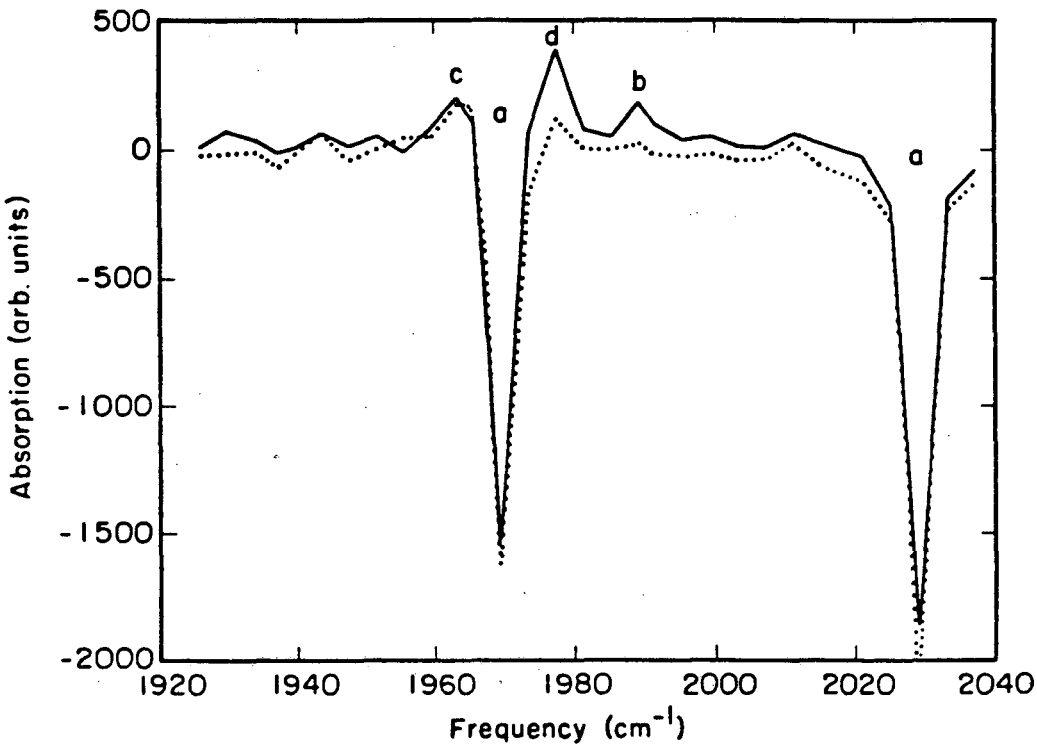

Figure 3-8. Transient spectra obtained 1 (solid line) and 4 μs (dotted) after the 308 nm photolysis of a 4.6×10^{-4} mol l^{-1} solution of $CpCo(CO)_2$ in cyclohexane also containing benzene at 0.022 mol l^{-1} concentration: a, $CpCo(CO)(c\text{-}C_6H_{12})$; c, $Cp_2Co_2(CO)_3$; d, $CpCo(CO)(C_6H_6)$.

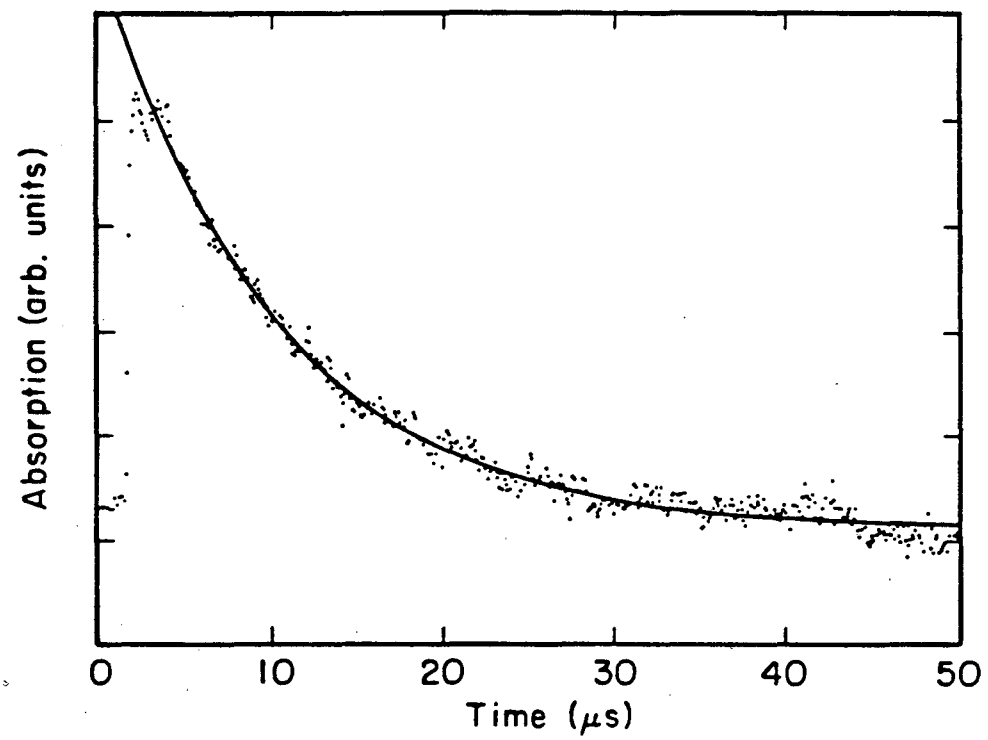

Figure 3-9. Transient absorption due to benzene solvate monitored at 1977 cm^{-1}. Concentrations of $CpCo(CO)_2$, C_6H_6, and $P(n\text{-}Bu)_3$ are 5.8×10^{-4}, 0.14, and 1.0×10^{-3} mol l^{-1}, respectively. The exponential fit to the decay is overlaid; lifetime of transient is $(9.8 \pm 0.2) \times 10^4$ s^{-1}.

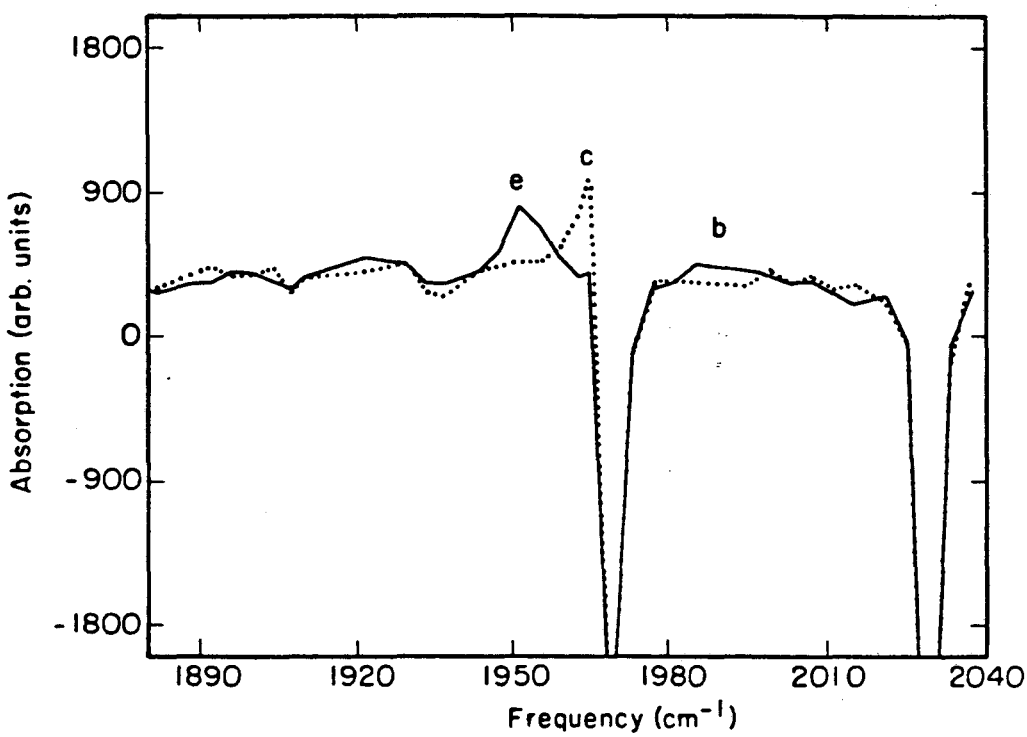

Figure 3-10. Transient spectra obtained 0.5 (solid line) and 2 μs (dotted) after the 308 nm photolysis of a 6.3×10^{-4} mol l^{-1} solution of $CpCo(CO)_2$ in cyclohexane solution also containing THF at 0.012 mol l^{-1} concentration: c, $Cp_2Co_2(CO)_3$; e, CpCo(CO)(THF). b marks the frequency at which absorption due to the cyclohexane solvate was seen previously.

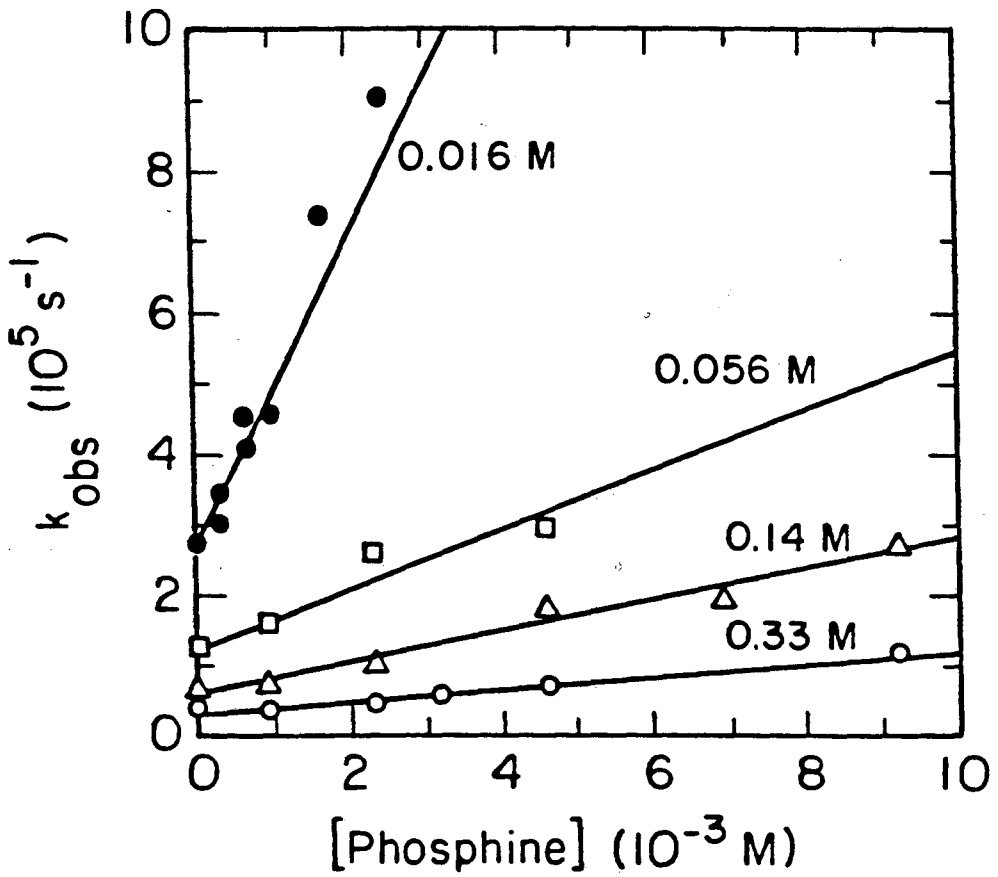

Figure 3-11. Dependence of the decay rate of the benzene solvate absorption upon the concentration of phosphine at four different benzene concentrations. The slopes are the effective rate constants for the reaction of the benzene solvate with phosphine.

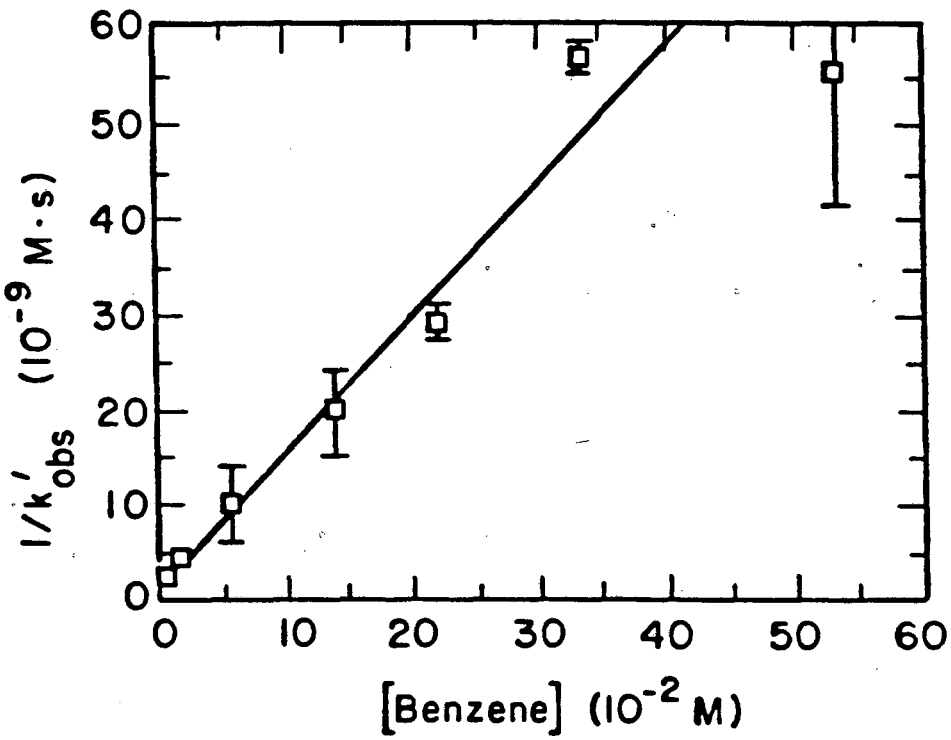

Figure 3-12. Dependence of the inverse of the effective rate constant for decay of the benzene solvate in the presence of phosphine upon benzene concentration.

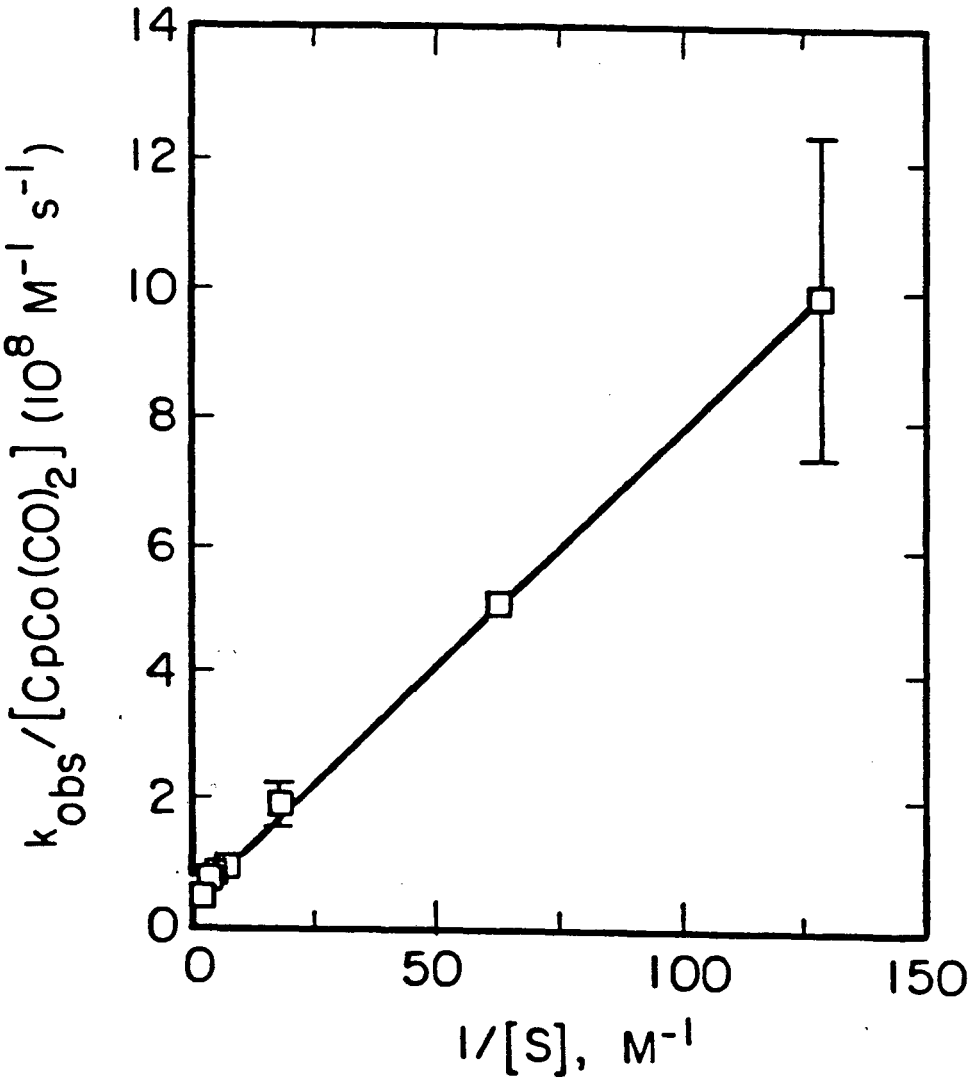

Figure 3-13. Dependence of $k_{obsd}/[CpCo(CO)_2]$ upon $1/[C_6H_6]$.

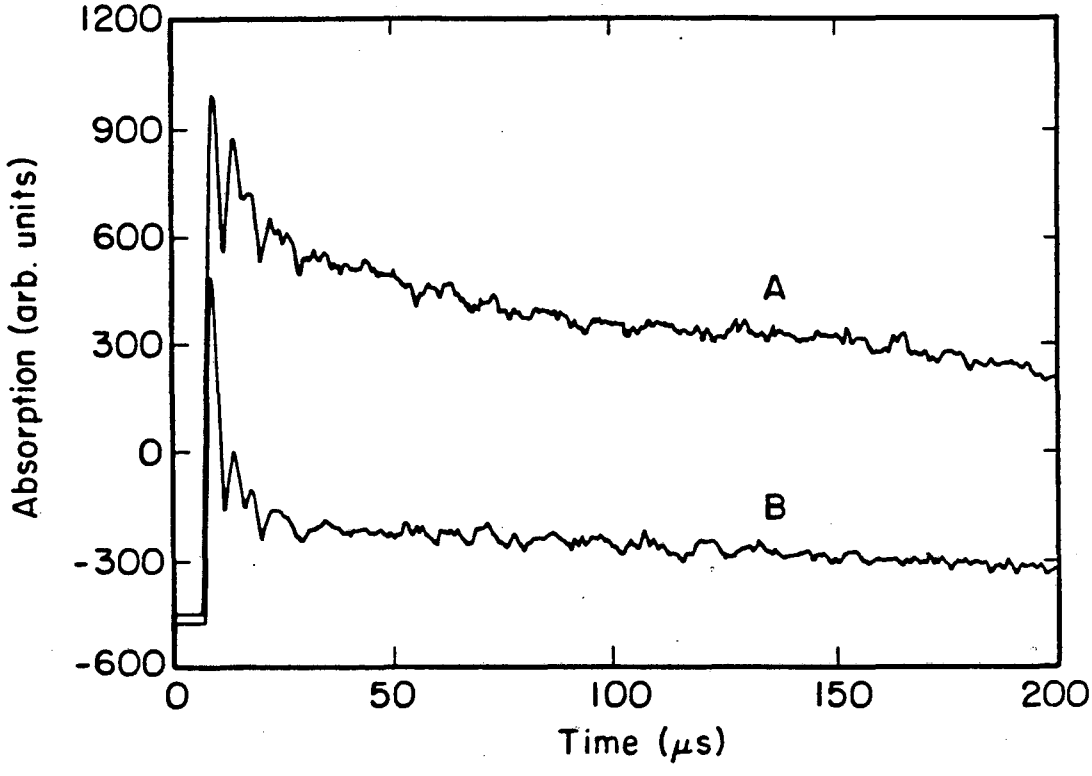

Figure 3-14. Transient absorption traces taken at 1977 cm^{-1} from solutions saturated with nitrogen. The initial oscillations in the transient absorptions are due to acoustic waves. A, that from a solution containing no phosphine; B, that from a solution containing 4.0×10^{-3} mol l^{-1} phosphine. The concentrations of $CpCo(CO)_2$ and benzene were 5.4×10^{-4} mol l^{-1} and 0.11 mol l^{-1}, respectively; the power of the CO laser for trace A versus that for trace B: 1.0:1.3.

Chapter 4. C-H Activation by Gas-Phase (η^5-C_5H_5)Rh(CO).

4.1. Introduction. Carbon-hydrogen insertion reactions, performed on otherwise inert hydrocarbons, show some promise in the effort to make alkanes a more useful feedstock in industrial chemistry. Inspired by recent advances in the field of the oxidative addition of alkanes to late transition metal centers,[1,2] we have investigated the photochemical reactivity of $CpRh(CO)_2$ and $Cp^*Rh(CO)_2$ ($Cp \equiv \eta^5$-C_5H_5; $Cp^* \equiv \eta^5$-C_5Me_5) toward alkanes using time-resolved infrared spectroscopy. These molecules are members of a growing family of soluble organometallic compounds which react stoichiometrically with hydrocarbon C-H bonds, with loss of one or more ligands (1).

$$L_nM\text{-}L' + R\text{-}H \xrightarrow{\Delta \text{ or } h\nu} L_nM(R)(H) + L' \qquad (1)$$

$$(R\text{-}H \equiv \text{alkane};\ L' \equiv CO, H_2)$$

The reactivity of C-H activation precursors toward common solvents has prevented direct observation of the intermediates responsible for the C-H activation process.

Two related questions present themselves: (a) what controls the reactivity of the metal center toward C-H bonds? (b) what is the mechanism of the insertion reaction? We have undertaken research to try to gain insight into these fundamental questions from two directions, both of which employ transient IR flash-kinetic spectroscopy. In chapter 5,[3] we describe the photochemical reactions of $Cp^*Rh(CO)_2$ toward several alkanes in liquid krypton. While the use of this solvent eliminates the problem of irreversible solvent activation, the kinetics of the reactions of the initially formed intermediates in liquified inert gases are quite complicated, due in part to the reversible formation of solvates. In this chapter we detail the results from the second avenue of research, in which we observe photo-induced C-H activation in the gas phase. Unfortunately, the involatility of

$Cp^*Rh(CO)_2$, the molecule used in our liquid krypton work, prevented a gas-phase study of this material. Instead, the more volatile, closely related complex $CpRh(CO)_2$ was chosen as the C-H activation precursor for the gas-phase experiments.

One goal of present C-H activation research is the development of a selective homogeneous organometallic catalyst which can attach organic functional groups to saturated hydrocarbons. The design of such a system must depend on an understanding of the patterns of reactivity of reactive metal centers toward C-H bonds of differing types. A substantial body of work has recently appeared on the transformations of alkanes by gas-phase inorganic ions containing transition metals[4,2d]. Application of this knowledge to more conventional chemistry is hampered by the lack of ligands around the metal ions, and also by the complexity of the net reactions, in which rearrangement of the carbon skeletons and extrusion of small daughter molecules often befall the initial, unobserved, C-H activation products. Hence the information gained on the propensities of hydrocarbons to undergo C-H activation is generally qualitative. Competition studies using soluble organometallic species[1c,e,5] are more relevant, but since the reaction products may often interconvert thermally, there is some uncertainty as to whether the branching ratios are kinetically or thermodynamically determined.

In the wake of pioneering efforts over the past several years,[6] the technique of flash photolysis with time-resolved infrared detection has been quite profitably applied to organometallic systems, particularly to homoleptic d^6-d^8 metal carbonyls studied in the vapor phase. In general, the coordinatively unsaturated metal carbonyl fragments formed upon photolysis react readily with two-electron (donor) ligands. Reactions with molecules such as hydrogen, alkanes, and silanes, however, have received relatively less attention. A recent study[7] by Ishikawa *et al.* revealed that $W(CO)_5$ binds to ethane strongly (ΔH^o = 9.7 ± 3 kcal mol^{-1}) in the gas phase. This result, when taken with information gained from photo-acoustic calorimetric studies[8] on the solvent-metal interaction, suggests that there exists a continuum of intermolecular bonding possibilities between a hydrocarbon moiety

and metal center which resembles the more familiar range of intramolecular bonding, from "agostic" interactions[9] to orthometallation. In several solution-phase experiments, complexes in which C-H bonds are weakly bound to metal centers are believed to function as intermediates in the activation of such bonds.[1c,e] Complexes of substituted silanes with the $16e^-$ species $CpMn(CO)_2$ are believed to exist in the gray area between σ-complexes and oxidative addition adducts.[10]

Both $CpRh(CO)_2$ and $Cp^*Rh(CO)_2$ have been subjects of studies of their photochemical reactivity toward alkanes.[11] The matrix-isolation work of Rest and co-workers[7a,b] showed these species to be photolabile at 12K, and lead, in the case of methane matrices, to methyl hydride products. The fact that such C-H activation is observed at all at cryogenic temperatures is indicative of a minuscule energy barrier for this process, although multiphoton processes may play a role in this chemistry.[12] These studies also yielded some interesting insights into the possible reactive intermediates in the C-H activation reaction, although one must be careful not to assume that new species created by continuous photolysis in the presence of methane are indeed steps on the reaction path to the methyl hydride. Intriguingly, these researchers assigned one new IR band in the CO stretching region to a "naked" unsaturated species, $Cp^{(*)}M(CO)$, and another to a methane complex, "$Cp^{(*)}M(CO)\cdots CH_4$", in which oxidative addition to the metal center has not occurred.

In recent years, Perutz *et al.* have contributed a series of illuminating papers[13] on the photochemistry of $CpRhL_2$ (L = CO, C_2H_4). These workers have demonstrated the high degree of reactivity of the $CpRh(C_2H_4)$ species toward donor ligands and silanes. Recently[14], this group has studied the photochemistry of $Cp^{(*)}Rh(CO)_2$ and of the dinuclear $Cp^{(*)}{}_2Rh_2(CO)_3$ toward hydrocarbons in organic solutions and in matrices. While unable to detect unsaturated intermediates, Perutz et al. were able to observe the decomposition of promptly-formed alkane activation products to various dimers and, in the presence of CO, to starting material.

In the following pages, we present evidence that $CpRh(CO)_2$ reacts with alkanes, upon photolysis in the gas phase, through an initially formed, coordinatively-unsaturated monocarbonyl species. In these experiments, we observe C-H activation to occur at rates close to gas-kinetic. There does not appear to be any strong dependence of the rate constant for this reaction upon alkane character. Rather, the reactive intermediate appears to be highly unselective, behaving in a manner similar to a free radical such as the fluorine atom. The magnitudes of the rates for C-H and H-H activation and the effect of isotopic substitution thereupon are somewhat surprising, and shed light on the mechanism of C-H activation in the gas phase.

4.2. Experimental. The flash-kinetic spectrometer and flowing-gas cell used in this experiment have been described in Chapters 2 and 3. Figure 4-1 illustrates the transient digitizer traces for the decay of CpRh(CO) at 1985 cm^{-1} and the concomitant rise of absorption at 2037 cm^{-1} due to Cp(CO)Rh(neopentyl)(H).

The sample, $CpRh(CO)_2$, is continuously evaporated by a stream of argon, mixed with the reactant gas, and flowed into the IR cell through a central port. Argon is flowed at a slow rate over the windows to prevent the build-up of photolysis residues on the inner surfaces. For this experiment, two sets of gas flowing conditions were used. This was dictated by a change in the method of measuring ligand concentrations. Spectra shown in Figures 4 and 7 were obtained using the previously-described system of pressure measurement in which two capacitance manometers (Validyne) are used (Chapter 3). For all other experiments, including all of those from which the rate constants were determined, we employed a system somewhat more sensitive to small reactant gas pressures. We use one 100 Torr-range capacitance manometer (MKS Baratron) to measure the total pressure and derive the reactant gas pressure from the readings of two mass-flow meters (Hastings), which monitor the flow rates of buffer and reactant gases, respectively. In this case, we ignore the contribution of buffer-gas flow through the window ports to the total flow of

buffer gas. The reactant-gas mass flow-meter was calibrated for all reactant gases individually except for CD_4 and D_2. For these gases, flow coefficients were derived from the adjustment of the empirically determined coefficients for the undeuterated molecules for differences in molar heat capacity.[15] In an attempt to demonstrate the validity of rate constants obtained using the new cell configuration, we repeated a previously studied reaction, $CpCo(CO) + CO = CpCo(CO)_2$. From our new system we find a rate constant for this reaction of $(6 \pm 2) \times 10^{-11}$ $cm^3 \cdot molec^{-1}s^{-1}$ which is somewhat larger than our previously determined value of $(3.3 \pm 0.6) \times 10^{-11}$ $cm^3 \cdot molec^{-1}s^{-1}$. We have greater confidence in the number more recently determined using our modified apparatus. We find there to be less room for systematic errors in our present system, since more variables (flow rates) are monitored. We have also found the flow meters and Baratron pressure sensor to be less susceptible to drifting baseline and slope.

The gaseous cyclohexane was flowed from a 9 l glass bulb with a stirring system in which 38.4 Torr cyclohexane (Fisher, >99%, degassed by several freeze-pump-thaw cycles) was mixed with 725 Torr Ar (Airco, 99.998%) and given 1 day to equilibrate. CO (99.5%), H_2 (99.99%), CH_4 (99.97%), and C_2H_6 (99.99%) were supplied by Matheson. D_2 (99.7%) was obtained from Liquid Carbonic, CD_4 (99 atom % D) from Cambridge Isotopes, and C_5H_{12} (99% by gas chromatography) from Chemical Samples Co.

$CpRh(CO)_2$ was synthesized according to a literature method[16] from NaCp and $[(CO)_2Rh(\mu\text{-}Cl)]_2$. The latter was prepared directly from $RhCl_3 \cdot 3H_2O$ and CO after the technique of Wilkinson.[17] The volatile liquid (partial pressure at 21°C ≈ 0.4 Torr) was purified by vacuum distillation, as well as by *in situ* Ar-assisted evaporation.

Inherent limitations of our experiment presented difficulties in the interpretation of some of the data presented here. We were restricted both by our desire to conserve the starting material and by the high-flow rate limit of our buffer-gas mass-flow meter to run at relatively slow flow rates (≤ 0.5 scc s^{-1}). Given a cell volume of ca. 770 cm^3 and a laser repetition rate of 4 Hz, this means that at the total pressures used (12-30 Torr), each gas

sample was exposed to ≈200 excimer laser flashes. Rough calculations indicate that the steady-state pressure of photo-generated CO should not be very significant (< 50 mTorr). However, under these conditions, a broad negative transient absorption feature, denoted A in Figures 4-2 and 4-9, can be seen from 1960 to 1990 cm^{-1}, perhaps due to the photolysis of a product of secondary reactions. Its identity has not been determined. This absorption overlaps with that assigned to the monocarbonyl species CpRh(CO) at 1985 cm^{-1}, imparting a negative baseline to its exponential decay traces, but apparently does not interfere with the kinetic analysis of the reaction of **2**, since product appearance rates generally agree with the corresponding decay rates to within experimental error.

4.3. Results and Discussion.

4.3.1. Photolysis of $CpRh(CO)_2$ in the Absence of Added Ligand.

Photolysis of $CpRh(CO)_2$ (compound **1** in Scheme I) in Ar results in the transient absorption spectra seen in Figure 4-2. Initially, one sees bleaching of infrared absorptions at 2003 and 2060 cm^{-1} due to loss of **1**, as well as the appearance of a new band peaking at 1985 cm^{-1}, labelled **2** in Figure 4-2. The wide negative absorption bands seen in this spectrum as well as others due to the destruction of **1** appear similar to the absorptions observed in the FTIR gas-phase spectrum of $CpRh(CO)_2$ (Figure 4-3). No other strong product bands are observed immediately after photolysis, although weaker bands at 1963 and 2035 cm^{-1} are noted. Based on previous work in matrices[11b] and in liquid Kr (see following chapter), we confidently ascribe band **2** to the monocarbonyl CpRh(CO) (compound **2** in Scheme I). The amplitude of the band due to **2** decays, while a shoulder grows in at *ca.* 1990 cm^{-1} which, along with a band at *ca.* 1858 cm^{-1}, is due to the production of the dinuclear adduct **5**. The reaction of **2** with **1** to form **5** causes an additional depletion of the starting material absorbances.

This process operates even in the presence of other introduced reactive gases such as CO. It manifests itself in a non-zero intercept in plots of the decay rate of **2** versus

reactant gas partial pressure (*vide infra*), and is a common characteristic of organometallic gas-phase chemistry.[18] For the reaction of **2** with **1**, however, we could not monitor the pressure of **1** as effectively as with $CpCo(CO)_2$ (due to a much smaller absorption cross-section at 308 nm). If we assume the pressure of **1** in our experiments to be its vapor pressure (roughly 400 mTorr at 20°), we obtain a value of 9×10^{-11} cm^3 $molecule^{-1}$ s^{-1} as a lower limit for the rate constant for this reaction. Although the amount of **1** in the gas mixture is not known, it is kept constant during the course of each series of rate determinations by keeping the flow rates and total pressure constant. Our ability to do this is supported by the fact that, under identical gas-flow conditions, the dimerization rate is reproducible, and always lies within the range $(4\text{-}8) \times 10^5$ s^{-1}.

4.3.2. Reaction of 2 with CO. The presence of the donor ligand molecule CO accelerates the decay of the monocarbonyl and predictably leads to the reformation of **1**. The spectral changes which accompany this transformation are seen in Figure 4-4. The rate constant for this reaction lies within an order of magnitude of the hard-sphere collision rate (derived from viscosity data[19]), and is similar to the rate constants derived for the analogous reactions of CpCo(CO), as well as for other unsaturated metal carbonyls (see Table 4.1). While a comparison of these rate constants reveals CpRh(CO) seemingly to be the most reactive, all the unsaturated species, with the important exception of $Fe(CO)_4$, undergo reaction with little or no activation barrier.

As has been noted[18b], it is necessary to ensure conditions in which vibrationally hot products of gas-phase addition reactions are quenched by third-body collisions in order to understand the rate behavior of these reactions. Studies[20] on the pressure dependences of the reaction of **2** with CO and CH_4 lead us to conclude, as we did for the reactions of CpCo(CO), that a buffer-gas pressure in excess of 10 Torr effectively cools and traps the products of these reactions. The rate constants for the reactions of **2** are taken from experiments with total pressures between 12 and 30 Torr.

4.3.3. Reaction of 2 with X_2 (X ≡ H, D). The monocarbonyl **2** reacts with H_2 to form an adduct with an absorption centered about 2055 cm^{-1}, as shown in Figure 4-5. By analogy with the carbonyl stretching frequencies assigned to various Rh(III) carbonyls[21], this band is assigned to the oxidative addition product **3**. The other viable candidate for the structure of the hydrogen addition product is an η^2- or σ-complex. This structure, in which there is little breaking of the H-H bond, does not agree with the following considerations. In known molecular hydrogen species, carbonyl absorptions do not shift to markedly higher frequency relative to corresponding precursors.[22] This reaction proceeds at nearly the gas-kinetic rate (Table 4.3), meaning that, given the H-H bond dissociation energy (BDE) of 104 kcal mol^{-1}, the Rh-H BDE must be at least 57 kcal mol^{-1}, when an appropriate reaction entropy for such a bimolecular reaction is chosen.[23] Such a value for the Rh-H bond seems reasonable, given the BDE's for comparable metal hydrides.[24]

A transient absorption spectrum for the reaction of **2** with deuterium is shown in Figure 4-6. Reaction with D_2 gives rise to the same new absorption feature as in reaction with H_2 (see Figure 4-5). This is to be expected, since the spectra are not sensitive to the small changes in carbonyl vibrations caused by isotopic substitution at other ligands.[25] It is noteworthy that **2** reacts with D_2 with the same rate constant as it does with H_2, well within our estimated error (Table 4.2, Figure 4-7). When the fact that the mass of D_2 is twice that of H_2 is taken into account, one realizes that the probability per collision of **2** with D_2 is greater than that for reaction with H_2, as seen in Table 4.3. While the discrepancy is not large (and is hardly statistically meaningful), it requires some explanation, since one would expect a "normal" kinetic isotope effect ($k_H/k_D > 1$) for a reaction in which one full X-X vibration is lost.[26]

The intermediacy of an η^2-X_2 or dihydrogen complex, in which H_2 is coordinated to the metal center but the H-H bond is not yet broken, suggests itself as a potential explanation for the slight inverse isotope effect. Many stable dihydrogen adducts are now

known.[27] If an η^2-X_2 complex is a metastable intermediate on the reaction path from reactants to **3**, it is possible that the highest energy transition state may involve the molecular coordination of X_2 to the metal center (eq. 3; R-H = H_2), rather than extensive X-X bond rupture, as prescribed by a one-step addition mechanism (eq. 2). The fact that such a complex is not observed spectroscopically implies that, were it to exist, its lifetime at room temperature would be <1 μs.

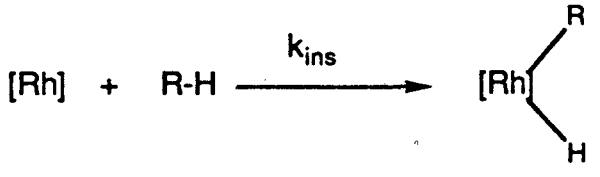

(2)

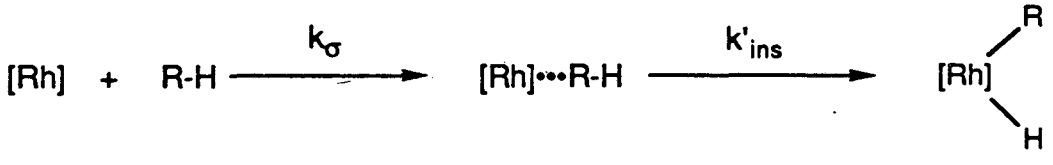

(3)

[Rh] ≡ CpRh(CO); R-H ≡ H_2, alkane

To explain the isotope effect observed within the context of this mechanism, one must account for the apparent lower free energy barrier for reaction with D_2 with changes in the vibrational frequency of X_2 and in the frequencies of the three new modes derived from the rotations of free X_2. Fuller investigation into the value of this hypothesis lies beyond the scope of our study, given the paucity of spectroscopic data in our system.

4.3.4. Reaction of 2 with Alkanes. In the presence of alkanes, a new transient absorption in the carbonyl spectrum is observed whose frequency (2033-2050 cm^{-1}) is consistent with an assignment to a C-H activation product **4** (see Table 4.2). Figures 4-8 and 4-9 show the transient absorption spectra from the reactions of **2** with ethane and cyclohexane, respectively. Given our limited (4 cm^{-1}) resolution, no specific dependence

of the peak frequency of the gas-phase carbonyl absorption upon either the size or the structure of the alkyl substituent of **4** was noted.

The alkyl hydride products appear to be stable over the timescale convenient for measurement in our system ($t_{1/2} > 1$ ms). This result agrees with the observations of Perutz and co-workers[14], who observed the rate of decay of CpRh(CO)(Cy)(H) in CO-free cyclohexane solution to be ca. 50 s^{-1}.[28]

Let us assume that the only route available for the decomposition of the alkyl hydride product molecule **4** involves reductive elimination of alkane, followed by the irreversible trapping of the newly-formed molecule of **2** by **1**, as shown in equations 4 and 5.

$$\mathrm{Cp(CO)Rh(R)(H)} \underset{k_i}{\overset{k_r}{\rightleftharpoons}} \mathrm{CpRh(CO)} + \mathrm{R\text{-}H} \qquad (4)$$

$$\mathrm{CpRh(CO)} + \mathrm{CpRh(CO)_2} \xrightarrow{k_d} \mathrm{Cp_2Rh_2(CO)_3} \qquad (5)$$

If a steady-state concentration of **2** is assumed, and the concentrations of **1** and the alkane are considered to be much greater than that of **4**, one finds the rate of decay of **4** to be described by equation 6.

$$k_{obs} = \frac{k_r k_d[\mathbf{1}]}{k_i[\mathrm{R\text{-}H}] + k_d[\mathbf{1}]} \qquad (6)$$

Since the quantity $k_d[\mathbf{1}]$ was estimated earlier, and k_i is known, we then obtain an upper limit for the unimolecular reductive elimination of alkane to be roughly 10^5 s^{-1}. Setting the preexponential factor to be equal to 10^{16}, that found for the elimination of cyclohexane from $Cp^*(P(CH_3))Ir(H)(c\text{-}C_6H_{11})$[1c], we obtain 15 kcal mol^{-1} as the estimated lower bound for the activation energy associated with reductive elimination of alkane from **4**.

Intermediate **2** reacts with alkanes at rates close to the hard-sphere collision frequency (see Table 4.3). This implies that the overall barrier to oxidative addition is negligible. The kinetic isotope effect for the reaction of **2** with CX_4 ($X \equiv H, D$) is small (see Figure 4-10), which also is consistent with a low entrance barrier for reaction. Our studies of C-H activation by Cp*Rh(CO) in liquid krypton yield a barrier for C-H activation of about 4.5 kcal mol^{-1}. Note, however, that this activation energy barrier represents the energy required for the transformation from an alkane-solvated intermediate to the alkyl hydride in liquid krypton, rather than the barrier for reaction of an unsolvated unsaturated species and the alkyl hydride (see Scheme II).

It is difficult to interpret small differences in rate constants which are close to gas-kinetic in magnitude.[29] An examination of the efficiencies for C-H activation *versus* several parameters relating to the nature of the C-H bonds of the hydrocarbons studied (Table 4.4) reveals no persuasive correlation. While it is true that the rate constants for C-H activation increase with decreasing C-H bond strength, they also increase with decreasing ionization potential and increasing polarizability. It is therefore difficult to determine whether the rate of oxidative addition depends more upon the propensity of the alkane to donate electron density to the metal center or upon the lability of the bond to be broken. A very similar pattern of reactivity has been shown[30] to hold for hydrogen atom abstraction by atomic fluorine, as seen in Table 4.4.

We must, however, consider the possibility of a molecular alkane adduct, similar to the η^2-X_2 complex proposed for H_2 activation in Scheme II, functioning as the initial intermediate in this system. As one follows the reaction path, one passes from the separated reactants over a near-zero energy barrier to a pair of potential wells. The first well represents a σ-type interaction similar to the η^2-H_2 species referred to above, while the second is the well for the alkyl hydride product. The enthalpic barrier for the process of going from the first well to the second is estimated at 4.5 kcal mol^{-1} based on our thermodynamic work on the Cp*Rh(CO) system in liquid krypton (see chapter 5) Based

Scheme II

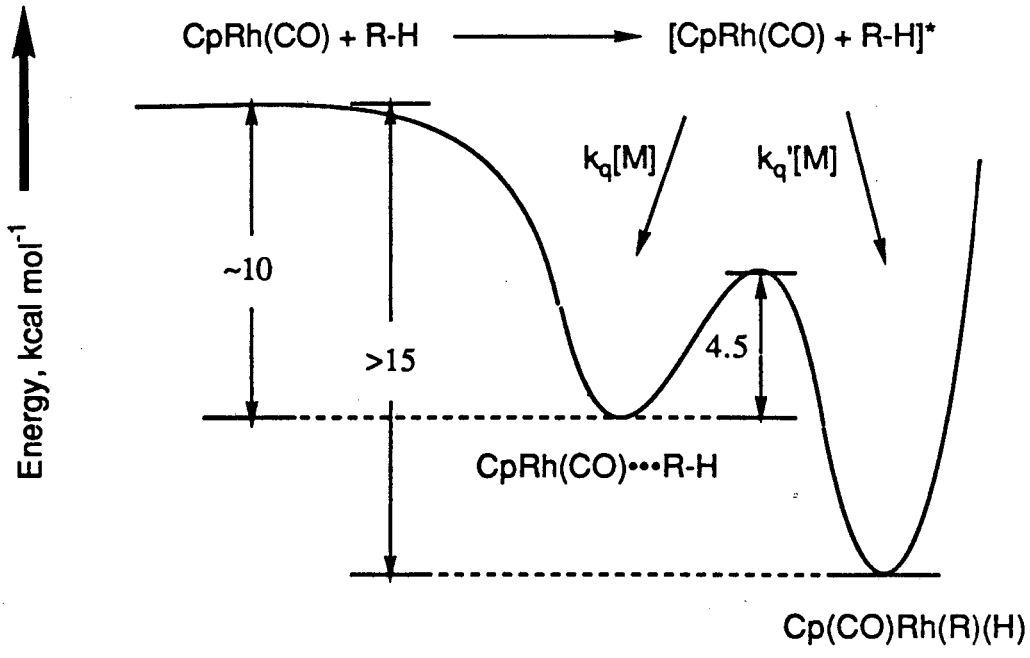

$$\text{CpRh(CO)}\cdots\text{R-H} \xrightarrow{k_i} \text{Cp(CO)Rh(R)(H)}$$

on the work of Rayner and co-workers,[7] we postulate that the σ-complex is approximately 10 kcal mol^{-1} lower in energy than the naked monocarbonyl **2**. Our crude calculation of the stability of Cp(CO)Rh(R)(H) (*vide supra*) yields an estimate of 5 kcal mol^{-1} as a lower limit for the relative stability of the alkyl hydride *versus* the σ-complex. Thus in the gas phase, the transition state for conversion of Cp(CO)Rh(R-H) to Cp(CO)Rh(R)(H) lies at lower energy than the separated reactants CpRh(CO) and R-H.

As radiative processes such as infrared fluorescence may be ignored for timescales shorter than ca. 100 μs, collisions with third-body molecules are required to drop the [CpRh(CO) • R-H] system into either potential well. Since the barrier between the two adduct wells lies lower in energy than the reactants, the rate constant for the conversion of the σ-complex to the alkyl hydride, k_i, will be greater than the rate of σ-complex dissociation. Consistent with this, we can use our data from the liquid Kr system to estimate k_i to be $\approx 3 \times 10^7$ s^{-1} at 22°C[31] This rate constant exceeds the frequencies of collision between **2** and R-H under the conditions of this experiment. For example, the collision frequency of CpRh(CO) with CH_4 per molecule CpRh(CO), in the presence of 2 Torr CH_4, is roughly 2.9×10^7 s^{-1}. (The pressure of alkane was rarely over 1 Torr, however.) Hence, even if the collisional trapping of the σ-complex were of unity efficiency and direct trapping of the oxidative addition product could be ignored, the concentration of the σ-complex would not build up. The sum of the rates for the quenching reactions, k_q[M][CpRh(CO)][R-H] + k_q'[M][CpRh(CO)][R-H], is then equal to the rate for appearance of the product **4**.

Larger, more polarizable hydrocarbons should be more strongly attracted to the unsaturated metal center than smaller molecules, such as methane. If the metal-alkane interaction is of Van der Waals type, one would expect the reaction efficiency to correlate either with the basicity of the alkane (which can be estimated using its ionization energy) or with the polarizibility of its electron cloud. As mentioned above, both the ionization energies and polarizibilities seem to show a correlation with reaction efficiency.

On the other hand, reaction with methane does exhibit a moderate isotope effect ($k_H/k_D \approx 1.3 \pm 0.3$, Figure 4-10), implying that there may be some degree of C-H bond breaking in the transition state, though the size of the isotope effect for the other alkanes has not yet been investigated. The small kinetic isotope effect for methane activation may be related to its small cross-section for reaction. Reaction of Cp*Rh(CO)(Kr) with CH_4 was not observed in liquid Kr, perhaps indicating a larger barrier for C-H activation relative to the larger alkanes cyclohexane and neopentane. If the barrier for C-H bond cleavage is significantly larger for methane than for other alkanes, the transition state for this reaction may lie above the ground-state energy of the reactant species, CpRh(CO) and CH_4.

Perhaps the strongest argument for an intermediate association complex lies in the sheer magnitude of the rate constants for the C-H activation reactions, which are all well within an order of magnitude of the collision frequency. It may be that the rate constants reflect an attractive interaction between the reactants which exists for many different orientations of approach. Also, the size of the rate constants may indicate the existence of a broad attractive potential extending into space in the region of the open coordination site in CpRh(CO), which increases the reaction cross-section relative to the hard-sphere collisional cross-section. In applying this second idea to the mechanism of Scheme II, one envisages this as meaning that a wide range of [CpRh(CO) + R-H]* configurations may be effectively trapped by collision.

4.3.5. Other Mechanistic Considerations. Recently, Lees *et al.* have reported[32] on studies of the photochemistry of $Cp^*Ir(CO)_2$ with benzene using UV-visible spectroscopy. Their experiment involved the photolysis of $CpML_2$ analogues in C_6F_6, in which small amounts of benzene were dissolved. The quantum yield of this reaction was reported to increase with increasing benzene concentration, but was not affected by added CO. To account for these observations, Lees postulated a mechanism involving direct reaction of benzene with electronically excited $Cp^*Ir(CO)_2$, followed by ligand loss in a second step, as shown in Scheme III.

Scheme III

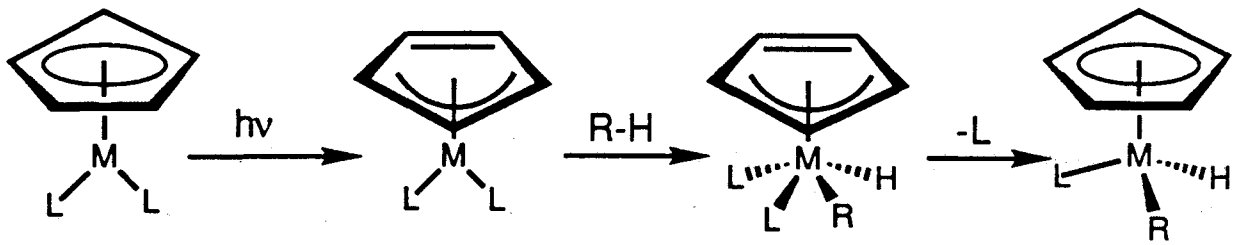

In this mechanism a new metal coordination site is made available by a change in cyclopentadienyl coordination (η^5 to η^3).

In contrast, our results, both in the gas phase and in liquid krypton,[2] suggest that ligand loss occurs prior to interaction with alkane, and that a coordinatively unsaturated intermediate is responsible for C-H activation. The strongest evidence for this mechanism is the direct gas-phase observation by IR of a monocarbonyl species which reacts with alkane to give an alkyl hydride species. How does one explain the discrepancy? Since no reactive transients were observed in Lees' study, the initial formation of the monocarbonyl Cp*Ir(CO) is not out of the question. One possible explanation is that in C_6F_6, the solvent may act to coordinate this intermediate and thus to inhibit attack by CO. In fact, Perutz and co-workers have observed the production of $Cp(PMe_3)Rh(C_6F_6)$ from the photolysis of $CpRh(PMe_3)(H)_2$ in C_6F_6.[33] Further work will be required to sort out Lees' puzzling observations.

4.4. Conclusions. The magnitude of all the rate constants for the reactions of CpRh(CO) with small molecules and alkanes indicates that this is one of the most reactive unsaturated organometallic fragments yet studied. These processes are marked by a lack of kinetic selectivity. This conclusion seems at odds with the results of competition studies in

solution which report sizable kinetic selectivities for C-H activation.[1e] There are some cases of apparent C-H activation selectivity in which the unfavored products may be unstable to the reaction conditions, and thus thermodynamic, rather than kinetic factors control the ratios of products formed. In other cases, however (*e. .g.* cyclopropane versus cyclohexane, which differ in reactivity with $Cp^*Rh(PMe_3)$ by a factor of 10.4 at -60°C), a real kinetic difference exists. In Chapter 5, we discuss the mechanism for C-H insertion in liquid Kr. In this medium, the rate of reaction of the unsaturated metal center with alkane is much less than that of diffusion, leaving open to the rhodium fragment the possibility of discriminating between substrates.

Several factors must be considered when comparing these solution-phase experiments with the gas-phase results reported here. First, the ligands attached to rhodium are different. This allows small differences in insertion rates among these solvates to become meaningful in determining product ratios. Also, in liquid alkane, the density of reactive C-H bonds is not a strong function of molecular size. This comes from the fact that intramolecular distances are comparable to molecular dimensions. This is not true in the gas phase, where the number of C-H bonds per unit concentration of alkane depends upon the size of the alkane.

Even if we take these reservations into account, and given the results from this gas-phase work, we would not expect to see the marked selectivities observed in solution. Based on the results described in Chapter 5, we believe that the main difference between the gas-phase and solution reactivity lies in the lack of solvent stabilization of the monocarbonyl intermediate in the gas phase. In condensed phase, the monocarbonyl species CpML does not exist for very long in non-solvated form, but is rapidly converted to a mixture of interconverting alkane complexes. The gas-phase monocarbonyl CpRh(CO), however, reacts with alkanes at a collision-limited rate. Our findings emphasize, therefore, the extraordinary reactivity of the CpRh(CO) fragment, which can be thought of as an "organometallic carbene".

Notes and References

[1](a) Janowicz, A. H.; Bergman, R. G. *J. Am. Chem. Soc.* **1982**, *104*, 352. (b) Janowicz, A. H.; Bergman, R. G. *J. Am. Chem. Soc.* **1983**, *105*, 3429. (c) Buchanan, J. M.; Stryker, J. M.; Bergman, R. G. *J. Am. Chem. Soc.* **1986**, *108*, 1537. (d) Wenzel, T. T.; Bergman, R. G. *J. Am. Chem Soc.* **1986**, *108*, 4856. (e) Periana, R. A.; Bergman, R. G. *J. Am. Chem. Soc.* **1986**, *108*, 7332. (f) Crabtree, R. H.; Mihelcic, J. M.; Quirk, J. M. *J. Am. Chem. Soc.* **1979**, *101*, 7738. (g) Crabtree, R. H.; Mellea, M. F.; Mihelcic, J. M.; Quirk, J. M. *J. Am. Chem. Soc.* **1982**, *104*, 107. .(h) Crabtree, R. H.; Holt, E. M.; Lavin, M.; Morehouse, S. M. *Inorg. Chem.* **1985**, *24*, 1986. (i) Baudry, D.; Ephritikhine, M.; Felkin, H. *J. Chem. Soc., Chem. Commun.* **1981**, 1243. (j) Ephritikhine, M. *New J. Chem.* **1986**, *10*, 9. (k) Cameron, C. J.; Felkin, H.; Fillebeen-Khan, T.; Forrow, N. J.; Guittet, E. *J. Chem. Soc., Chem. Commun.* **1986**, 801. (l) Hoyano, J. K.; Graham, W. A. G. *J. Am. Chem. Soc.* **1982**, *104*, 3723. (m) Ghosh, C. K.; Graham, W. A. G. *J. Am. Chem. Soc.* **1987**, *109*, 4726. (n) Jones, W. D.; Feher, F. J. *J. Am. Chem. Soc.* **1984**, *106*, 1650. (o) Jones, W. D.; Feher, F. J. *Acc. Chem. Res.* **1989**, *22*, 91. (p) Hackett, M.; Whitesides, G. M. J. Am. Chem. Soc. 1988, 110, 1449. (q) Harper, T. G.P.; Shinomoto, R. S.; Deming, M. A.; Flood, T. C. *J. Am. Chem. Soc.* **1988**, *110*, 7915.

[2]For reviews on this subject, see: (a) Muetterties, E. L. *Chem. Soc. Revs.* **1983**, *12*, 283. (b) Shilov, A. E. *Activation of Saturated Hydrocarbons by Transition Metal Complexes*; D. Riedel Publishing Co.: Dordrecht, 1984. (c) Bergman, R. G. *Science (Washington, D. C.)*, **1984**, *223*, 902.(d) Crabtree, R. H. *Chem. Rev.* **1985**, *85*, 245. (e) Halpern, J. *Inorg. Chim. Acta*, **1985**, *100*, 41. (f) Graham, W. A. G. *J. Organomet. Chem.* **1986**, *300*, 81.

[3]This experiment has been described in a forthcoming communication: Weiller, B. H.; Wasserman, E. P.; Bergman, R. G.; Moore, C. B.; Pimentel, G. C., in press.

[4]See, for example: (a) Jackson, T. C.; Carlin, T. J.; Freiser, B. S. *J. Am. Chem. Soc.* **1986**, *108*, 1120. (b) Tolbert, M. A.; Mandich, M. L.; Halle, L. F.; Beauchamp, J. L. *J. Am. Chem. Soc.* **1986**, *108*, 5675. (c) Cassady, C. J.; Freiser, B. S. *J. Am. Chem. Soc.* **1986**, *108*, 5690. (d) Georgiadis, R.; Fisher, E. R.; Armentrout, P. B. *J. Am. Chem. Soc.* **1989**, *111*, 4251.

[5]Renneke, R. F.; Hill, C. L. *J. Am. Chem. Soc.* **1988**, *110*, 5461.

[6]For reviews of recent progress in this area, see: (a) Schaffner, K.; Grevels, F.-W. *J. Mol. Struct.* **1988**, *173*, 51. (b) Weitz, E. *J. Phys. Chem.* **1987**, *91*, 3945. (c) Poliakoff, M.; Weitz, E. *Adv. in Organomet. Chem.* **1986**, *25*, 277. (c) Ishikawa, Y.; Hackett, P. A.; Rayner, D. M. *J. Mol. Struct.* **1988**, *174*, 113. (d) Weiller, B. H.; Grant, E. R. *Gas Phase Inorganic Chemistry*. Russel, D. H., ed. New York: Plenum Press, 1987.

[7]Ishikawa, Y.; Brown, C. E.; Hackett, P. A.; Rayner, D. M. *Chem. Phys. Lett.* **1988**, *150*, 506.

[8]Yang, G. K.; Peters, K. S.; Vaida, V. *Chem. Phys. Lett.* **1986**, *125*, 566.

[9]Brookhart, M; Green, M. L. H. *J. Organomet. Chem.* **1983**, *250*, 395.

[10]See: Lichtenberger, D. L.; Rai-Chaudhuri, A. *J. Am. Chem. Soc.* **1989**, *111*, 3583, and references therein.

[11](a)Rest, A. J.; Whitwell, I.; Graham, W. A. G.; Hoyano, J. K.; McMaster, A. D. *J. Chem. Soc., Chem. Commun.* **1984**, 624. (b) Rest, A. J.; Whitwell, I.; Graham, W. A. G.; Hoyano, J. K.; McMaster, A. D. *J. Chem. Soc., Dalton Trans.* **1987**, 1181. (c) Haddleton, D. M. *J. Organomet. Chem. 1986, 311*, C21.

[12]The possibility of multiphoton effects in cw irradiation cannot be ruled out, especially when the extent of photochemical conversion is large.

[13](a) Haddleton, D. M.; Perutz, R. N.; *J. Chem. Soc., Chem. Commun.* **1985**, 1372. (b) Haddleton, D. M.; Perutz, R. N.; Jackson, S. A.; Upmacis, R. K.; Poliakoff, M. *J. Organomet. Chem.* **1986**, *311*, C15. (c) Belt, S. T.; Haddleton, D. M.; Perutz, R. N.; Smith, B. P. H.; Dixon, A. J. *J. Chem.Soc., Chem. Commun.* **1987**, 1347. (d) Duckett, S. B.; Haddleton, D. M.; Jackson, S. A.; Perutz, R. N.; Poliakoff, M.; Upmacis, R. K. *Organometallics*, **1988**, *7*, 1526.

[14]Belt, S. T.; Grevels, F.-W.; Klotzbuecher, W. E.; McCamley, A.; Perutz, R. N. *J. Am. Chem. Soc.*, in press.

[15]*Thermophysical Properties of Matter*, Vol. 6. Eds.: Touloukian, Y. S.; Makita, T. New York: Plenum Press, 1970.

[16]Fischer, E. O.; Bittler, K. *Z. Naturforsch. B*, **1961**, *16b*, 225.

[17]McCleverty, J. A.; Wilkinson, G. *Inorg. Syn.* **1966**, *8*, 211.

[18]In several of the metal carbonyl systems studied in the gas phase, attack by unsaturated photoproducts upon starting material competes with other reactions. See: (a) Chapter 3; (b) Fletcher, T. R.; Rosenfeld, R. N. *J. Am. Chem. Soc.* **1988**, *110*, 2097.

[19]Hirschfelder, J. O.; Curtiss, C. F.; Bird, R. B. *Molecular Theory of Gases and Liquids*. New York: Wiley, 1954.

[20]In the reaction of CH_4 with CpRh(CO), for example the quantity $k_{obs}/[CH_4]$ was not affected by the total pressure under conditions in which the total pressure was >10 Torr.

[21]Hill, R.; Knox, A. R. *J. Chem. Soc., Dalton Trans.* **1975**, 2622.

[22](a) Andréa, R. R.; Vuurman, M. A.; Stufkens, D. J.; Oskam, A. *Recl. Trav. Chim. Pays-Bas* **1986**, *105*, 372. (b) Upmacis, R. K.; Poliakoff, M.; Turner, J. J. *J. Am. Chem. Soc.* **1986**, *108*, 3645.

[23]This simplistic analysis assumes that there are no changes in the bond energies of the CpRh(CO) moiety upon reaction. Using the M-H IR frequencies of $(CO)_4FeH_2$ (Stobart, S. R. *J. Chem. Soc., Dalton Trans.* **1972**, 2442), we arrive at a value of 64 for the ratio of vibrational partition functions of $Cp(CO)Rh(H)_2$ and CpRh(CO) at 293K. Knowing the

partition functions of hydrogen, we estimate the ratio of the total partition functions to be 3.5×10^{-4} atm^{-1}.

[24]Pearson, R. G. *Chem. Rev.* **1985**, *85*, 41.

[25]Note, for example, the calculated shifts in carbonyl frequencies upon deuteration in: Sweany, R. L.; Russell, F. N. *Organometallics* **1988**, *7*, 719.

[26]By comparison, see: (a) Reference 18b; (b) Ishikawa, Y.; Hackett, P. A.; Rayner, D. M. *J. Phys. Chem.* **1989**, *93*, 652.

[27]For reviews, see: (a) Kubas, G. J. *Acc. Chem. Res.* **1988**, *21*, 120. (b) Kubas, G. J. *Comments Inorg. Chem.* **1988**, *7*, 17.

[28]Greater rates were seen when CO was present.

[29]The pitfalls in such an analysis are severalfold: (a) with enthalpic barriers to reaction which may be very small or negative, one must have an accurate knowledge of the partition functions of the reactants and the resulting transition state before one can predict a rate constant; (b) the participation of a third body in removing energy from the activated complex may unpredictably effect the efficiency of reaction; (c) collision frequencies cannot be calculated exactly.

[30]Smith, D. J.; Setser, D. W.; Kim, K. C.; Bogan, D. J. *J. Phys. Chem.* **1977**, 898.

[31]For this calculation, the following parameters were taken from the temperature dependence of the C-H activation of cyclohexane in liquid krypton (see Reference 3): $\log_{10}A = 10.6$; $E_a = 4.6$ kcal mol^{-1}. $T = 290$ K.

[32]Marx, D. E.; Lees, A. J. *Inorg. Chem.* **1988**, *27*, 1121.

[33]Belt, S. T.; Duckett, S. B.; Helliwell, M.; Perutz, R. N. submitted to *J. Chem. Soc., Chem. Commun.*

Table 4.1. Rate Constants for the Gas-Phase Reactions of Singly-Unsaturated Organometallic Species with CO.

Reactant	10^{11} k, cm^3 $molecule^{-1}$ s^{-1}
CpRh(CO)	15[a]
CpCo(CO)	6[a,b]
$Fe(CO)_4$	0.006[c]
$Ru(CO)_4$	2.8[d]
$Cr(CO)_5$	2.5[e], 6.4[f]
$W(CO)_5$	5[g]
$V(CO)_5$	5[h]

[a]this work; [b]see Experimental Section; [c]Seder, T. A.; Ouderkirk, A. J.; Weitz, E. *J. Chem. Phys.* **1986**, *85*, 1977; [d]Bogdan, P. L.; Weitz, E. *J. Am. Chem. Soc.* **1989**, *111*, 3163; [e]Seder, T. A.; Church, S. P.; Weitz, E. *J. Am. Chem. Soc.* **1986**, *108*, 4721; [f]Fletcher, T. R.; Rosenfeld, R. N. *J. Am. Chem. Soc.* **1988**, *110*, 2097; [g]Reference 18b; [h]Ishikawa, Y.; Hackett, P. A.; Rayner, D. M. *J. Am. Chem. Soc.* **1987**, *109*, 6644.

Table 4.2. Carbonyl Stretching Frequencies for CpRh(CO) and its Reaction Products (in cm^{-1}).

	this work	literature
$CpRh(CO)_2$	2003, 2060	1989, 2050[a]
CpRh(CO)	1987	1969[b]
$CpRh(CO)(H)_2$	*ca.* 2055	
$CpRh(CO)(H)(CH_3)$	2040	2022[b]
$CpRh(CO)(H)(C_2H_5)$	2037	
$CpRh(CO)(H)(CH_2C(CH_3))$	2044	
$CpRh(CO)(H)(c\text{-}C_6H_{11})$	2033	
$Cp_2Rh_2(CO)_3$	1858, 2000	1834, 1981[c]
$[CpRh(\mu\text{-}CO)]_2$		1778[c]

[a]Reference [p 2:2a]; [b]Reference 11b; [c]Anderson, F. R.; Wrighton, M. S. *Inorg. Chem.* **1986**, *25*, 112.

Table 4.3. Rate Constants for Reactions of CpRh(CO).

reactant	$10^{10}k_{obsd}$, $cm^3molecule^{-1}s^{-1}$	efficiency[a]
CO	1.5 ± 0.3	0.43
H_2	1.6 ± 0.3	0.17
D_2	1.6 ± 0.7	0.22
CH_4	0.58 ± 0.26	0.14
CD_4	0.47 ± 0.10	0.11
C_2H_6	1.8 ± 0.5	0.49
$C(CH_3)_4$	2.1 ± 0.6	0.60
c-C_6H_{12}	2.8 ± 0.9	0.82

[a] fraction of gas-kinetic

Table 4.4. Efficiency of C-H Activation versus Alkane Properties.

Reactant	Eff[a]	B.E.[b]	I.P.[f]	a[g]	DH_a[i]	k_F[k]
H_2	0.17	104.2[c]	15.427	0.79		0.37
CH_4	0.14	104.3[c]	12.6	2.62[h]	416.6[j]	1
C_2H_6	0.49	100.4[d]	11.5	4.48[h]	420.1[j]	2.1
$C(CH_3)_4$	0.60	100[e]	10.35	10.2[h]	408.9[j]	4.5
c-C_6H_{12}	0.82	95.5[e]	9.8	11.0[h]		4.3

[a]fraction of gas-kinetic; [b]kcal mol^{-1}; [c]Griller, D.; Kanabus-Kaminska, J. M.; Maccoll, A. *J. Mol. Struct.* **1988**, *163*,125; [d]Parmar, S. S.; Benson, S. W. *J. Am. Chem. Soc.* **1989**, *111*, 57; [e]McMillen, D. F.; Golden, D. M. *Ann. Rev. Phys. Chem.* **1982**, *33*, 493; [f]ionization potential, eV; [g]polarizability, cm^{-24}; [h]Applequist, J.; Carl, J. R.; Fung, K.-K. *J. Am. Chem. Soc.* **1972**, *94*, 2952, and references therein.; [i]gas-phase acidity, kcal mol^{-1}; [j]DePuy, C. H.; Gronert, S.; Barlow, S. E.; Bierbaum, V. M.; Damrauer, R. *J. Am. Chem. Soc.* **1989**, *111*, 1968; [k]reaction rate with atomic fluorine, Reference 30.

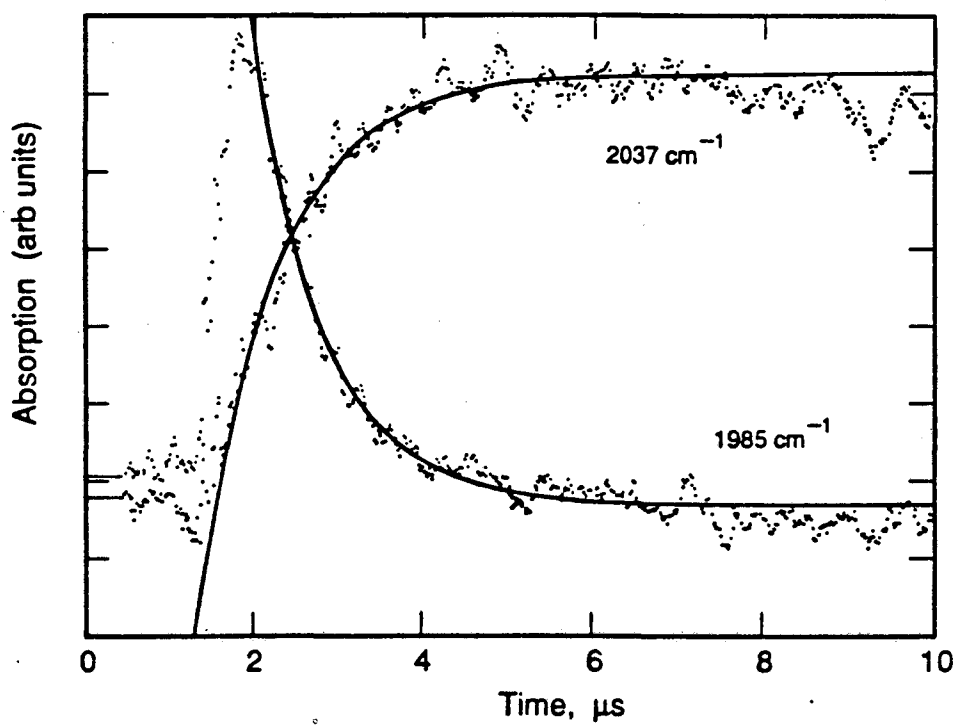

Figure 4-1. Transient absorption traces taken at 1985 and 2037 cm^{-1}, following the decay of CpRh(CO) and formation of Cp(CO)Rh($CH_2C(CH_3)_3$)(H), respectively, from the reaction of CpRh(CO) with neopentane. Pressure of gases: 12.6 Torr Ar; ca. 0.08 Torr neopentane. Shock wave transient removed from traces (see Chapter 2). Superimposed fits: 1.2×10^6 s^{-1} (decay), 1.1×10^6 s^{-1} (rise).

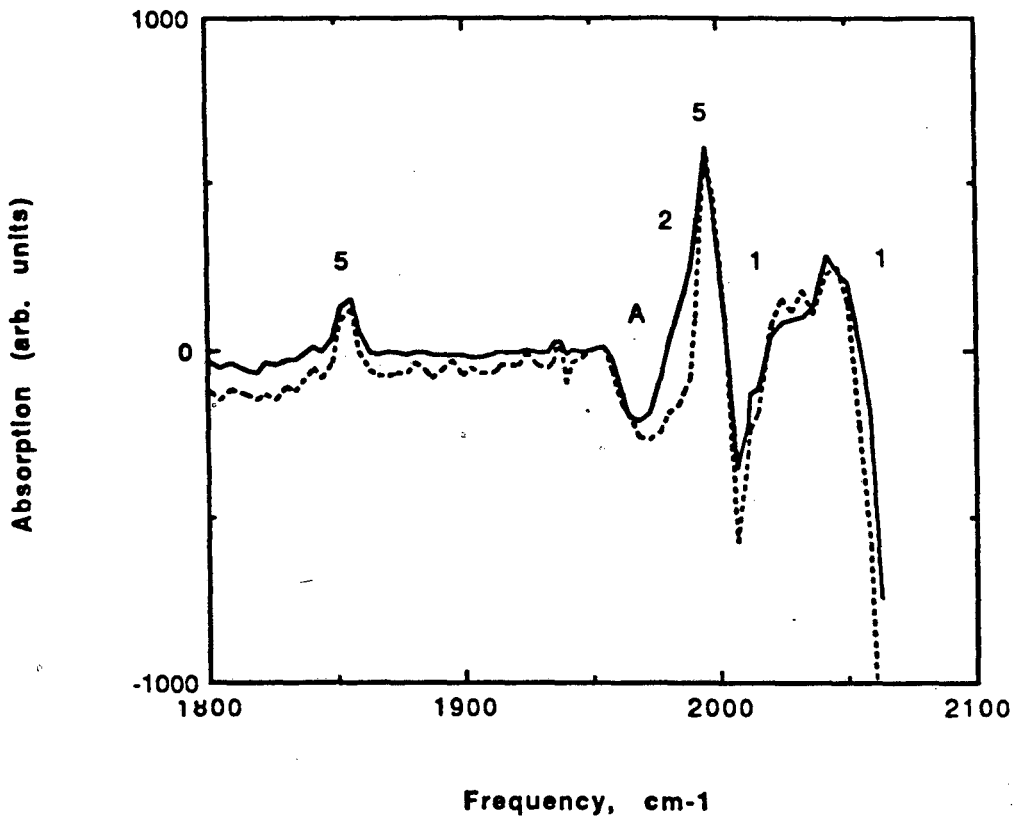

Figure 4-2. Transient absorption spectra observed following the 308 nm photolysis of $CpRh(CO)_2$ in ca. 22 Torr Ar. Solid line: 1 μs after photolysis; dotted: 9 μs after photolysis. Band labels for this figure and for subsequent transient absorption spectra refer to Scheme I.

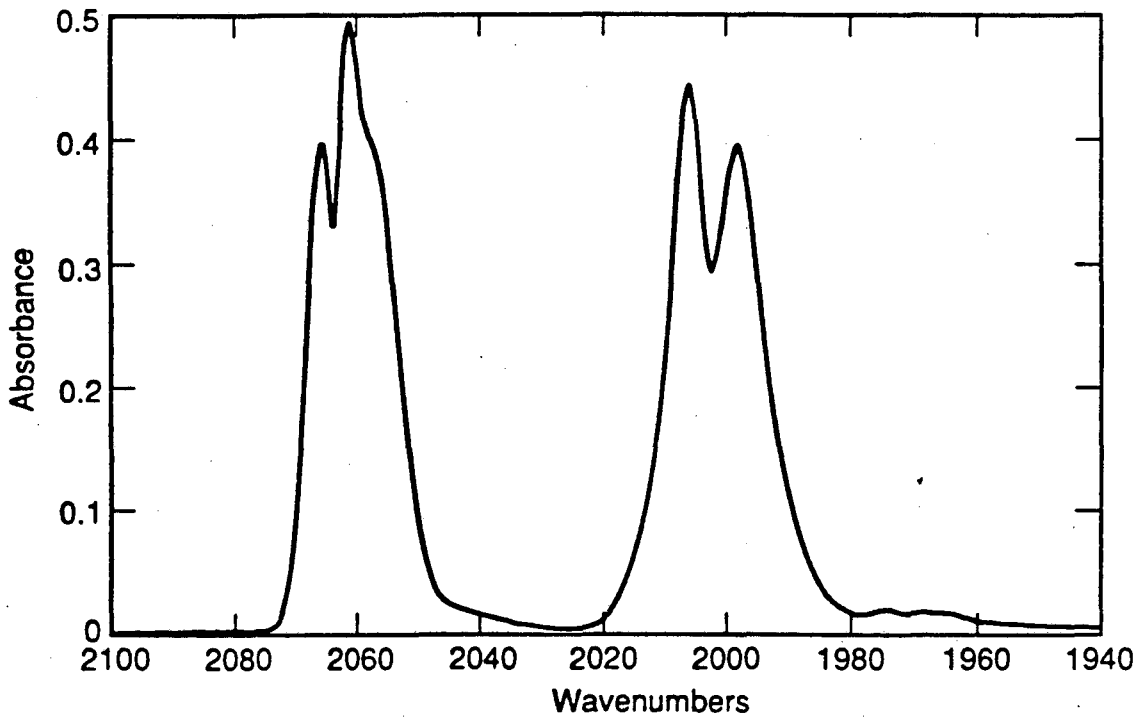

Figure 4-3. FTIR spectrum of 0.37 Torr $CpRh(CO)_2$. Resolution: 0.5 cm^{-1}. Pathlength of cell: 8 cm. 100 scans acquired.

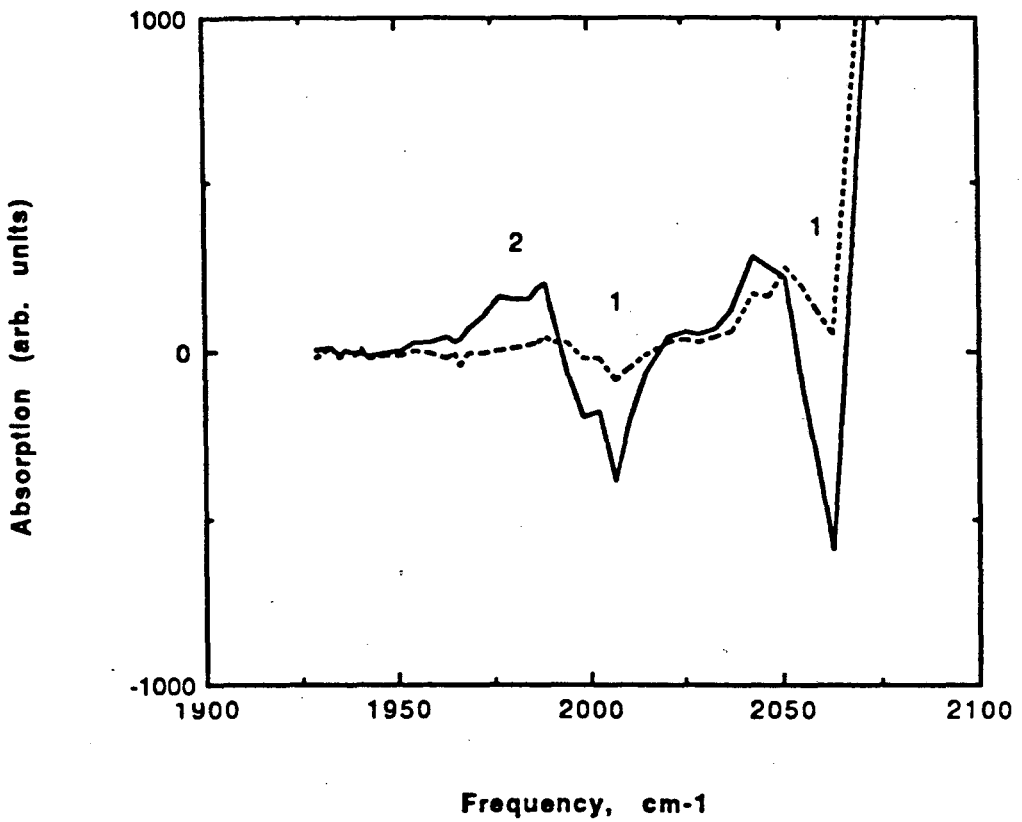

Figure 4-4. Transient absorption spectra from the photolysis of $CpRh(CO)_2$ in *ca.* 18 Torr Ar with 0.6 Torr CO added. Solid line: 0.2 μs after photolysis; dotted: 1.8 μs after photolysis.

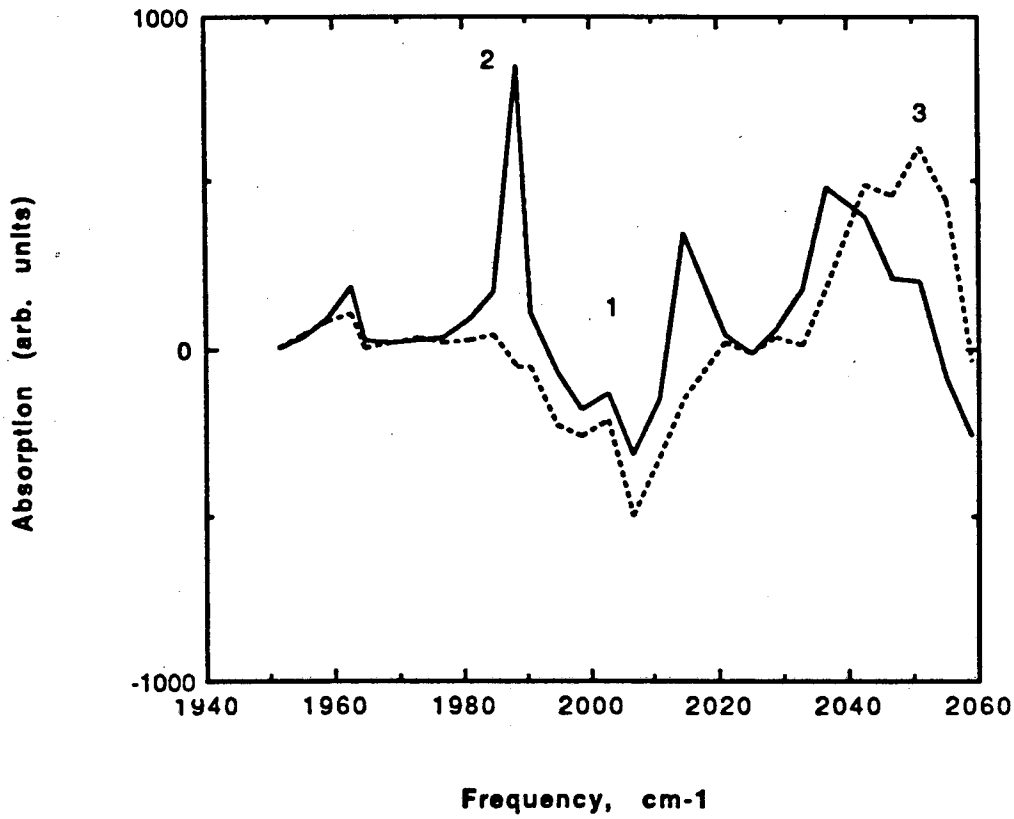

Figure 4-5. Transient absorption spectra from the photolysis of $CpRh(CO)_2$ in *ca.* 35 Torr Ar with *ca.* 0.3 Torr H_2 added. Solid line: 0.2 μs after photolysis; dotted: 1.8 μs after photolysis.

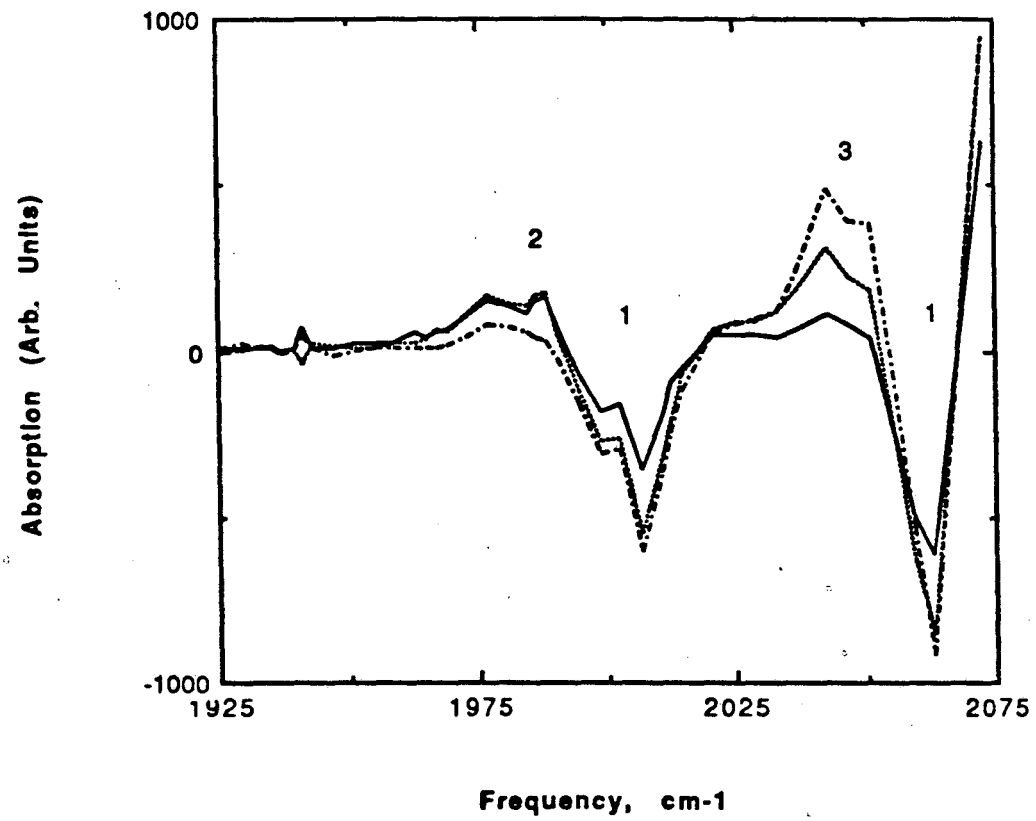

Figure 4-6. Transient absorption spectra from the photolysis of $CpRh(CO)_2$ in *ca.* 17 Torr Ar with *ca.* 0.3 Torr D_2 added. Solid line: 0.2 μs after photolysis; dotted: 1.8 μs after photolysis.

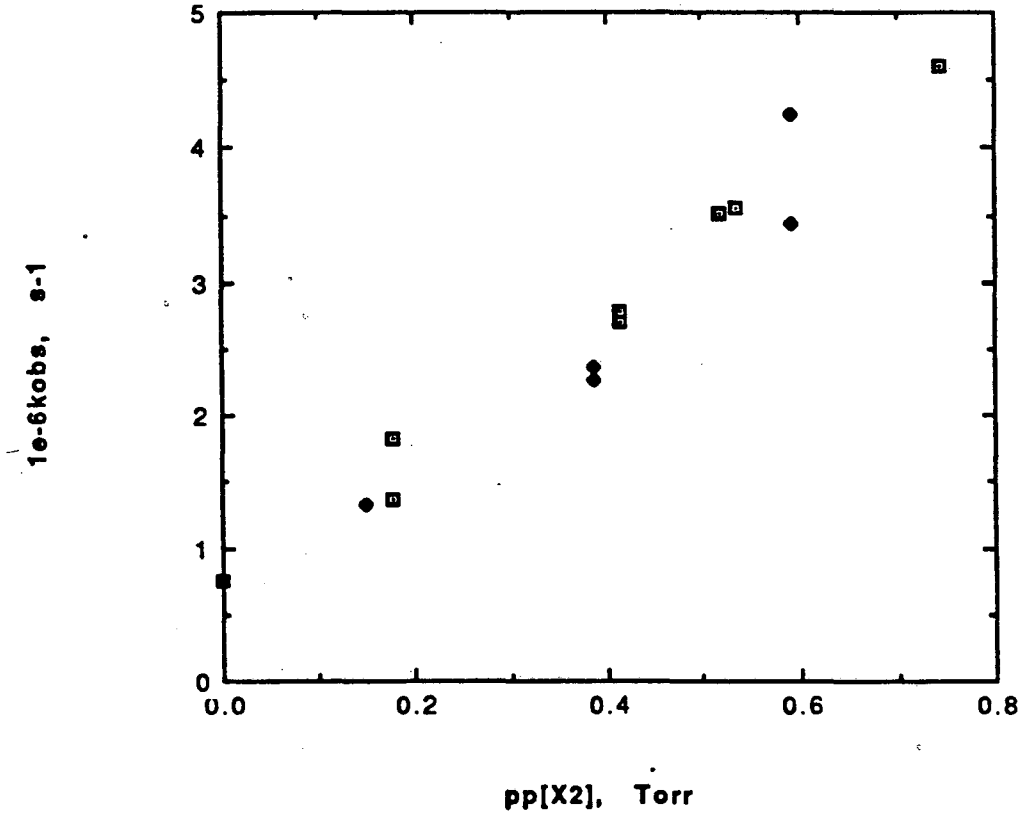

Figure 4-7. Plot of observed rates for decay of CpRh(CO) and for appearance of $Cp(CO)Rh(X)_2$ (X = H, D), versus the partial pressure of X_2. Open squares: H_2; filled lozenges: D_2.

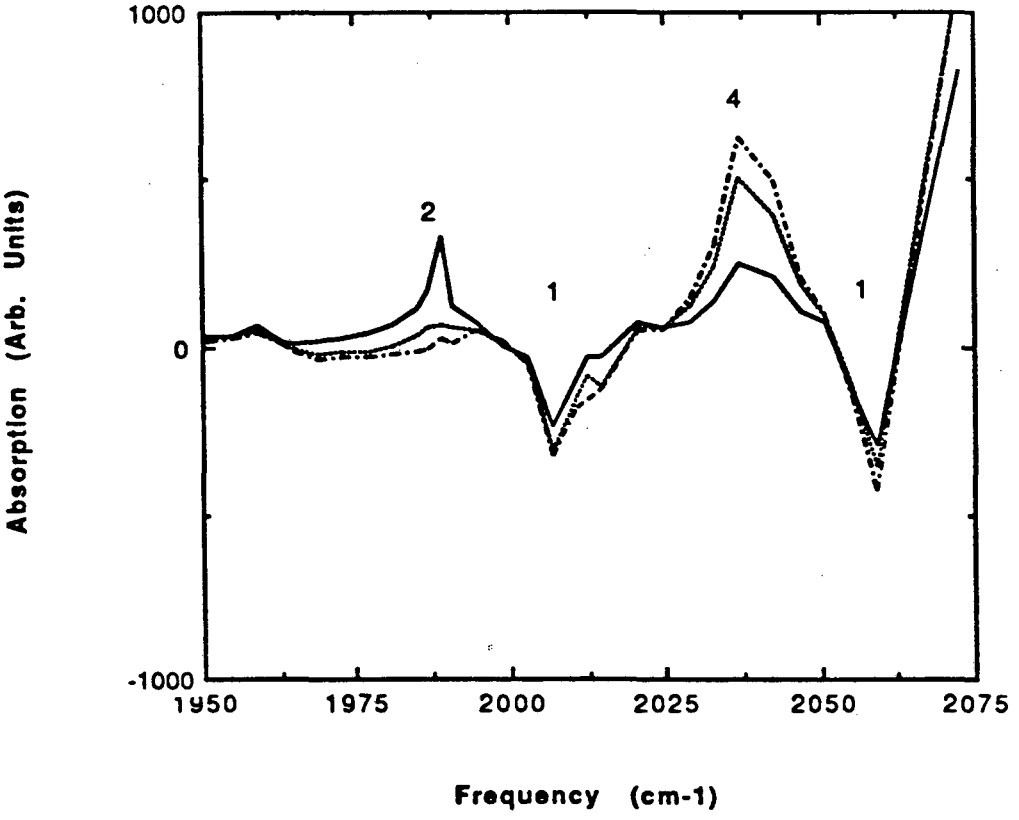

Figure 4-8. Transient absorption spectra from the photolysis of $CpRh(CO)_2$ in *ca.* 50 Torr Ar with 0.4 Torr C_2H_6 added. Solid line: 0.2 μs after photolysis; dotted: 0.4 μs after photolysis; dot-dash: 0.6 μs after photolysis.

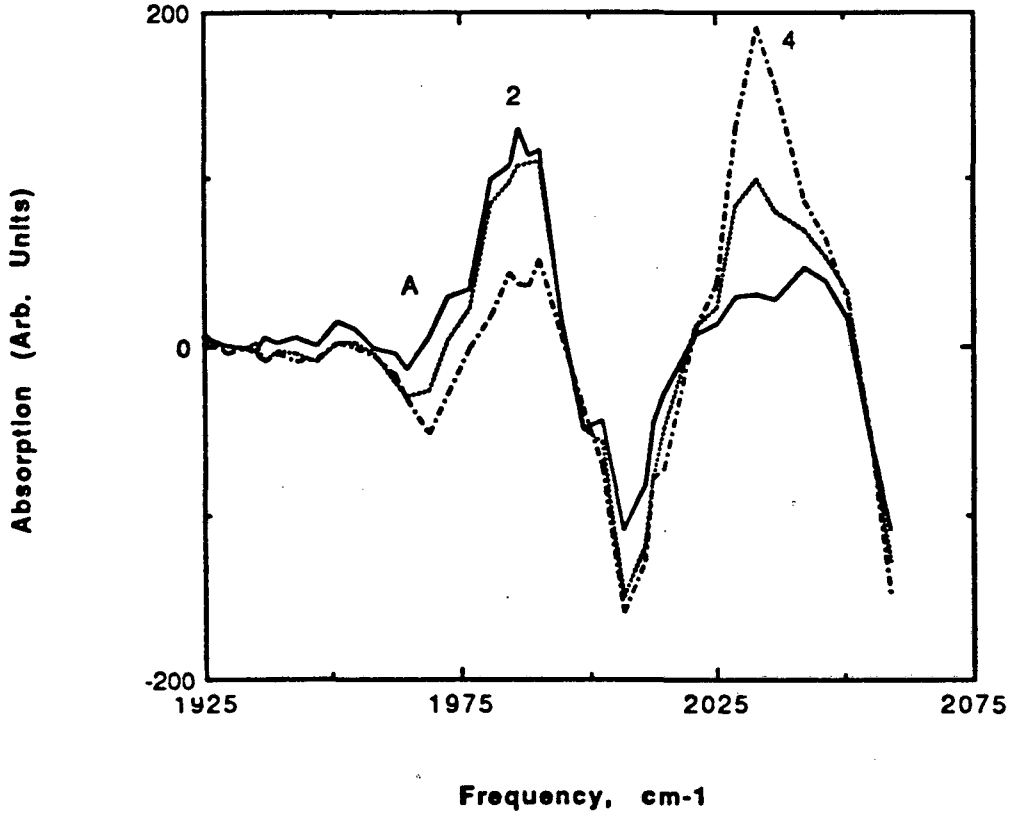

Figure 4-9. Transient absorption spectra illustrating the reaction of **2** with 0.3 Torr *c*-C_6H_{12} in 28 Torr Ar. Solid line: 0.2 μs after photolysis; dotted: 0.4 μs after photolysis; dot-dash: 0.6 μs after photolysis.

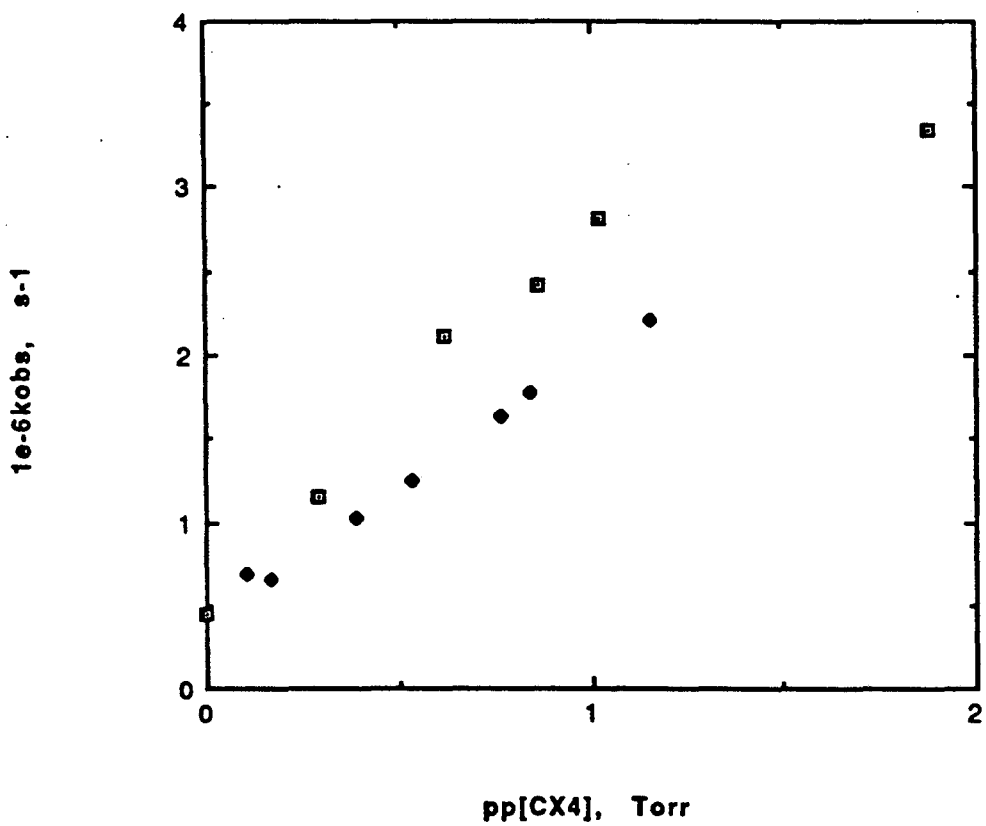

Figure 4-10. Plot of the decay rate of **2** versus the partial pressure of CX_4 (X = H, D). Open squares: CH_4; closed lozenges: CD_4.

Chapter 5. The Reactivity of $(\eta^5\text{-}C_5Me_5)Rh(CO)$ in Liquid Krypton: Oxidative Addition of Alkanes.

5.1. Introduction. The oxidative addition of alkanes, normally considered inert, to transition metal centers is an interesting example of controlled reactivity.[1] In this reaction, (C-H activation), the C-H bond of a saturated hydrocarbon is broken and metal-carbon and -hydrogen bonds are formed. This reaction is especially intriguing because, unlike other reactions which involve alkanes such as attack by main-group radicals or light-sensitized reaction with mercury, C-H activation yields transition-metal alkyl hydride adducts. These species can then, in principle, act as intermediates in the conversion of alkanes to more synthetically useful species. We have made an effort to understand one subset of C-H activation reactions, those which employ compounds of the family $(\eta^5\text{-}C_5R_5)ML_2$ (R ≡ H, Me; L ≡ CO, H_2, or trialkyl phosphine; M ≡ Rh, Ir) as starting materials.[2] Here, photochemical or thermal excitation of these organometallic species in the presence of saturated hydrocarbons leads to loss of one ligand and insertion into the C-H bond (eq. 1).

$$(\eta^5\text{-}C_5R_5)MLL' + R\text{-}H \xrightarrow{h\nu \text{ or } \Delta} (\eta^5\text{-}C_5R_5)(L)M(R)(H) + L' \qquad (1)$$

(R-H ≡ alkane; L ≡ phosphine or CO; L' ≡ CO or H_2)

In a search for solvents inert to C-H activating metal centers, Graham and co-workers found that conversion of $Cp^*Ir(CO)_2$ to the methyl hydride $Cp^*(CO)Ir(CH_3)(H)$ proceeded in perfluoromethylcyclohexane.[2e] In studies of the photochemical reactivity of $Cp^*(PMe_3)IrH_2$ ($Cp^* \equiv \eta^5\text{-}C_5Me_5$), however, *no* solvent has been found to be unreactive toward the intermediate generated by photolysis of starting material. Seemingly inert solvents such as fluorocarbons, SF_6, and SiF_4 undergo reaction, often leading to metal-fluoride species through routes not yet understood.[3] Belt *et al.* note[4] that hexafluorobenzene can function as a donor ligand in the photochemistry of

$Cp^*Rh(PMe_3)(C_2H_4)$, leading to the formation of $Cp^*(PMe_3)Rh(\eta^2\text{-}C_6F_6)$. Kinetic studies aimed at understanding the mechanism of C-H oxidative addition require the ability to vary the concentration of the alkane substrate in a controlled fashion, yet this is impossible when one is restricted to studying the C-H activation of solvent.

As almost a last resort, we initiated research into C-H activation in rare-gas solutions. Happily, this finally provided a medium in which irreversible reaction of metal with solvent was not observed, and C-H oxidative addition using variable concentrations of alkanes could be carried out. Using this approach, Sponsler *et al.* found[3] liquid Xe to be an excellent medium for the preparation of alkyl hydride products that have previously been difficult to obtain for reasons of solubility (*e. g.* naphthalene) or by the difficulty of liquifaction (*e. .g.* methane).

Liquified rare gases have found use as solvents since the 1960's.[5] Solutions of the heavier rare gases Kr and Xe have solvent properties surprisingly similar to those of alkanes.[6] The fact that solutes such as cubane and naphthalene can be dissolved in liquid Xe[3] is a clear demonstration of the applicability of liquid rare gases to the study of reactions involving large organic molecules. This is some compensation for the difficulties inherent in working with liquid inert gases, which include design of reaction chambers suitable for use at high pressures and low temperatures.

Turner and co-workers pioneered the use of liquid inert gas solutions in organometallic photochemistry in the early 1980's.[7] Since then, this group and others[8] have shown the possibilities of rare-gas solutions in the preparation of unusual coordination complexes (such as dinitrogen[7a] and molecular hydrogen[7g] adducts) in liquid Xe and Kr. Recent work by Perutz *et al.* has brought the technique to bear on the subject of oxidative addition. These researchers have examined the photochemistry of $CpRh(C_2H_4)_2$ ($Cp \equiv \eta^5\text{-}C_5H_5$) in liquid inert gases, and have found that an intermediate with the formula $CpRh(C_2H_4)$ can react with silanes to produce the rhodium silyl hydride adducts by Si-H activation.[8c,d]

These last studies represent the latest attempts at providing a mechanism for oxidative addition by molecules of the type $CpML_2$. Perutz and co-workers have also studied[9] the C-H activation reaction by photolysis of $CpRh(CO)_2$ in cyclohexane solution using transient infrared spectroscopy and found, as we did for $Cp^*Rh(CO)_2$ photolyzed in alkane solution at room temperature,[10] that the intermediate responsible for C-H activation could not be detected because of the swiftness of reaction. The alkyl hydride C-H activation products were observed, however, and their decay to dimeric species was noted. Marx and Lees have also performed transient UV-visible spectroscopic experiments in C-H activation, as well as quantum yield studies, using perfluorobenzene as an inert solvent.[11] Another approach, that of matrix isolation, has been employed by Rest's group and others.[12] These endeavors have led to the discovery of methane C-H activation from the photolysis of the carbonyl species $Cp^{(*)}M(CO)_2$ ($M \equiv Rh, Ir$) in methane matrices at 12K. These studies have identified by infrared spectroscopy several species of the form $Cp^{(*)}ML$.[12]

In this chapter, I will give an account of our research into C-H activation processes that occur upon photolysis of $Cp^*Rh(CO)_2$ in liquid krypton. These studies represent the first time-resolved detection of the reaction of an organometallic intermediate with alkane to form a C-H activation product. We use the method of transient infrared spectroscopy with CO laser detection, following the photochemistry by the organometallic species' ν_{CO} absorptions. This technique has become an important tool in the study of organometallic carbonyl photochemistry, notably in the UV-laser photodissociation of gas-phase metal carbonyls,[13] though recently it has been applied to the solution-phase photolyses of transition-metal compounds as well.[14] We have also investigated the temperature and alkane concentration dependences of the rate constants for C-H activation.

5.2. Experimental. The transient infrared spectrometer (Figure 5-1) has been described in chapter 2, so we will provide only its salient features. A liquid nitrogen-

cooled CO laser (cw, 3-10 mW; 1800-2080 cm^{-1}) is used to monitor the carbonyl absorptions of organometallic species produced by flash photolysis (XeCl excimer, 308 nm) of a precursor molecule, such as in this case, $Cp^*Rh(CO)_2$. The CO laser beam then impinges upon a photoconductive IR detector (Ge:Cu, 3 × 10 mm, ca. 150 ns risetime) whose output, after amplification, is fed into a transient digitizer (Tektronix, 7912AD). Signals are acquired and the laser frequency controlled from the environment of a Pascal computer program on a personal computer (Fountain XT).

$Cp^*Rh(CO)_2$ was synthesized according to a literature method[15] from the dimer $[Cp^*Rh(Cl)(\mu\text{-}Cl)]_2$, which itself was synthesized from $RhCl_3 \cdot 3H_2O$ and C_5Me_5H[16]. The volatile solid was sublimed from the crude product and stored in a drybox under nitrogen. Sample solutions were made up by first charging a small flask with a small amount of $Cp^*Rh(CO)_2$ in hexanes or pentane (concentration roughly 10^{-3} mol l^{-1}), which afforded a stock solution from which dilutions appropriate for the liquid krypton study were made. The stock solution was kept under a blanket of Ar for no longer than 3-5 days, during which time little decomposition was observed by qualitative IR spectroscopy. CO (99.5%), CH_4 (99.97%), and ethane (99.99%) were supplied by Matheson, neopentane (99% by gas chromatography) by Chemical Samples Co., cyclohexane (99.7% by gas chromatography) by Fisher, cyclohexane-d_{12} (99.7 atom % D) by Cambridge Isotopes, neopentane-d_{12} (98 atom % D) by MSD Isotopes, and Kr (99.995%) by Airco.

The cell used for this experiment was designed by G. E. Gadd, and is similar in construction and capability to those in use by Turner *et al.*[7b] It consists of a copper block through which two perpendicular channels of lengths 1.43 and 5 cm have been drilled for holding the liquid krypton solutions. Sample solutions are stirred by a magnetically coupled stirbar. The temperature range accessible is ca. -150 to 30°C; the cell can withstand pressures up to 900 psi, although pressures above 700 psi are in general to be avoided, as such conditions apparently reduce the lifetime of the vacuum seal. The cell temperature is kept stable (± 1°C) by a program of pulsed heating and cooling set at a

temperature controller (Omega, model CN2002-T). Heating is effected by DC current flow through two resistors (total resistance 100 Ω) in contact with the copper block, while liquid nitrogen or cold nitrogen vapor flowing through channels in the block provide for cooling. The cell is thermally isolated from the environment by placement in an evacuated dewar housing. BaF_2 or CaF_2 windows are used on the dewar and cell body. Two thermocouples (copper-constantan) monitor the temperature at two points on the assembly: on the cell body, and on the inlet tube leading to the cell. Heating tape wrapped around the inlet tube allows input of condensible gases into the cell volume with minimal loss. The stainless steel vacuum line which accompanies the cell has a diffusion pump, an ion gauge, and two capacitance manometers (ranges 10 and 1000 Torr, MKS Baratron).

The following procedure is used to produce samples in liquid krypton solution. First, an aliquot (0.5-2 ml) of the $Cp^*Rh(CO)_2$ solution is withdrawn from a dilute solution (see above) and injected into the cell volume. Argon is then flowed over the sample until the solvent is evaporated, at which point the cell volume is evacuated to remove residual solvent. The cell is then cooled to the temperature of interest (-140 to -80°C). Krypton gas is then flowed through a volume containing a gaseous sample of the reactive substrate (*e. g.* cyclohexane) into the cell to high pressure until condensation of the mixture occurs.

5.3. Estimation of Reagent Concentrations. The concentrations of the organometallic (*ca.* 10^{-5} mol l^{-1}) and substrate are derived from the integrated infrared absorbances obtained by a single-beam FTIR spectrometer (P-E 1750) equipped with a deuterated triglycine sulfate (DTGS) detector and operating with a nominal resolution of 2 cm^{-1}. The FTIR beam passes through the short cell axis, while the CO and excimer laser beams proceed along the long axis. The integrated absorption cross-sections of the infrared alkane bands (cyclohexane[17], neopentane[18], methane[19], and ethane[20]) and CO[21] are taken from the literature. In cases in which more than one infrared band was used for

concentration determinations, an average of derived concentrations was taken. The deviation between the two derived concentrations was rarely >10%. When the integrated absorbance of only one band was measurable, as was often the case at high concentrations of cyclohexane, the concentration of the alkane was estimated from the absorbance of the measurable band.

For *c*-C_6H_{12}, the absorption cross-sections are taken to be equal to those determined from the neat alkanes, after correction for the change in the index of refraction.[5] For *c*-C_6D_{12}, methane, ethane, and CO, values for the integrated absorptions were taken from gas-phase studies. In the case of neopentane, we noted that the absorption cross-sections for two infrared fundamentals changed in relative magnitude when going from the gas phase to liquid krypton solution. Neither of the bands in question is a C-H stretching vibration. Therefore, we made the assumption that the integrated absorption cross-sections for the C-H stretching modes did not vary with the medium, when adjusted for changes in refractive index. All other bands were then compared with the C-H stretch, and empirical ratios for the absorption intensities for these other bands *versus* the C-H stretch were calculated. For larger concentrations of neopentane, a very weak fundamental absorption around 925 cm^{-1} was used for determining its concentration. A "double bootstrap" was then performed in which empirical ratios of the low-frequency band versus the intermediate bands were calculated, followed by extrapolation of the C-H stretching integrated absorption, from which the concentration was estimated.

We found in the literature no values for the integrated IR absorption cross-sections of perdeuteroneopentane, although its fundamental bands have been assigned.[22] Therefore, we measured the infrared spectrum of $C(CD_3)_4$ in the gas phase at several pressures < 20 Torr $C(CD_3)_4$, using an 8 cm gas cell, with 1 atm SF_6 present to pressure-broaden the individual gas-phase lines. We used a Nicolet 8000 FTIR spectrometer operating with 0.5 cm^{-1} nominal resolution, collecting 100 scans. From the two spectra taken in which the peak absorbance of the neopentane-d_{12} C-D stretching frequency region

was less than 2.4 (i. e., in which the spectrometer gave reliable band integrals), we estimate the integrated absorption cross-section of the sum of the anti-symmetric and symmetric C-D stretching bands (2250-2000 cm^{-1}) to be 154 km mol^{-1}. Using this number, we were able to estimate the concentration of neopentane-d_{12}, with the aid of the empirical method of extrapolation of the C-D stretching absorption used in the determination of $C(CH_3)_4$ concentrations (*vide supra*).

5.4. Results

5.4.1. Photolysis in the Absence of Added Ligands. Photolysis of $Cp^*Rh(CO)_2$ (**1**) in liquid krypton causes transient bleaching of absorbance at 1969 and 2029 cm^{-1}, due to depletion of the starting material, as well as transient increase in absorption at 1947 cm^{-1}. At -80°C, the half-life of this transient species (**2**) in the absence of any added reactant is roughly 1 ms. We believe that the positive transient is due to the production of a rhodium mono-carbonyl complex for several reasons. First, it is the only carbonyl absorption observed in the CO laser range formed promptly after the photolysis event (within the detector risetime of 200 ns). In addition, this species reacts with CO to reform the dicarbonyl **1**. The frequency of this absorbance also corresponds well with a feature seen by Rest *et al.*[12b] in the photolysis of $Cp^*Rh(CO)_2$ in cryogenic matrices which was assigned as the monocarbonyl $Cp^*Rh(CO)$.

The monocarbonyl transient appears to regenerate the dicarbonyl starting material after photolysis by the capture of CO generated from photolysis. This we conclude from the behavior of transient absorption at the frequency of starting material absorption. Starting material does not return to its original concentration after each photolysis event, however, indicating that other reactions compete for the monocarbonyl intermediate. We surmise that one of these reactions could be reaction with starting material to produce dimeric species.

5.4.2. Photolysis in the Presence of CO. In liquid krypton, the monocarbonyl transient reacts with CO at rates which approach the diffusion-controlled limit. Figure 5-2 shows the essentially temperature-independent behavior of the rate constant for decay of **2** in the presence of CO. (These rate constants were determined using one value of k_{obs} for each temperature. A preliminary study of k_{obs} versus [CO] at -80° implies a linear dependence.) In such a situation, the rate is equal to the Arrhenius pre-exponential factor A; note that the value of k or A derived from this experiment is nearly the rate of diffusion in most solvents (ca. 10^9 l mol^{-1} s^{-1}). This result agrees with recent time-resolved studies of the reactivity of CpRh(CO) in the gas phase (see chapter 4), in which the monocarbonyl reacts with CO and several other species with nearly gas-kinetic rate constants.

5.4.3. Photolysis in the Presence of Cyclohexane and Neopentane. In the presence of either cyclohexane or neopentane the rate of disappearance of the monocarbonyl is faster than that observed with no added ligand, but is slower than that seen in the presence of similar concentrations of CO. The rate at which **2** decays is matched by the rate of appearance of a new positive transient absorption centered at 2003-2007 cm^{-1} (see Figure 5-3). The relatively high frequency of this absorption indicates formal oxidation of the metal center from Rh(I) to Rh(III) based on the carbonyl absorptions of several previously-characterized molecules of the form Cp*Rh(CO)RR'[23]. The *ca.* 2005 cm^{-1} transient also agrees in frequency with rhodium alkyl hydrides seen both in matrices[12b] and in alkane solution[9]. To our knowledge, this is the first time-resolved experiment in which a coodinatively unsaturated intermediate in solution-phase C-H activation has been observed.

A transient absorption spectrum taken from the photolysis of **1** in the presence of cyclohexane is shown in Figure 5-4. We note depletion of absorption at 1969 and 2033 cm^{-1} due to the destruction of starting material, as well as transient absorption by the monocarbonyl **2** at 1947 cm^{-1}. The species **2** then decays as a new absorption due to formation of **3** appears at 2003 cm^{-1}. We should point out that the appearance of the

transient absorption spectrum changes significantly with temperature, primarily because the carbonyl absorptions are narrow (2-5 cm^{-1} FWHM) and shift to lower frequency as the temperature is lowered. Since our spectrometer can only monitor transient absorption at frequencies separated by 4 cm^{-1}, the carbonyl stretching absorptions pass in and out of resonance with these frequencies of detection, causing the measured relative magnitudes of the transients to change.

We have also observed by FTIR spectroscopy the photochemical conversion of the starting material to the cyclohexyl hydride in the presence of cyclohexane in liquid Kr at -100°. A small fraction (<10%) of the starting material may be converted to the rhodium cyclohexyl hydride by exposing the liquid Kr solution of **1** and cyclohexane to several hundred excimer shots or to the focussed output of a cw Hg arc lamp with a quartz filter. (No absorptions around 1947 cm^{-1}, corresponding to the monocarbonyl species observed by transient IR spectroscopy, is seen.) The production of the alkyl hydride can be monitored by its carbonyl absorbance at 2004 cm^{-1}, although the metal-hydride stretching vibration absorption has not been observed, presumably because of the relative weakness of its absorption cross-section. The half-life of the alkyl hydride complex is *ca.* 4 min at -85°C. A FTIR difference spectrum taken from the arc-lamp photolysis of $Cp^*Rh(CO)_2$ in liquid Kr at -100°C in the presence of cyclohexane is shown in Figure 5-5. Note the difference in magnitude between the negative changes in absorption due to destruction of $Cp^*Rh(CO)_2$ and the positive absorption from $Cp^*Rh(CO)(H)(R)$ (3); ($R \equiv c\text{-}C_6H_{11}$).

We have since discovered that the alkyl hydrides are themselves photolabile. In flash-kinetic experiments, after *ca.* 100 shots, the appearance of the kinetic traces taken at the frequency characteristic of the alkyl hydride species changes. Initially, within the detector risetime limit, absorption tends to decrease (see Figure 5-3). Absorption then increases with a first-order exponential risetime which again corresponds well to the rate for decay of the monocarbonyl transient. Apparently, the C-H activation product undergoes photolytic loss of alkane to regenerate the monocarbonyl, which can then react

with alkane as before. Thus a photo-stationary concentration of **3** can be realized, in which the amount of alkyl hydride generated equals the amount destroyed on each photolysis shot. We attribute the relatively small amount of alkyl hydride produced to one or both of the following: (1) the product **3** may have a greater UV absorption cross-section; (2) **3** may have a greater quantum yield for photolysis. While it is possible that thermal reactions act to consume the alkyl hydride molecules, this seems an unlikely explanation for the effects seen here. At room temperature, Perutz and co-workers examined the thermal decomposition of Cp*Rh(CO)(H)(Cy) in cyclohexane, and found it to decay with a unimolecular rate constant of roughly 50 s^{-1}.

If the rate for the C-H activation reaction with either cyclohexane or neopentane, as determined from both the rate of decay of the monocarbonyl **2** and the rate of appearance of the alkyl hydride **3**, is plotted against the concentration of alkane, pronounced curvature can be observed. This deviation from a first-order dependence on alkane is especially pronounced at high concentrations of this alkane; it can be seen at all temperatures studied (see Figures 5-6, 5-7).

Upon photolysis of **1** in the presence of perdeuterated alkanes instead of their proteated analogues, we observe similar features of the transient spectroscopy, namely the depletion of transient absorption of **2** concurrent with the appearance of transient absorption in the 2003-2007 cm^{-1} region. We note, though, sharply lower rate constants for oxidative addition of the perdeuterated alkanes relative to their proteated analogues under almost all conditions. Figures 5-8, 5-9 display the temperature and concentration dependences of rate constants for reaction with c-C_6D_{12} and $C(CD_3)_4$, respectively. Two aspects of the concentration dependence should be noted. First, as [alkane-d_{12}] increases, the rates approach limiting values which are as much as a factor of 15 smaller than those for the rates of activation of alkane-d_0 at the corresponding temperatures. Second, for each temperature, the initial rise of alkane-d_{12} activation rate with alkane concentration appears to be as fast or faster than the initial rise for the alkane-d_0 complex.

5.4.4. Other Alkanes. Several attempts were made to observe C-H activation of methane, with little success. Even at the highest methane concentration (0.046 mol l^{-1}), the rate of decomposition of **2** did not differ substantially from its rate of decay in the absence of CH_4. We estimate an upper bound of 1.2×10^4 s^{-1} for the C-H activation of methane at -100°C in the presence of 0.046 mol l^{-1} CH_4, at least a factor of 5 slower than for the reaction with neopentane at similar concentration and temperature. In the presence of *ca.* 0.01 mol l^{-1} ethane at -80°C, a slow reaction was noted, yielding the growth of a transient at about 2007 cm^{-1}. Unfortunately, the reaction was too slow to make a detailed variable-temperature investigation possible.

5.4.5. Comparison with Results in Liquid Xenon.

As part of our effort to understand the role of rare gas molecules in these C-H activation reactions, we have begun the investigation of alkane oxidative addition in liquid xenon solution. Although our results are preliminary, it is appropriate to summarize them here.

The photolysis of $Cp^*Rh(CO)_2$ in liquid Xe at temperatures between -70 and -20°C leads to the appearance of a transient infrared absorption at 1943 cm^{-1}. In the absence of any other reactant such as CO or alkane, the new species does not decay appreciably over a period of 1 ms. The transient absorption, apparently that of a rhodium monocarbonyl similar to that seen in liquid Kr, decays in the presence of CO to reform starting material. However, unlike in the liquid Kr system, the rate of this reaction is much slower than the rate of diffusion, implying an energy barrier. We have not fully investigated the concentration dependence of the reaction, but, having examined the reaction with CO over the temperature range -70 to -30°C, we estimate the enthalpy of activation for the CO recombination to be about 3 kcal mol^{-1}.

Reaction of the rhodium monocarbonyl with cyclohexane also occurs, as noted by transient absorption at 2003 cm^{-1}. Again, this reaction is much slower than is the same reaction in liquid Kr at the same [alkane], despite the fact that the temperature is about 100°C higher for the liquid Xe experiments. As we have not yet examined the dependence

of k_{obs} upon [cyclohexane], it would be premature to compare the results too closely with those from the liquid Kr study. However, we did note the overall temperature dependence of k_{obs}/[cyclohexane] from a set of experiments in which the rate constant for C-H activation was measured at only one cyclohexane concentration for each temperature. The results from this analysis yield an overall activation energy for C-H activation of approximately 8 kcal mol^{-1}. In both the reactions with CO and with cyclohexane, it is apparent that the interaction of the rhodium monocarbonyl with Xe is stronger than that with Kr, contributing a barrier to the substitution of Xe by another ligand. An understanding of the mechanistic implications of our results must await a more detailed investigation of the concentration dependences of and isotope effects in these reactions.

5.5. Discussion.

5.5.1. Possible Mechanisms. One may attempt to explain the levelling off of the rates at high alkane concentration in several ways. First, hydrocarbon aggregation may affect the accurate measurement of high alkane concentrations. (We have eliminated the possibility of a non-linear FTIR response at these high alkane absorbances independently.[24]) In this scenario, we imagine that at low cyclohexane concentrations, for example, solutions consist largely of solvent-separated, independently diffusing monomers, and this might become a mixture of monomers and higher clusters of cyclohexane molecules at high concentration. We may then propose the mechanism outlined in Scheme I, which represents attack on the alkane cluster by the reactive transient, with equilibria existing among clusters of all sizes.

Scheme I

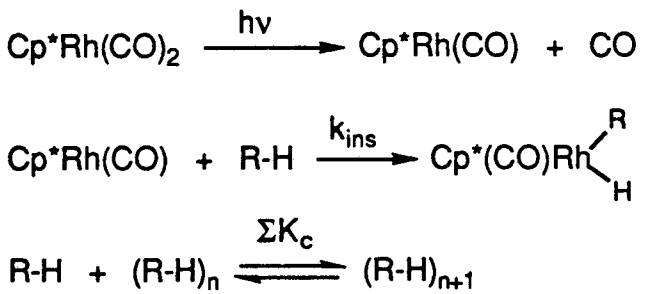

Since a cluster of a certain size would tend to have absorption cross-sections equal to the cross-section of the monomer multiplied by the number of molecules in the cluster[25], but would diffuse through the solution as a single particle, the collision frequency per molecule of reactive intermediate and consequently the rate of reaction would cease to be proportional to the infrared absorbance. Aggregation in liquid rare gases has been observed for hydrogen-bonding solutes such as methanol,[26,27] although it has not been reported for alkanes.

Other evidence does not support this hypothesis, however. First, one would expect that solute cluster formation would, for entropic reasons, be less pronounced at higher temperatures, causing the curvature to be less. However, no such trend can be seen from Figures 5-8 and 5-9. Second, it seems unlikely that cyclohexane and neopentane, compounds with large differences in their melting and boiling points and heats of vaporization, would behave in such a strikingly similar manner in liquid krypton. Finally, an Arrhenius analysis of the data (see Table 5.1) based on linear fits to the low-concentration data (in which curvature is not very prominent), yields activation energies for C-H insertion of 4.4 and 5.3 kcal mol^{-1} and pre-exponential factors of *ca.* 10^{12} and 10^{13}, for cyclohexane and neopentane, respectively. The latter are most difficult to accept, being several orders of magnitude greater than that for diffusion-controlled reactions, and much larger than that for the reaction of Cp*Rh(CO) with CO in liquid Kr.

A second possible mechanism may be invoked to understand the non-first order dependence of rate upon alkane concentration. This mechanism, laid out in Scheme II, calls for a pre-equilibrium to exist between Cp*Rh(CO)•••Kr, a krypton solvate, and Cp*Rh(CO), the non-solvated or "naked" monocarbonyl.

Scheme II

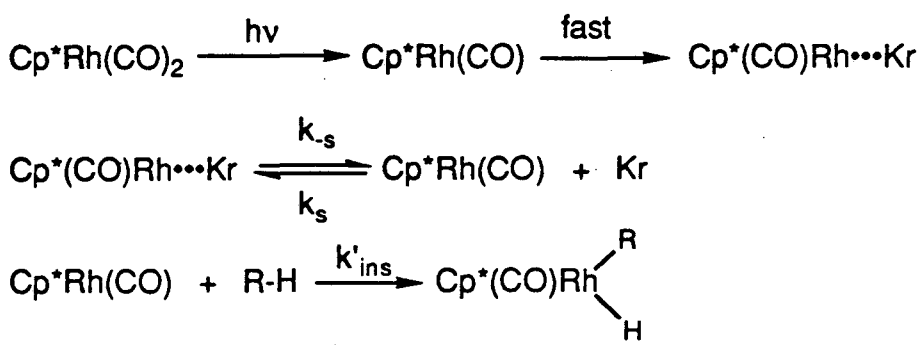

Only the naked unsaturated species is deemed reactive toward alkane. Upon photolysis, the naked species is formed, and reacts initially with Kr or with alkane in a branching ratio reflective of their relative abundances; this initial relaxation would be undetectable using our apparatus. Subsequently, the krypton-metal complex dissociates reversibly, leading to the naked species, which reacts with alkane. As the alkane concentration increases, the rate of production of alkyl hydride approaches k_{-s} in eq. (2), the rate of krypton detachment, and loses its dependence on [R-H]. This fact can be readily drawn from inspection of the rate expression which can be derived from a steady-state analysis of the kinetics (eq. 2):

$$k_{obs} = \frac{k_{-s}k'_{ins}[R\text{-}H]}{(k_s[Kr] + k'_{ins}[R\text{-}H])} \qquad (2)$$

In support of this mechanism, we recall that organometallic complexes with rare-gas molecules have been discovered, and a few have been shown to consist of a metal interacting with a unique rare-gas atom.[28] Recently, some researchers have claimed to

observe the fleeting existence of non-solvated or "naked" unsaturated metal carbonyls in solution,[29] although considerable controversy now surrounds these findings. One point against this scheme is that it requires k'_{ins}[R-H] to become of comparable magnitude to k_s[Kr] at the high range of alkane concentration. Since even with [R-H] ≈ 0.05 mol l^{-1}, [Kr]/[R-H] > 300, k_{ins} must be at least 100•k_s. Considering the lack of steric demand by the krypton atom and the nature of the metal-rare gas interaction[30], this requirement seems unreasonable. The most formidable objection to this mechanism, however, lies in the fact that it predicts the limiting rate constant (k_{-s}) for C-H activation to be independent of the nature of the alkane. This is clearly contradicted by the large positive isotope effect on the high-concentration rates for oxidative addition of cyclohexane and neopentane (Figures 5-6 through 5-9).

The mechanism we have settled upon to explain the rate behavior of C-H activation is laid out in Scheme III.

Scheme III

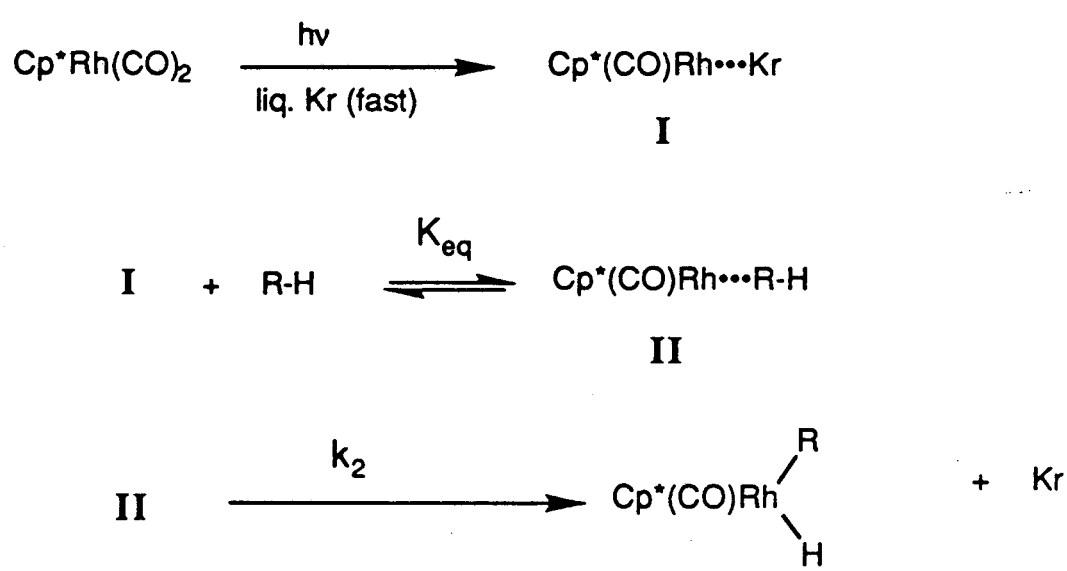

Similar to Scheme II, a krypton solvate, labelled I in Scheme III, is formed immediately after photolysis. This rare-gas solvate is then in equilibrium with an alkane-solvated species (II) in which the alkane C-H bond is largely intact. The mechanism requires that the krypton and alkane solvates be indistinguishable by our spectrometer.[31] Finally, in an "intramolecular" process, the C-H bond is broken and the alkyl hydride molecule is irreversibly formed. The kinetic analysis of this scheme, shown in equations 3-5, provides for the curvature seen in Figures 5-6 and 5-7 in the following way: as the alkane concentration increases, the fraction of unsaturated Cp*Rh(CO)•••X (X = Kr, alkane) which is solvated by alkane increases, tending toward 100% at infinite [R-H]/[Kr]. The rate then asymptotically approaches k_2, the intramolecular insertion rate. This mechanism predicts the observed independence of the rate constant upon [R-H] at high alkane concentration, and also (unlike the dissociative mechanism in Scheme II) accounts for the *dependence* of k_{obs} on the *nature* of the alkane.

$$k_{obs} = \frac{[II]}{[I]_o} k_2 = \left(\frac{K_{eq}}{1 + K_{eq}}\right) \cdot k_2 \qquad (3)$$

$$K_{eq} = \frac{k_1[R\text{-}H]}{k_{-1}[Kr]} = K \left(\frac{[R\text{-}H]}{[Kr]}\right) \qquad (4)$$

$$k_{obs} = \left(\frac{K \left(\frac{[R\text{-}H]}{[Kr]}\right)}{1 + K \left(\frac{[R\text{-}H]}{[Kr]}\right)} \right) \cdot k_2 \qquad (5)$$

{I = Cp*Rh(CO)(Kr); II = Cp*Rh(CO)(R-H)}

One can fit the experimental data at each temperature to curves with the following functional form:

$$y = \frac{x}{a + bx}, \qquad (6)$$

where x and y represent the alkane concentration and rate for C-H activation, respectively, while a and b are fitting parameters. The parameters a, b are defined as follows:

$$a = \frac{1}{k_2}; \qquad b = \frac{[Kr]}{k_2 K}. \qquad (7)$$

From a non-linear least-squares fit of the data using the above model, we arrive at the best values for a and b, which when inserted into (eq. 6), yield the curves overlaid upon the data points in Figures 5-6 and 5-7. As the equation of state of krypton is well-known[32], the krypton concentration for each temperature can easily be derived.

The kinetic scheme used in this model is a simplification of the chemical system in at least one sense. Since we observe decay, albeit slow, of the monocarbonyl species **2** even in the absence of alkane, provision should be made for a non-zero y intercept of the model function. The reactions which comprise the removal of **2** in the absence of alkane probably include reaction of **2** with $Cp^*Rh(CO)_2$ to produce dinuclear species and reaction of the monocarbonyl with impurities dissolved in the krypton such as oxygen, as well as recombination of **2** with photo-generated CO. The magnitude of this intercept is quite small, however, compared to the range of rates studied, and is even less than the magnitude of the scatter in most of the data taken with non-zero alkane concentration, as can be seen from Figure 5-6 and 5-7. For this reason, a separate parameter for baseline offset was not included.

From the parameters a and b, we obtain values for k_2, the "intramolecular" C-H activation rate constant, and for K, the constant of equilibrium between the krypton and alkane solvates. The temperature dependences of these quantities is represented, for

cyclohexane, in Figures 5-10 and 5-11, and for neopentane in Figures 5-12 and 5-13. It is clear from these figures that the value for the activation energy for the C-H bond-breaking step is more accurately known than the value for the energy difference between the krypton and alkane solvates. The temperature dependences of K and k_2 for the neopentane complex yield similar numbers for ΔH_σ (the enthalpy difference between the Kr and alkane solvates) and E_a (the activation energy barrier for the k_2 step) respectively, as can be seen in Tables 5.2 and 5.3.

5.5.2. Isotope Effects. The rate constants for the reactions of the monocarbonyl with c-C_6D_{12} and $C(CD_3)_4$ are much slower than those for reaction with the proteated alkanes. In consequence, we could not perform as thorough an investigation of the temperature dependences of these rate constants. Given this limitation, we may apply a similar analysis of the concentration dependence of the C-D activation. The results are startling, since they imply large differences between isotopomers in both the alkane-metal binding enthalpy as well as the barrier for C-H insertion. For example, at -80°C, a fit of the data for C-D activation of neopentane-d_{12} to the model in Scheme III yields values of 8.9×10^3 for K and 3.8×10^4 s^{-1} for k_2.[33] When we compare these values to those from reaction with neopentane-d_0 at the same temperature (see Table 5.3), we find K for neopentane-d_{12} to be much larger, while k_2 is much smaller. This results from the fact that the rate constant for C-D activation levels off at lower concentration and reaches a plateau at a much lower rate constant, as noted in section 5.4.3. The behavior of the rate versus [c-C_6D_{12}] is similar. We can put a lower bound of 2×10^4 on the value of K for cyclohexane-d_{12} at -80° using the data shown in Figure 5-8. Again, $k_2^H/k_2^D >> 1$, with $k_2^D \approx 3.6 \times 10^4$ s^{-1}.

We can understand the isotope effect on k_2 in conventional terms. Thus, it may reflect the lower zero-point energy of the C-X (X ≡ H, D) bond undergoing cleavage. In support of this, a plot of $\ln(k_2^H/k_2^D)$ versus 1/T for cyclohexane (Figure 5-14) reveals a $\Delta\Delta H^\dagger$ of 0.9 kcal mol^{-1}. Since the zero-point energy difference between C-H and C-D bonds is 1.2 kcal mol^{-1}, this value is not unreasonable. The value for $\Delta\Delta S^\dagger$, 1.5 cal mol^{-1}

deg^{-1} is reassuring, since we would not expect a large difference in entropy of reaction. When extrapolated to 298K, this free energy difference predicts an isotope effect of roughly 10 for k_2.

We cannot as easily account for the increase in the magnitude of ***K*** upon deuteration. Inverse isotope effects have been observed for the reverse of oxidative addition, the reductive elimination of hydrocarbons from metal centers. We note with interest that Buchanan *et al.*[2c] found a larger rate for reductive elimination of cyclohexane-d_{12} over cyclohexane-d_0 from the alkyl hydride isotopomers $Cp^*(PMe_3)Ir(H)(c\text{-}C_6H_{11})$ and $Cp^*(PMe_3)Ir(D)(c\text{-}C_6D_{11})$. The researchers postulated the existence of an intermediate alkane complex $Cp^*(PMe_3)Ir$(cyclohexane), and explained the inverse isotope effect for reductive elimination as leading from a higher steady-state concentration of the alkane complex of the perdeuterated alkane system. Jones and Feher[2g] observed a large inverse isotope effect in another reductive elimination reaction, the loss of benzene-d_n from $Cp^*(PMe_3)Rh(C_6H_{6-n}D_n)(H)$, which they attributed to the existence of an intermediate π-complex. This isotope effect is most likely a secondary effect due to the strengthening of the C-X bonds during coordination.

In explaining the inverse isotope effects seen in the binding of alkane complexes seen in this work and in that of Buchanan *et al.*, we must invoke secondary effects. It is hard to imagine a metal-alkane complex in which the C-X bond is not directly involved in donation of electron density to the metal center. Metal-bonding through the C-X bond should weaken the alkane C-X bond, favoring C-H attachment over C-D because of the higher zero-point energy in the uncomplexed alkane. The favored binding of the deuterated alkanes must be explained in terms of one or both of the following: (a) lower zero-point energy in modes of the metal-alkane complex other than the C-X stretch, such as hindered rotations of the alkane; (b) differences in entropy of solvation.

We must also consider the possibility that the rhodium complex reacts with residual partially protonated alkanes in the perdeuterated alkane solutions. The deuterated solvents

were quoted to be 98% atom D for neopentane-d_{12} and 99.7% atom D for cyclohexane-d_{12}. (The isotopic purities of the deuterated alkanes were confirmed to ±1% atom D by IR and GC analysis, ±1% atom D.) Therefore, as much as one quarter of our deuterated neopentane could possibly have been neopentane-d_{11}, although significantly less cyclohexane-d_{11} contaminates the cyclohexane-d_{12}. We note from Figures 5-8 and 5-9 that there is little difference between the concentration dependences for the C-X activation rate constant of the two deuterated compounds; this parallels the similarity between the cyclohexane-d_0 and neopentane-d_0 systems. One would not expect such resemblance between the behavior of the two deuterated substrates if the concentration of residual C-H bonds affected the rate of reaction.

5.5.3. Solvation by Kr and Alkanes. The model we have constructed to explain the concentration and temperature dependences of C-H activation in liquid Kr, shown in Scheme III, relies on the existence of metal-alkane and -krypton complexes. We can justify their participation in the mechanism on the basis of previous spectroscopic and kinetic evidence.

The interaction of coordinatively unsaturated organometallic fragments with rare gases in liquid rare-gas solution was first demonstrated by Turner[7c] in 1983. In this experiment, the Xe solvate of $Cr(CO)_5$ in liquid Kr was observed by FTIR, and was found to have a half-life of *ca.* 2 s at -98°C. This experiment followed almost a decade of research into metal complexes with various "inert" species which resulted in a qualitative table of relative metal-solvent interaction magnitudes based on UV-visible spectroscopy.[34] We note that the UV-visible spectrum of $Cr(CO)_5$ is perturbed to nearly the same extent by krypton and methane.[36] The metal-rare gas interaction is apparently strong enough to effectively occupy the open site of the unsaturated molecule and to cause a significant shift in the frequencies of its carbonyl stretching vibrations compared with its naked coordinatively unsaturated analogue.

Metal-alkane complexes have often been implicated in reaction schemes. Buchanan *et al.*[2c], as mentioned above, attributed the curious deuterium scrambling patterns in the isotopically labelled $Cp^*(PMe_3)Ir(cyclohexyl)(H)$ to the intermediacy of a σ-complex. In such a complex, the metal site is considered to interact with one or possibly two C-X bonds. Periana and Bergman found more indirect kinetic evidence for the existence of an alkane-solvate intermediate in the rearrangement of $Cp^*(PMe_3)Rh(H)(n\text{-alkyl})$.[2d] Isotopic scrambling in $Cp_2W(H)(CH_3)$ isotopomers caused Bullock *et al.* to invoke[35] the intermediacy of the methane σ-complex $Cp_2W(CH_4)$. As we discussed in Chapter 4, metal-alkane interactions may be considered a close relation to the so-called "agostic" complexes that are characterized by formally coordinatively unsaturated metal centers and short distances between the metal and the C-H bond of a ligand attached covalently at another site.[36] Some theoretical studies of the reaction path for the oxidative additions of alkanes by metals have detected energy minima consistent with dative metal-alkane complexes.[37] In the gas phase, Ishikawa *et al.* claim to observe an equilibrium between $W(CO)_5$ and ethane with a W-ethane enthalpy of complexation of *ca.* 10 kcal mol^{-1}.[38] Similar metal-alkane bond energies have been indirectly found using photoacoustic calorimetry.[39] Adsorption of alkanes on some metal surfaces appears to involve substantial C-H bond weakening, indicated by the appearance of so-called "soft" C-H stretching IR absorptions.[40]

5.5.4. Reaction Path and Selectivity. Our results suggest that the energetics of C-H activation in liquid Kr may be represented by the reaction coordinate diagram shown in Figure 5-15. Photolysis of the starting material produces an initial statistical mixture of krypton and alkane complexes, which quickly reaches equilibrium. The barrier between the krypton and alkane complexes must be much lower than the 4-5 kcal mol^{-1} measured for the C-H insertion step itself, since the kinetic scheme we employed to fit the data assumes a pre-equilibrium between the solvates. The exact mechanism of alkane displacement of Kr (and *vice versa*) is unknown, but we propose that it resembles an S_N2-

type displacement, in which the Cp*Rh(CO) fragment is never totally uncomplexed by either alkane or rare gas. This we infer from the fact that the naked monocarbonyl most probably lies some 10 kcal mol^{-1} higher in energy than the alkane solvate, and thus is an unlikely transition state for the pre-equilibrium between solvates. After the equilibration, the alkane complexes pass over the 4-5 kcal mol^{-1} barrier to the C-H activation products. There is a slightly higher barrier for neopentane activation than there is for cyclohexane activation. Interestingly, the energy for the rhodium-neopentane complex appears to be slightly lower than that for the cyclohexane complex based and the greater absolute value of ΔH_{σ} for neopentane complexation.

The energy barrier to C-H insertion in liquid Kr (E_a of k_2 step) is close to those proposed in other studies. Bergman and co-workers propose[2c] a barrier of ≤5 kcal mol^{-1} for the activation of cyclohexane by the fragment $Cp^*Ir(PMe_3)$, and based this on the energies of the Ir-cyclohexyl, Ir-H, and cyclohexane C-H bonds and the magnitude of the enthalpic barrier to reductive elimination of cyclohexane from $Cp^*(PMe_3)Ir(c\text{-}C_6H_{11})(H)$.[41] In recent theoretical work on C-H activation by CpML species (M ≡ Rh, Ir; L ≡ CO, PH_3), Ziegler *et al.* hold that there is a *ca.* 2.5 kcal mol^{-1} activation barrier to C-H activation of methane by the Ir complex, while the Rh complex activates methane with a somewhat larger barrier of *ca.* 9 kJ mol^{-1}. Such estimates of activation barriers to C-H activation appear to contradict the matrix isolation evidence presented by Rest and co-workers,[12b] who found C-H activation after prolonged photolysis of $Cp^{(*)}Ir(CO)_2$ in 12K methane matrices.

In our examination of the gas phase reactions of CpRh(CO) (chapter 4), we found that the rate constants for the oxidative addition of alkanes to Rh was nearly diffusion-controlled and comparable to the rate constant for addition of CO. If the effect of the change in ligand from Cp to Cp* is ignored, how do we explain the difference in reactivity between the gas-phase and liquid Kr rhodium monocarbonyl systems? The major difference is that in the gas phase, the rhodium monocarbonyl is not solvated, and thus lies

at much higher energy than either the krypton- or alkane- solvated monocarbonyls; C-H insertion takes place rapidly following rate-determining formation of a metal-alkane complex. In liquid Kr, however, the monocarbonyl intermediate is stabilized by solvation, and must undergo an increase in enthalpy on its way to the oxidative addition product; that is, our kinetic experiments monitor an activated, rather than a collision-controlled, process.

We believe this picture rationalizes the facts that (a) large selectivities have been observed for the C-H activation of alkanes by photolysis of $Cp^*(L)M(H)_2$ (M ≡ Rh, Ir) in mixed hydrocarbon solvents,[42] but (b) the gas-phase results for CpRh(CO) show no such selectivity, since reaction occurs upon nearly every collision, preventing discrimination among different substrates. As shown in the potential energy diagram for C-H activation in liquid Kr (Figure 15), we propose that, in mixed alkane solution, a pre-equilibrium exists between different alkanes. (Such an equilibration may resemble that between krypton and alkane solvates in the liquid Kr system.) This is shown schematically for a two-substrate system in Figure 16. The energies of both solvates, as well as the barrier between them, lie well below the transition state energies for C-H activation of either alkane. Since the alkane complexes rapidly interconvert, the relative selectivity for alkane activation is determined by the energy difference between the transition states of the two activation processes, from the Curtin-Hammett principle.[43] A critical requirement of this mechanistic hypothesis is that interchange of alkane complexes occurs rapidly -- and therefore cannot proceed by full dissociation of alkane from the metal center to regenerate "naked" Cp*Rh(CO).

We are intrigued by the results that C-H activation of methane and ethane proceeds much more slowly than do the activation reactions of cyclohexane and neopentane. We find this surprising since previous work has indicated that relative rates for oxidative addition should follow the order 1° > 2° > 3°.[43] By extension, the C-H bonds in CH_4 and C_2H_6 should react rapidly. If the mechanism in Scheme III is accepted, then in liquid Kr, either the metal-alkane complexes of methane and ethane are of lower energy than the corresponding complexes of cyclohexane and neopentane, slowing the C-H activation of

these two small alkanes, or else the transition state for C-H insertion lies higher in energy for the methane and ethane solvates. Further work will be required to address this question.

5.6. Conclusions. We find that photolysis of $Cp^*Rh(CO)_2$ in liquified krypton at T = 153-193K produces a monocarbonyl intermediate which, when generated in the presence of the alkanes cyclohexane and neopentane, reacts to form products assigned as the metal alkyl hydrides formed by C-H bond activation. A large kinetic isotope effect is observed. The rate of reaction is proportional to the concentration of added alkane only at low substrate concentrations, and levels off at higher concentrations. We can fit the alkane concentration dependence of the rate by a model which posits a pre-equilibrium to exist between a rare-gas- and an alkane-solvate of the rhodium monocarbonyl. We think of the alkane solvate as having a nearly complete C-H bond. The actual C-H bond cleavage is thought to occur in a second, intramolecular step, in which the alkane-solvated monocarbonyl isomerizes to the alkyl hydride product. By fitting the concentration and temperature dependences of the C-H activation to this model, we obtain barriers to C-H activation in the second step of about 5 kcal mol^{-1}, while the alkane solvate is 0-2 kcal mol^{-1} more stable than the Kr-solvate.

Notes and References

[1]For reviews on this subject, see: (a) Muetterties, E. L. *Chem. Soc. Revs.* **1983**, *12*, 283. (b) Shilov, A. E. *Activation of Saturated Hydrocarbons by Transition Metal Complexes*; D. Riedel Publishing Co.: Dordrecht, 1984. (c) Bergman, R. G. *Science (Washington, D. C.)*, **1984**, *223*, 902.(d) Crabtree, R. H. *Chem. Rev.* **1985**, *85*, 245. (e) Halpern, J. *Inorg. Chim. Acta*, **1985**, *100*, 41. (f) Graham, W. A. G. *J. Organomet. Chem.* **1986**, *300*, 81.

[2](a) Janowicz, A. H.; Bergman, R. G. *J. Am. Chem. Soc.* **1982**, *104*, 352. (b) Janowicz, A. H.; Bergman, R. G. *J. Am. Chem. Soc.* **1983**, *105*, 3429. (c) Buchanan, J. M.; Stryker, J. M.; Bergman, R. G. *J. Am. Chem. Soc.* **1986**, *108*, 1537. (d) Periana, R. A.; Bergman, R. G. *J. Am. Chem. Soc.* **1986**, *108*, 7332. (e) Hoyano, J. K.; Graham, W. A. G. *J. Am. Chem. Soc.* **1982**, *104*, 3723. (f) Ghosh, C. K.; Graham, W. A. G. *J. Am. Chem. Soc.* **1987**, *109*, 4726. (g) Jones, W. D.; Feher, F. J. *J. Am. Chem. Soc.* **1984**, *106*, 1650. (h) Jones, W. D.; Feher, F. J. *Acc. Chem. Res.* **1989**, *22*, 91.

[3]Sponsler, M. B.; Weiller, B. H.; Stoutland, P. O.; Bergman, R. G. *J. Am. Chem. Soc.* **1989**, *111*, 6891.

[4]Belt, S. T.; Duckett, S. B.; Helliwell, M.; Perutz, R. N., submitted to *J. Chem. Soc., Chem. Commun.*

[5]For an early review of work in liquid inert solutions, see: Bulanin, M. O. *J. Mol. Struct.* **1973**, *19*, 59.

[6]The diffusion constant for Kr in liquid Kr at 160 K is 5.6×10^{-5} cm^2 s^{-1} [Cowgill, D. F.; Norberg, R. E. *Phys. Rev. B* **1976**, *13*, 2773], while that for Kr in cyclohexane at 298 K is 3.57×10^{-5} cm^2 s^{-1} [Chen, S. H.; Davis, H. T. *J. Chem. Phys.* **1981**, *75*, 1422]. The dielectric constant for liquid Kr is 1.67 at 126 K [Sinnock, A. C.; *J. Phys. C* **1980**, *13*, 2375] while it is 2.023 for cyclohexane at 293 K.

[7](a) Maier, W. B., II; Poliakoff, M.; Simpson, M. B.; Turner, J. J. *J. Chem. Soc., Shem. Commun.* **1980**, 587. (b) Maier, W. B., II; Poliakoff, M.; Simpson, M. B.; Turner, J. J. *J. Mol. Struct.* **1982**, *80*, 83. (c) Simpson, M. B.; Poliakoff, M.; Turner, J. J.; Maier, W. B., II; McLaughlin, J. G. *J. Chem. Soc., Chem. Commun.* **1983**, 1355. (d) Turner, J. J.; Simpson, M. B.; Poliakoff, M.; Maier, W. B., II *J. Am. Chem. Soc.* **1983**, *105*, 3898. (e) Turner, J. J.; Simpson, M. B.; Poliakoff, M.; Maier, W. B., II; Graham, M. A. *Inorg. Chem.* **1983**, *22*, 911. (f) Gadd, G. E.; Poliakoff, M.; Turner, J. J. *Inorg. Chem.* **1984**, *23*, 630. (g) Upmacis, R. K.; Gadd, G. E.; Poliakoff, M.; Simpson, M. B.; Turner, J. J.; Whyman, R.; Simpson, A. F. *J. Chem. Soc., Chem. Commun.* **1985**, 27. (h) Gregory, M. F.; Jackson, S. A.; Poliakoff, M.; Turner, J. J. *J. Chem. Soc., Chem. Commun.* **1986**, 1175. (i) Upmacis, R. K.; Poliakoff, M.; Turner, J. J. *J. Am. Chem. Soc.* **1986**, *108*, 3645. (j) Gadd, G. E.; Poliakoff, M.; Turner, J. J. *Organometallics* **1987**, *6*, 391.

[8](a) Andrea, R. R.; Luyten, H.; Vuurman, M. A.; Stufkens, D. J.; Oskam, A. *Appl. Spectrosc.* **1986**, *40*, 1184. (b) Andrea, R. R.; Vuurman, M. A.; Stufkens, D. J.; Oskam,

A. *Recl. Trav. Chim. Pays-Bas* **1986**, *105*, 372. (c) Haddleton, D. M.; Perutz, R. N.; Jackson, S. A.; Upmacis, R. K.; Poliakoff, M. *J. Organomet. Chem.* **1986**, *311*, C15. (d) Howdle, S. M.; Poliakoff, M. *J. Chem. Soc., Chem. Commun.* **1989**, 1099.

[9]Belt, S. T.; Grevels, F.-W.; Klotzbuecher, W. E.; McCamley, A.; Perutz, R. N., submitted to *J. Am. Chem. Soc.*

[10]Wasserman, E. P.; Bergman, R. G.; Moore, C. B. unpublished results.

[11]Marx, D. E.; Lees, A. J. *Inorg. Chem.* **1988**, *27*, 1121.

[12](a) Haddleton, D. M. *J. Organomet. Chem.* **1986**, *311*, C21. (b) Rest, A. J.; Whitwell, I.; Graham, W. A. G.; Hoyano, J. K.; McMaster, A. D. *J. Chem. Soc., Dalton Trans.* **1987**, 1181. (c) Bloyce, P. E.; Rest, A. J.; Whitwell, I.; Graham, W. A. G.; Holmes-Smith, R. *J. Chem. Soc., Chem. Commun.* **1988**, 846.

[13]See review: Weitz, E. *J. Phys. Chem.* **1987**, *91*, 3945.

[14](a) Moore, B. D.; Simpson, M. B.; Poliakoff, M.; Turner, J. J. *J. Chem. Soc., Chem. Commun.* **1984**, 973. (b) Dobson, G. R.; Hodges, P. M.; Healy, M. A.; Poliakoff, M.; Turner, J. J.; Firth, S.; Asali, K. J. *J. Am. Chem. Soc.* **1987**, *109*, 4218.; (c) Belt, S. T.; Haddleton, D. M.; Perutz, R. N.; Smith, B. P. H.; Dixon, A. J. *J. Chem. Soc., Chem. Commun.* **1987**, 1347. (d) Creaven, B. S.; Dixon, A. J.; Kelly, J. M.; Long, C.; Poliakoff, M. *Organometallics*, **1987**, *6*, 2600.

[15]Kang, J. W.; Maitlis, P. M. *J. Organomet. Chem.* **1971**, *26*, 393.

[16]Booth, B. L.; Haszeldine, R. N.; Hill, M. *J. Chem. Soc. A* **1969**, 1299.

[17]Hogan, T. R.; Steele, D. *J. Mol. Struct.* **1986**, *141*, 315.

[18]Stal'makhova, I. P.; Finkel', A. G.; Sverdlov, L. M. *Zh. Prikl. Spekt.* **1969**, *11*, 132.

[19]Saeki, S.; Mizuno, M.; Kondo, S. *Spectrochim. Acta A* **1976**, *32A*, 403.

[20]Kondo, S.; Saeki, S. *Spectrochim. Acta A* **1973**, *29A*, 735.

[21]Penner, S. S.; Weber, D. *J. Chem. Phys.* **1951**, *19*, 807.

[22]Shimizu, K.; Murata, H. *Bull. Chem. Soc. Jpn.* **1957**, *30*, 487.

[23]Hill, R.; Knox, A. R. *J. Chem. Soc., Dalton Trans.* **1975**, 2622.

[24]By using solutions of cyclohexane in CCl_4, we found that the intergrated absorption of the cyclohexane band at 1453 cm^{-1} FTIR is a linear function of concentration through concentrations which give peak absorbances larger than 2.5 (*i. e.*, saturated the spectrometer). Since we avoided peak absorbances above 2.5, we feel that the FTIR gave an accurate estimation of integrated IR absorbances.

[25]We assume largely non-interacting oscillators (no exciplexes).

[26](a) Beattie, W. H.; Maier, W. B., II; Freund, S. M.; Holland, R. F. *J. Phys. Chem.* **1982**, *86*, 4351. (b) Tokhadze, K. G.; Tkhorzhevskaya, N. A.; *J. Mol. Liquids*, **1986**, *32*, 11.

[27]See also: (a) Schauer, M. W.; Lee, J.; Bernstein, E. R. *J. Chem. Phys.* **1982**, *76*, 1982. (b) Rest, A. J.; Scurlock, R. G.; Wu, M. F. *Cryogenics* **1985**, *25*, 591.

[28](a) Simpson, M. B.; Poliakoff, M.; Turner, J. J.; Maier, W. B., II; McLaughlin, J. G. *J. Chem. Soc., Chem. Commun.* **1983**, 1355. (b) Fairhurst, S. A.; Morton, J. R.; Perutz, R. N.; Preston, K. F. *Organometallics*, **1984**, *3*, 1389.

[29]See, for example: (a) Simon, J. D.; Peters, K. S. *Chem. Phys. Lett.* **1983**, *98*, 53. (b) Joly, A. G.; Nelson, K. A. *J. Phys. Chem.* **1989**, *93*, 2876. (c) Wang, L.; Zhu, X.; Spears, K. G. *J. Phys. Chem.* **1989**, *93*, 2.

[30]We assume that this interaction is dominated by dispersion forces.

[31]This assumption is not unreasonable given the resolution of the spectrometer (4 cm^{-1}) and the similar IR absorptions of Ar and methane complexes of $W(CO)_5$: see Reference 8b.

[32]Streett, W. B.; Staveley, L. A. K. *J. Chem. Phys.* **1971**, *55*, 2495.

[33]Fits to the data acquired at lower temperatures were not meaningful, as the scatter in the data was too large.

[34]See the following matrix isolation review: Perutz, R. N.; Turner, J. J. *J. Am. Chem. Soc.* **1975**, *97*, 4791.

[35]Bullock, R. M.; Headford, C. E. L.; Hennessy, K. M.; Kegley, S. E.; Norton, J. R. *J. Am. Chem. Soc.* **1989**, *111*, 3897.

[36]See, for example: Crabtree, R. H.; Holt, E. M.; Lavin, M.; Morehouse, S. M. *Inorg. Chem.* **1985**, *24*, 1986.

[37](a) Low, J. J.; Goddard, W. A., III *J. Am. Chem. Soc.* **1984**, *106*, 8321. (b) Saillard, J.-Y.; Hoffmann, R. *J. Am. Chem. Soc.* **1984**, *106*, 2006. (c) Ziegler, T.; Tschinke, V.; Fan, L.; Becke, A. D., submitted for publication.

[38]Ishikawa, Y.; Brown, C. E.; Hackett, P. A.; Rayner, D. M. *Chem. Phys. Lett.* **1988**, *150*, 506.

[39]See references in: Peters, K. S.; Snyder, G. J. *Science* **1988**, *241*, 1053.

[40](a) Madey, T. E.; Yates, J. T. *Surf. Sci.* **1978**, *76*, 397. (b) Hoffmann, F. M.; Felter, T. E.; Thiel, P. A.; Weinberg, W. H. *Surf. Sci.* **1983**, *130*, 173. (c) Hoffmann, F. M.; Upton, T. H. *J. Phys. Chem.* **1984**, *18*, 6209. (d) Avery, N. R. *Surf. Sci.* **1985**, *163*, 357.

[41]A similar estimate may also be found in: Stoutland, P. O.; Bergman, R. G.; Nolan, S. P.; Hoff, C. D. *Polyhedron* **1988**, *7*, 1429.

[42]Janowicz, A. H.; Periana, R. A.; Buchanan, J. M.; Kovac, C. A.; Stryker, J. M.; Wax, M. J.; Bergman, R. G. *Pure and Appl. Chem.* **1984**, *56*, 13.

[43]Hammett, L. P. *Physical Organic Chemistry: Reaction Rates, Equilibria, and Mechanisms*, 2nd Ed. New York: McGraw-Hill, 1970, p. 119.

Table 5.1. Parameters from the Linear Fits of Rates at Low Alkane Concentration[a]

A. Cyclohexane

T, K	$10^{-6}k_{ins}$[b], l mol^{-1} sec^{-1}
193	16.9
183	8.7
173	4.8
163	2.2
153	0.85

B. Neopentane

T, K	$10^{-6}k_{ins}$[b], l mol^{-1} sec^{-1}
193	10.6
183	4.6
173	1.8
163	0.90
153	0.26

[a]Concentrations of cyclohexane, neopentane less than 0.02 mol l^{-1}. [b]See Scheme I.

Table 5.2. Reaction of Cp*Rh(CO) with Cyclohexane in Liquid Krypton[a]

T^b, K	$10^{-3}k_2$, l mol^{-1} s^{-1}*	Kr, l mol^{-1}[c]	K*	$\ln(k_2)$†	$\ln(K)$†
193	690 ± 70	20.15	943 ± 24	13.44(10)	6.85(13)
183	313 ± 28	21.98	1151 ± 153	12.67(9)	7.05(13)
173	156 ± 13	23.44	1240 ± 155	11.96(9)	7.12(13)
163	65 ± 5	24.66	1612 ± 203	11.09(8)	7.39(13)
153	29 ± 3	25.73	1672 ± 300	10.27(11)	7.42(18)

[a]Parameters taken from fits of data to kinetic model in Scheme III; [b]Precision: ± 1K; [c]Concentration derived from a cubic spline fit to experimental data found in Reference 32. *Uncertainties are 1σ confidence limits. †Numbers in parentheses are 1σ error limits of last digit of value.

Table 5.3. Reaction of Cp*Rh(CO) with Neopentane in Liquid Krypton[a]

T[b], K	$10^{-3}k_2$, l mol^{-1} s^{-1}*	Kr, l mol^{-1}[c]	*K**	ln(k_2)†	ln(*K*)†
193	667 ± 62	20.15	452 ± 49	13.41(9)	6.12(11)
183	228 ± 24	21.98	699 ± 93	12.34(11)	6.55(13)
173	110 ± 19	23.44	667 ± 138	11.61(18)	6.50(21)
163	32 ± 2	24.66	1965 ± 297	10.37(7)	7.58(15)
153	13.4 ± 0.2	25.73	1931 ± 57	9.50(1)	7.56(3)

[a]Parameters taken from fits of data to kinetic model in Scheme III; [b]Precision: ± 1K; [c]Concentration derived from a cubic spline fit to experimental data found in Reference 32. *Uncertainties are 1σ confidence limits. †Numbers in parentheses are 1σ error limits of last digit of value.

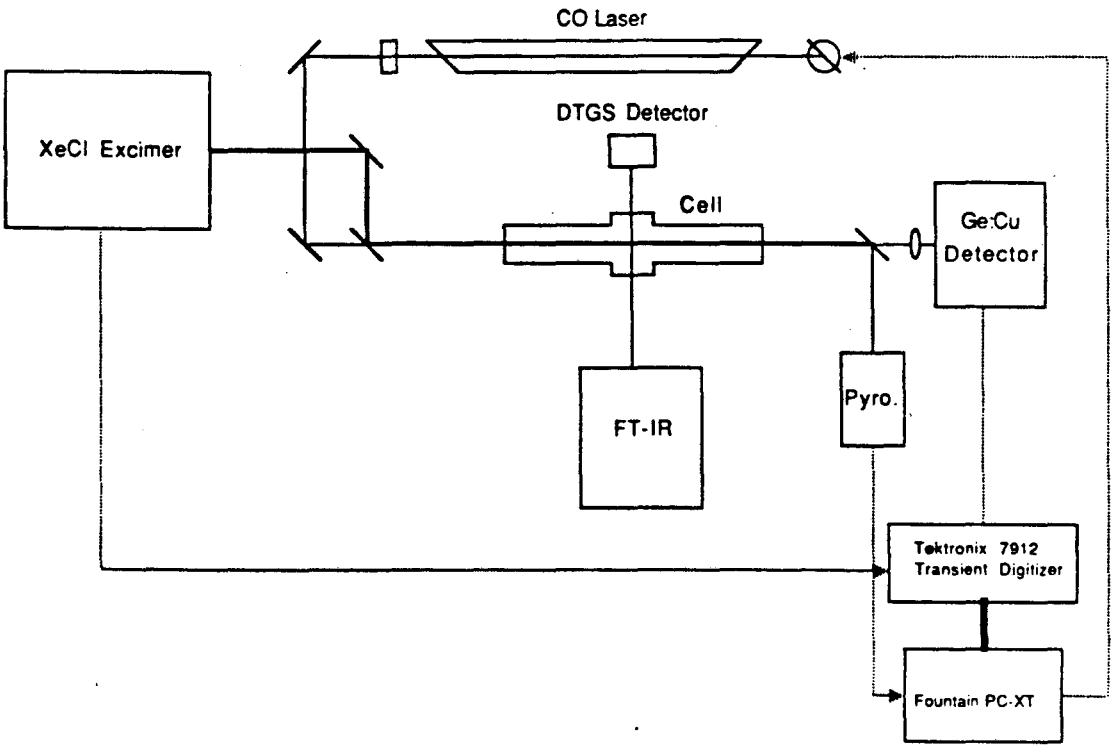

Figure 5-1. Schematic of the experiment. Solid lines show light beams, while dotted lines show electronic connections.

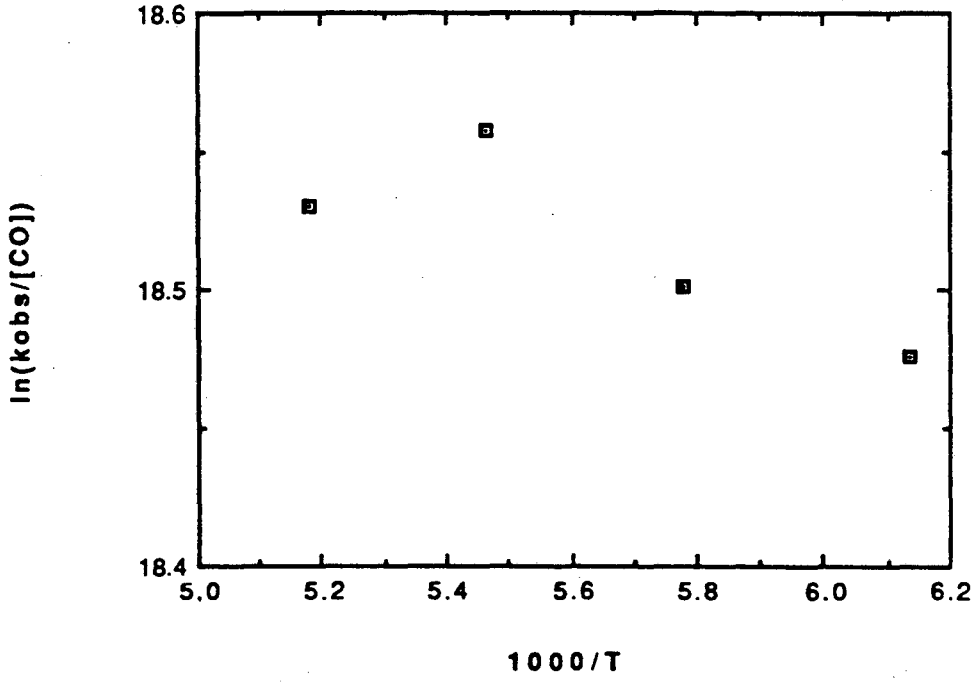

Figure 5-2. Plot of the logarithm of the quantity k_{obs} (the observed rate for the decay of the 1947 cm^{-1} transient) divided by the concentration of CO taken at four different temperatures.

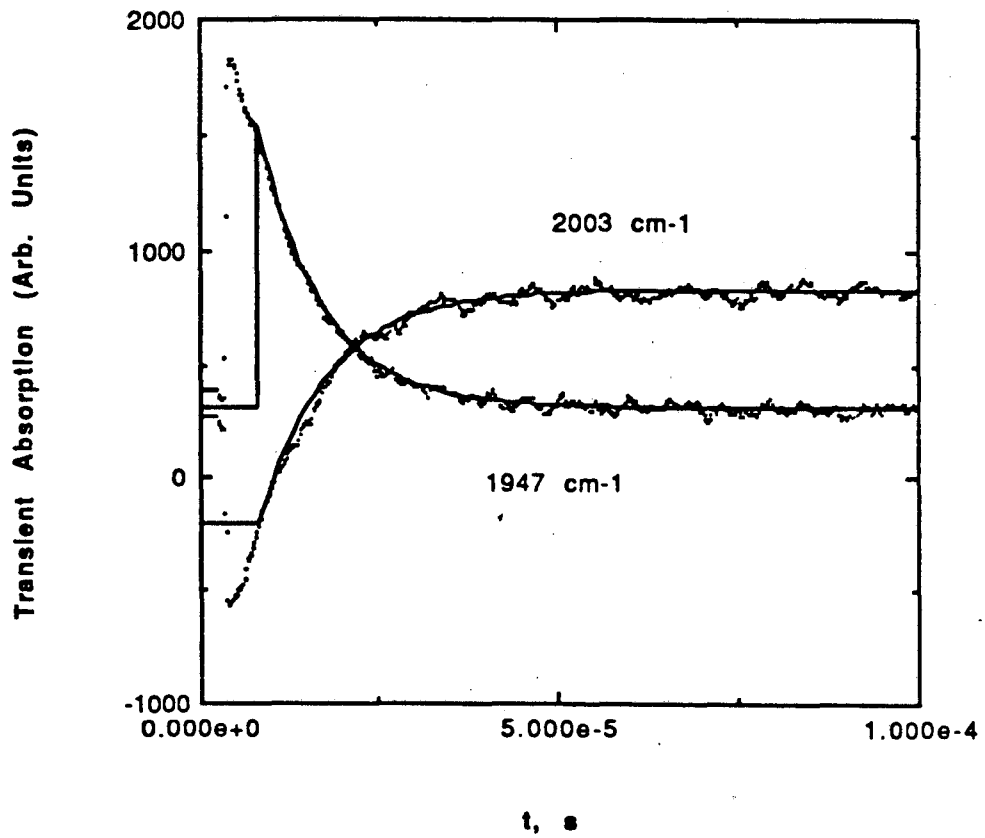

Figure 5-3. Two transient absorption traces showing the destruction of the monocarbonyl Cp*Rh(CO) monitored at 1947 cm^{-1} and the appearance of the alkyl hydride Cp*(CO)Rh(cyclohexyl)(H) observed at 2003 cm^{-1}. Solid lines are overlaid exponential fits to the data, with $k_{obs} = 1.1 \times 10^5\ s^{-1}$ for the decay and $1.0 \times 10^5\ s^{-1}$ for the growth.

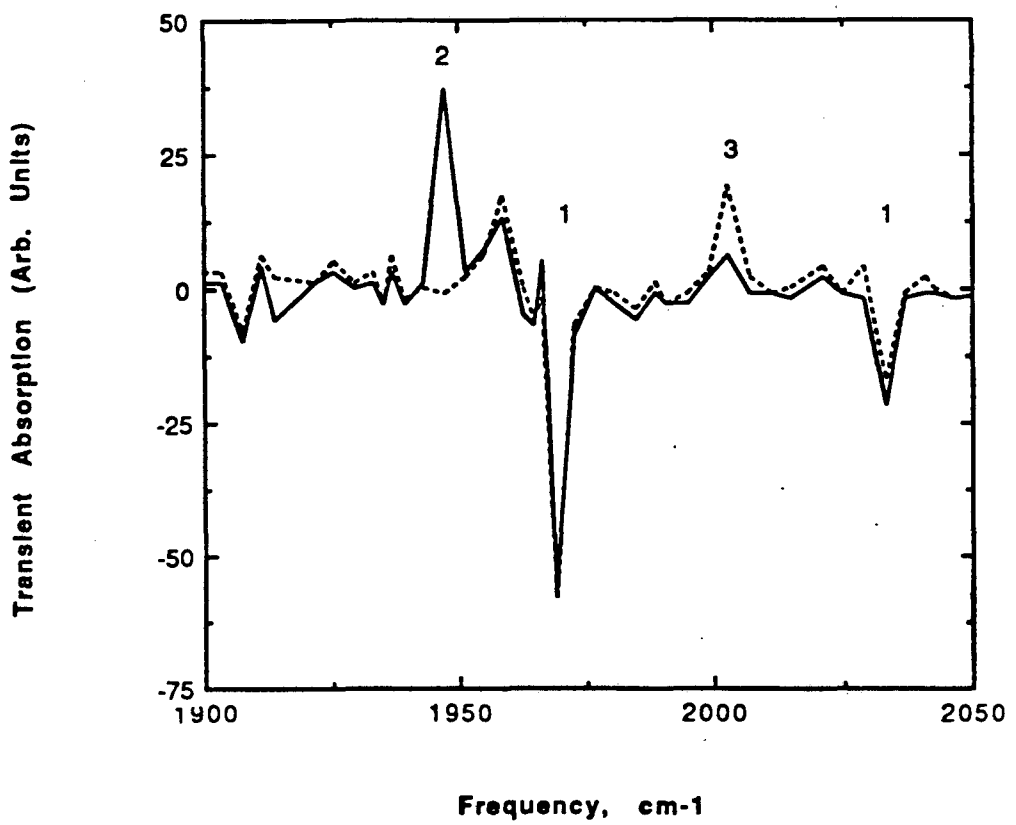

Figure 5-4. Transient absorption spectra from the photolysis of $Cp^*Rh(CO)_2$ in the presence of *ca.* 0.001 mol l^{-1} cyclohexane in liquid Kr at -90°C. Solid line: 30 μs after photolysis; dotted line: 120 μs after photolysis. Number labels on spectra refer to text. 11 point smoothing procedure applied to digitizer data. 1977 cm^{-1} trace subtracted from data to remove shock wave artifact.

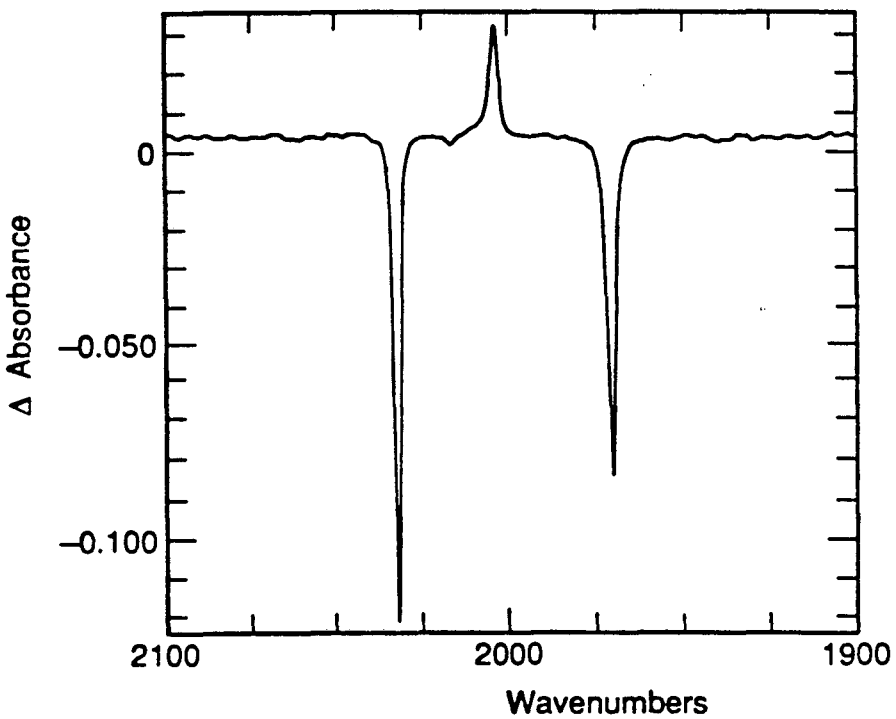

Figure 5-5. FTIR difference spectrum showing spectral changes after 5 min photolysis using a cw Hg lamp of a solution of *ca.* 0.012 cyclohexane in liquid Kr at -100°C.

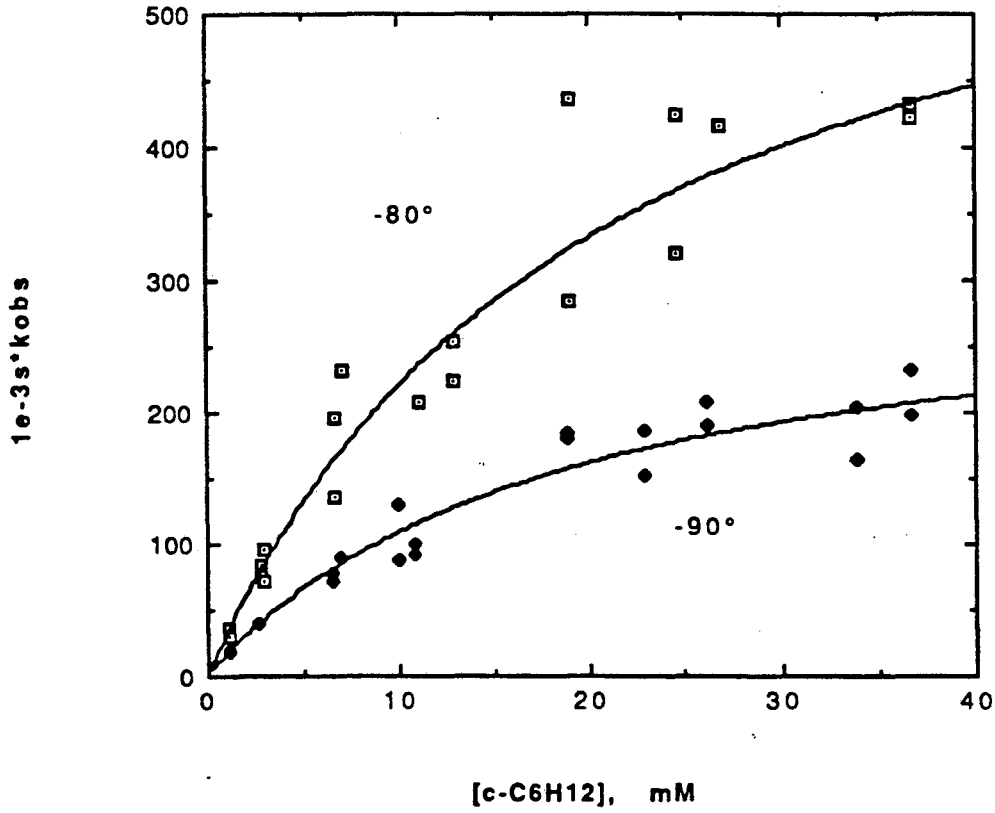

Figures 5-6. Dependence of the observed rate constants for the decay of the monocarbonyl and the appearance of the cyclohexyl hydride upon the concentration of cyclohexane, for five temperatures. Solid lines represent fits to the model given in Scheme III.

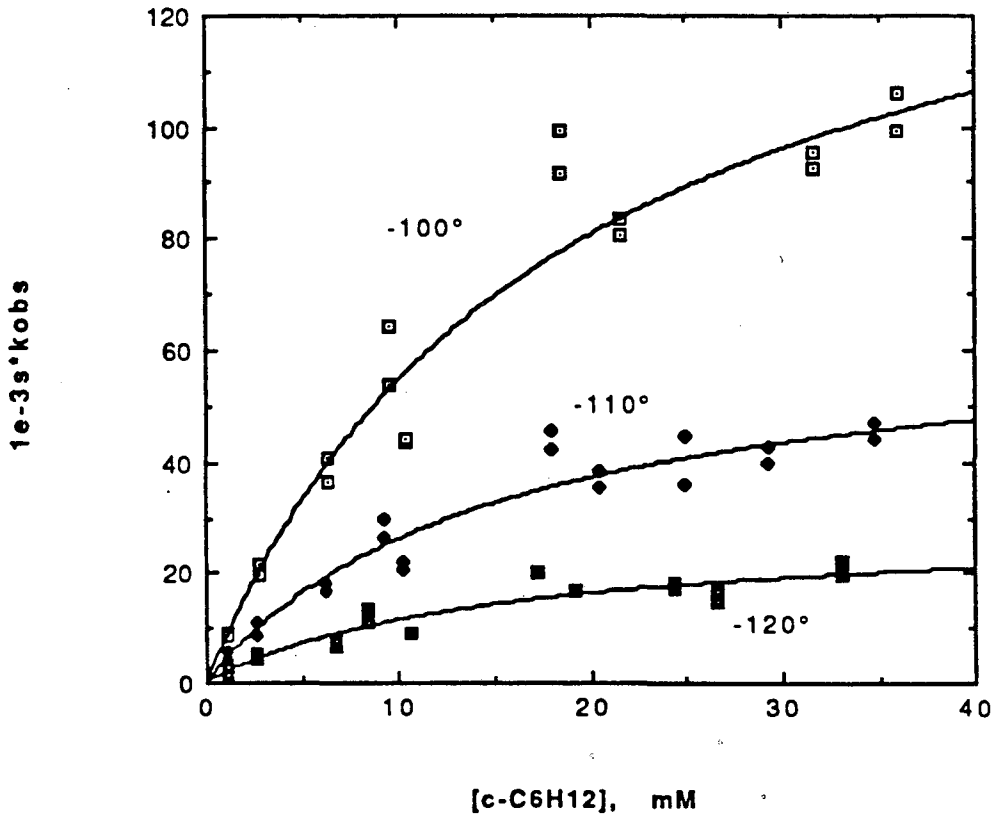

Figures 5-6 (continued)

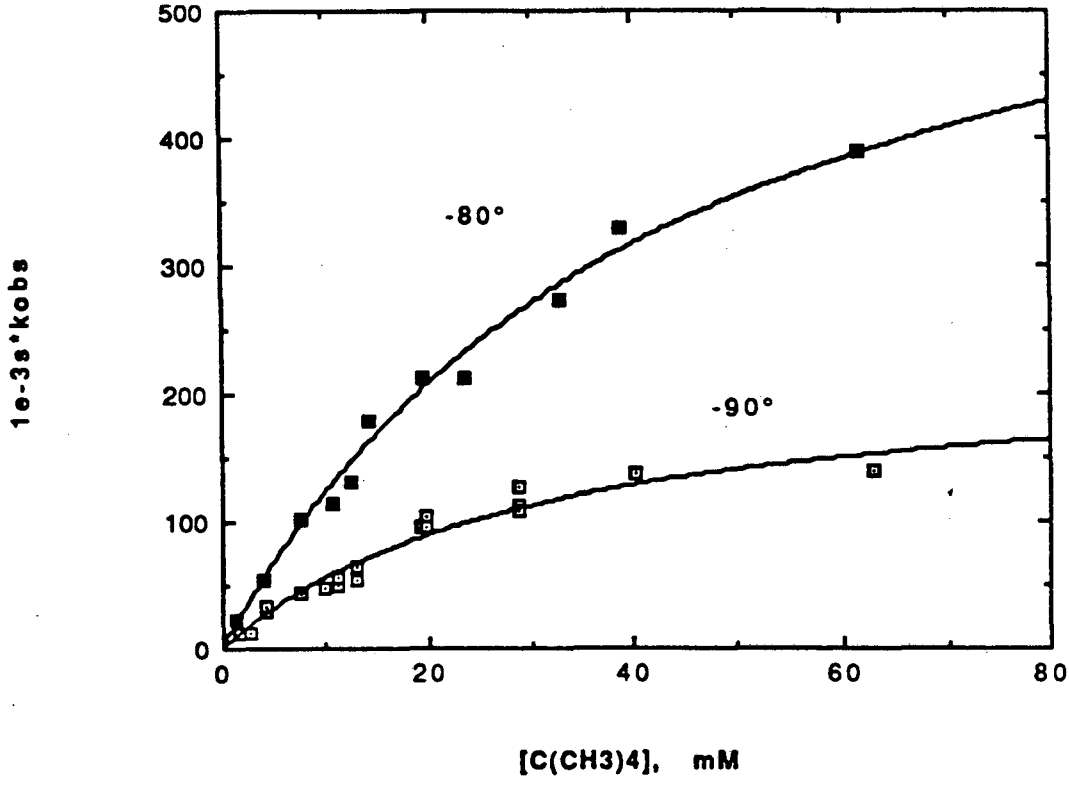

Figures 5-7. Dependence of the observed rate constants for the decay of the monocarbonyl and the appearance of the neopentyl hydride upon the concentration of neopentane, for five temperatures.

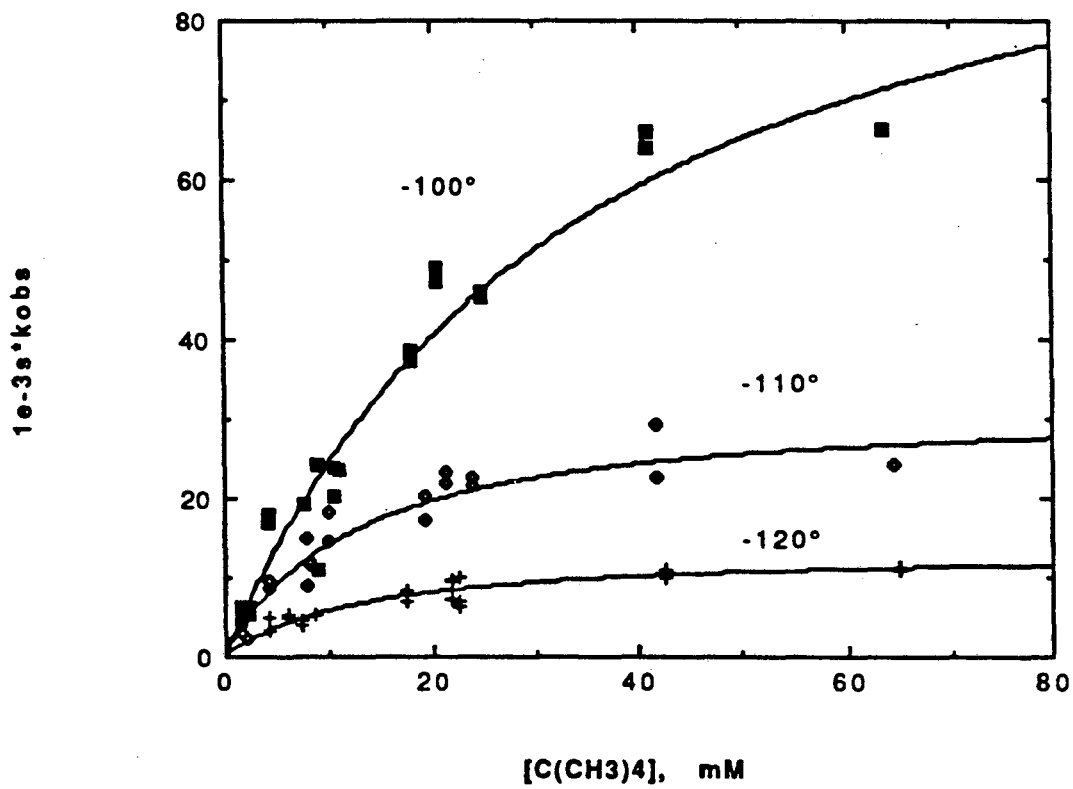

Figures 5-7. (continued)

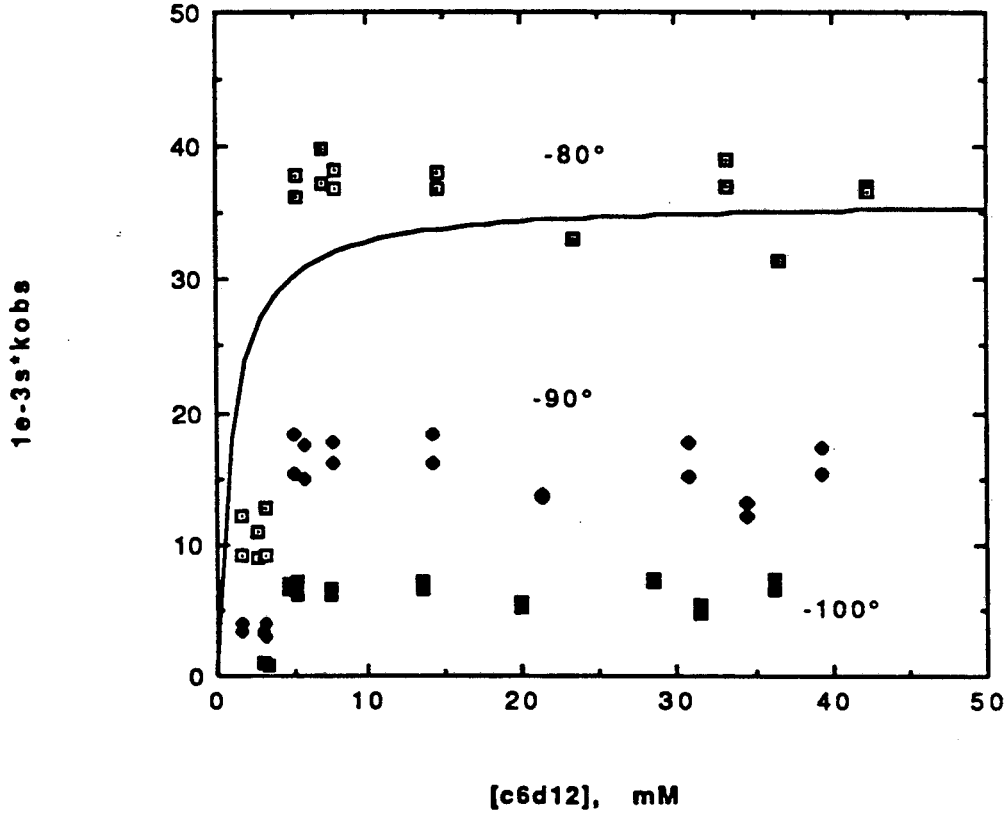

Figure 5-8. Dependence of the rate constant for C-D activation of cyclohexane-d_{12} upon c-C_6D_{12} concentration. See text for parameters of overlaid fit.

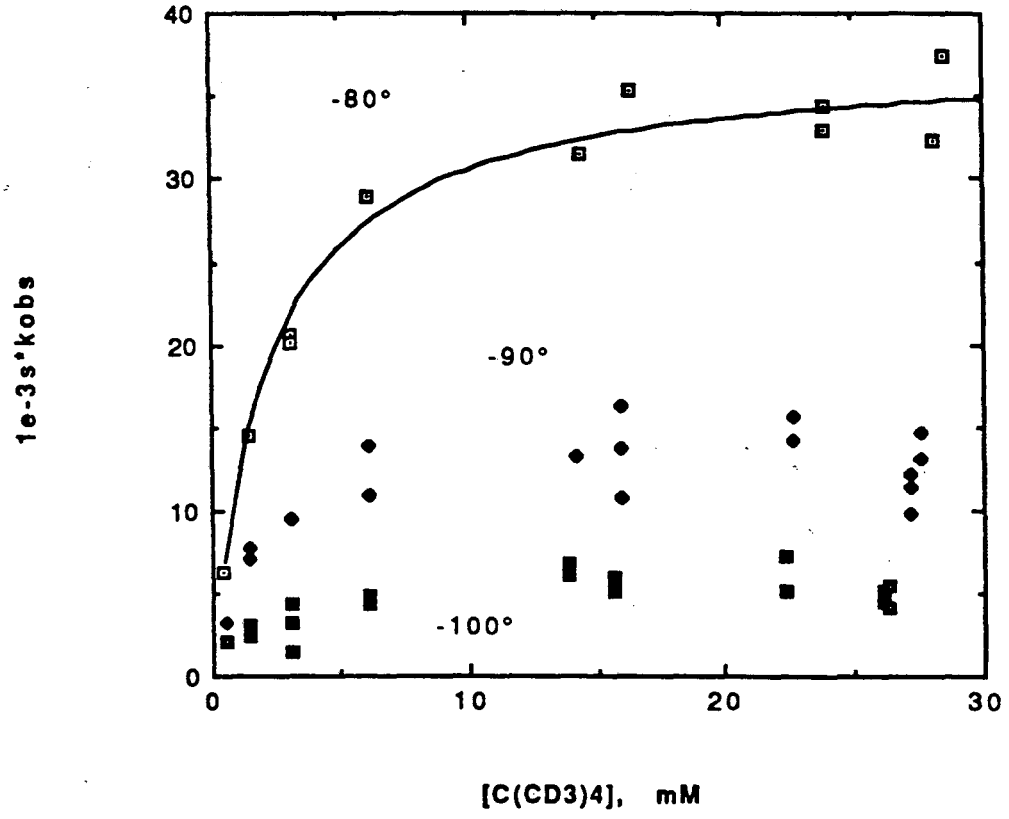

Figure 5-9. Dependence of the rate constant for C-D activation of neopentane-d_{12} upon $C(CD_3)_4$ concentration. See text for parameters of overlaid fit.

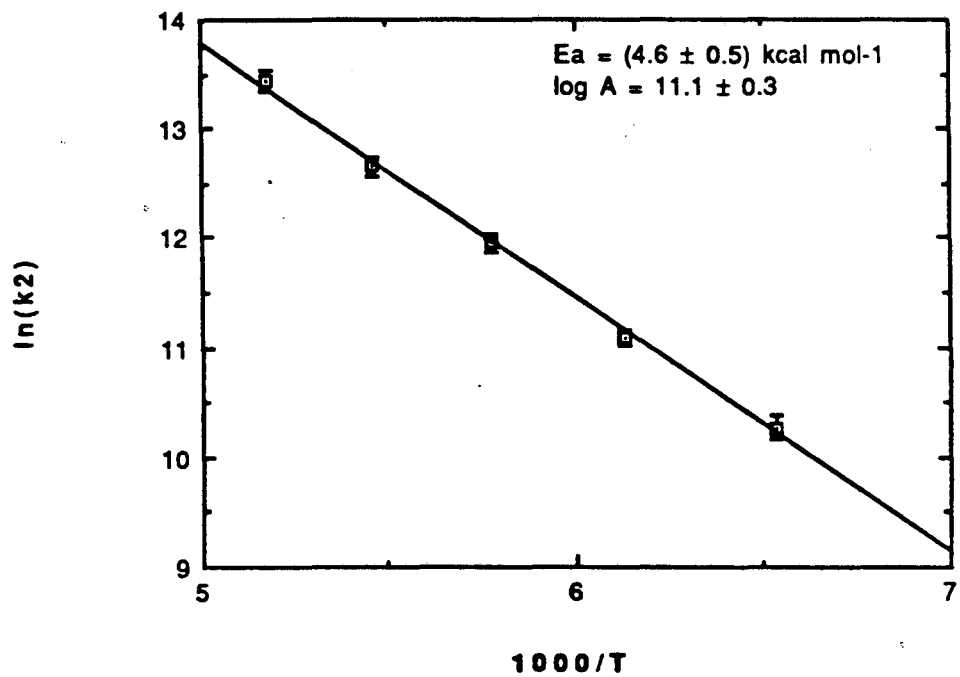

Figure 5-10. Arrhenius plot for derived values of k_2 for cyclohexane activation.

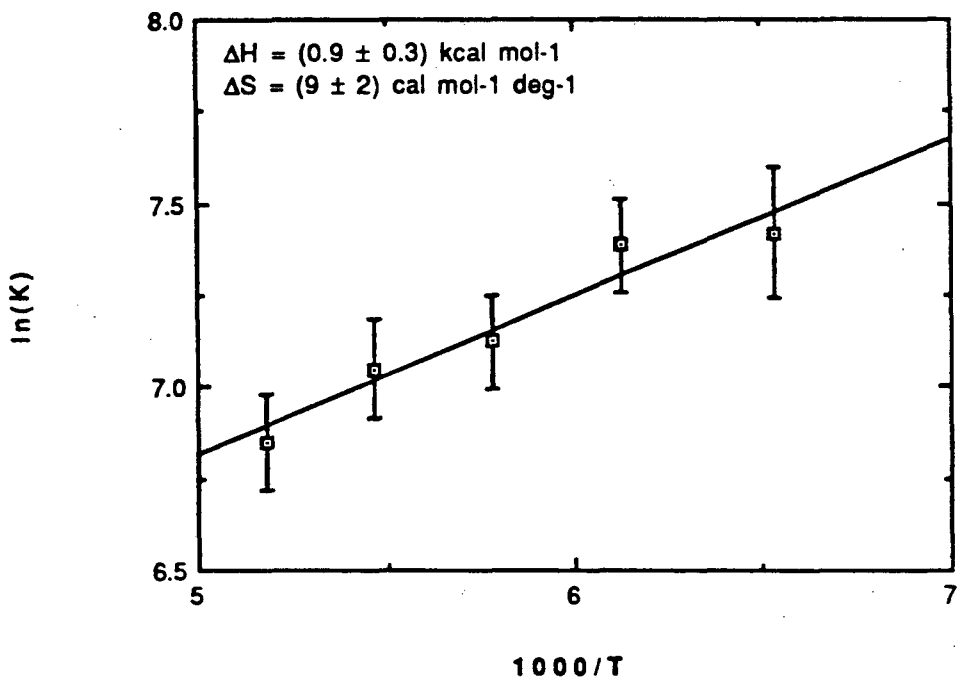

Figure 5-11. Plot of the logarithm of the equilibrium constant *K* versus 1000/T for cyclohexane.

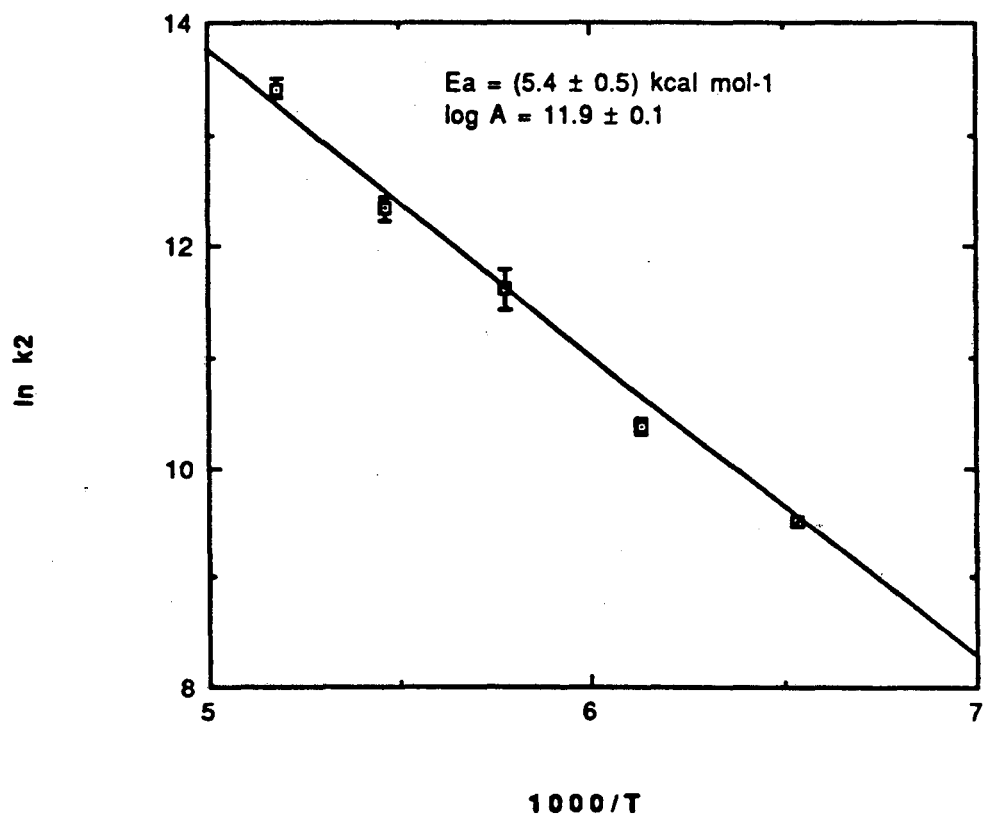

Figure 5-12. Arrhenius plot for derived values of k_2 for neopentane activation.

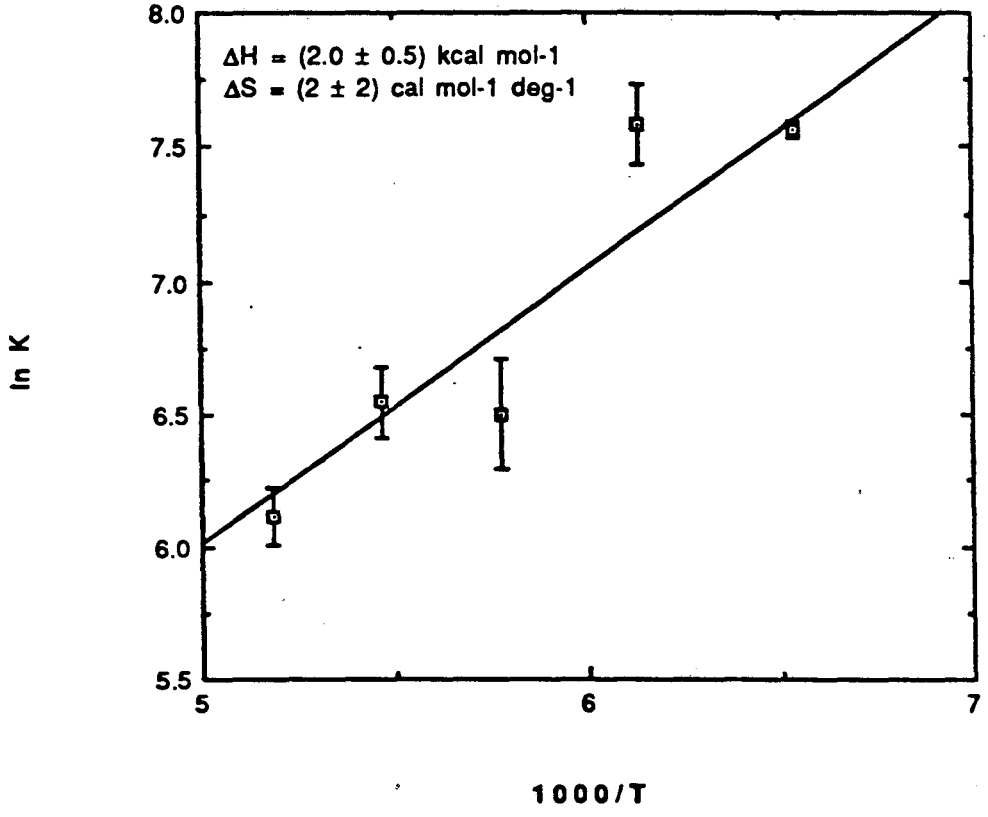

Figure 5-13. Plot of the logarithm of the equilibrium constant *K* versus 1000/T for neopentane.

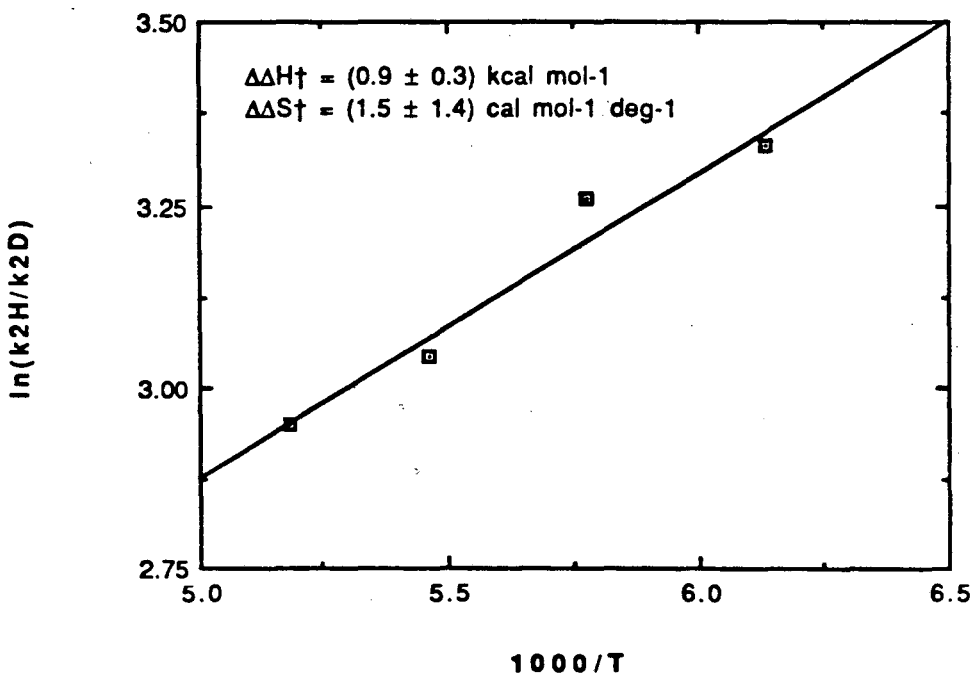

Figure 5-14. Plot of the logarithm of the ratio of k_2 values for cyclohexane-d_0 and cyclohexane-d_{12} versus 1000/T.

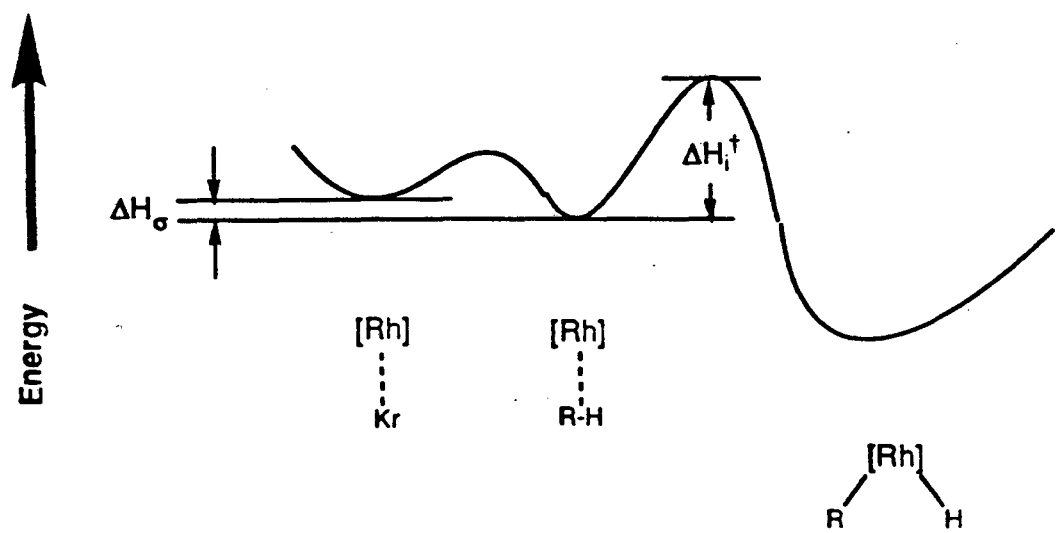

Figure 5-15. Diagram of energy versus reaction coordinate for alkane activation in liquid krypton. $\Delta H_i^{\dagger}$ represents the activation enthalpy for C-H activation in the intramolecular k_2 step, while ΔH_{σ} stands for the enthalpy of relative stabilization of the unsaturated Rh site by alkane over krypton.

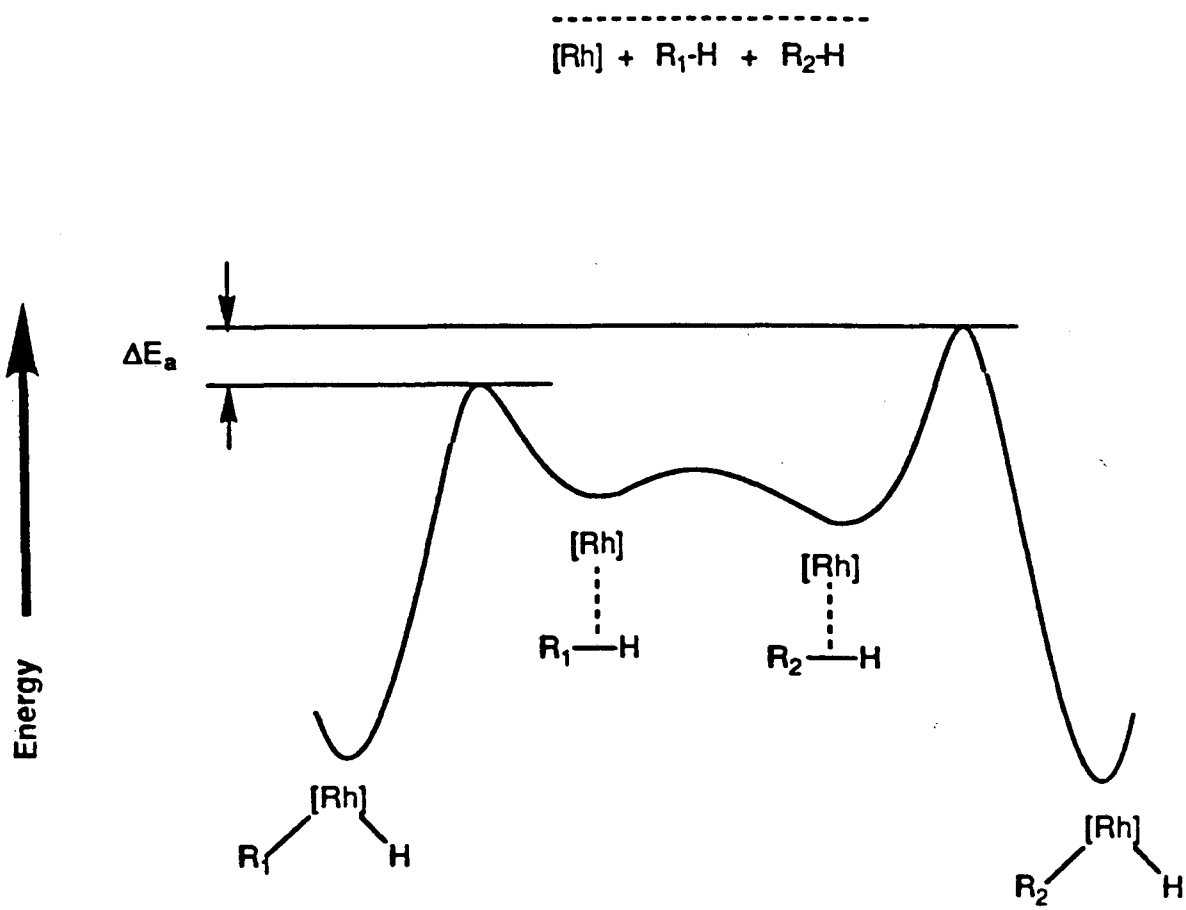

Figure 5-16. Potential energy diagram for C-H activation in liquid mixture of two alkanes.

Appendix 1.

Turbo-Pascal 3.0 program for operation of the CO laser, solenoids, and digitizer. The include files were written by Will Polik (except for GPIB and Dash-8 software), and are all in the Moore group software archives. The program C.PAS is essentially an extensively modified version of TAKEDATA.PAS, originally written by Will Polik.

```
(*{$U+,C+}*)

program c;
{.PA}

label
  BackToMain;

const
  IEEEStrLength = 50;
  {MAXIBBUF declared in TPDECL.PAS  to be $400}
  BoardNum = 0;
  BaseAddress = $300;
  IntLev = 2;

  LineFileName = 'LINEFILE.BNK';
  StartFileName = 'START.CFG';
  Minimum  :real = 0.10;
type
  IEEEString    = String[IEEEStrLength];
  DataArray     = Array[1..512] of Real;
  DataPointer   = ^DataArray;
  String50      = String[50];
  String80      = String[80];

var
  Key               : Integer;          {Menu option chosen
by user}
  Digitizer         : Integer;          {7912AD digitizer}
  Brd0              : Integer;          {GPIB Interface Board
in IBM PC}
  AveragedData      : Array[1..512] of Integer;   {Average of
8 traces}
  SummedData        : Array[1..512] of Real;      {Summed
data from N*8 traces}
  TimeBase          : Array[1..512] of Real;      {Time base
for plotting}
  Xdata             : DataPointer;      {Pointer to data for
plotting}
  YData             : DataPointer;      {Pointer to data for
```

```
plotting}
  TracesAdded       : Real;              {Total traces added
in SummedData}
  TracesSubtracted : Real;               {Total traces
subtracted in SummedData}
  VerticalScaleStr : IEEEstring;         {Vertical 7912AD
setting}
  VerticalUnitStr  : IEEEstring;         {Vertical Units,
e.g., Volts}
  HorizScaleStr    : IEEEstring;         {Horizontal 7912AD
setting}
  HorizUnitStr     : IEEEstring;         {Horizontal Units,
e.g., Seconds}
  HorizScale       : Real;               {Numerical Value of
HorizScaleStr}
  CursorX,CursorY  : Integer;            {Temporary cursor
position}
  DefaultDrive     : Char;               {Drive for data
storage}
  DefaultDirectory : String[15];         {Directory for data
storage}
  InputString      : String[20];
  Drive            : String[15];         {Default drive, full
name}
  Chanlo           : Integer;            {Selection of ref.
input channel}
  Ntr              : Integer;            {Number of shots per
trace}
  StepNum          : Integer;            {Stepper mike
"address"}
  NewFreq,                               {Frequency of line}
  NewPwr,                                {Chopped power of
laser}
  Freq2,TrialFreq   : Real;
  ErrCode,
  ErrCode3          : Integer;           {Dash-8 error codes}
  StartFreq         : Real;
  Volts             : Real;
  SavPwr            : Real;
  Suffix            : String[6];
  OldStep,
  Increment         : Integer;
  TrialStep         : Integer;
  Answer2           : Char;
  Sol1,Sol2,Okay2   : Boolean;
  LineArray         : Array[1..2,1..200] of Real;
  LineBankFile      : Text;
  LineNum           : Integer;
  j                 : Integer;
  StartFile         : Text;              {Start-up freq. of
laser}
  PwrArray          : Array[1..64] of Real;
```

```
  PwrSum              : Real;
  RepRate             : Real;
  Intern                 : Boolean;

{$I C:\TURBO\PASLIB\GRAPHLIB.TGT}
{Graphics Library}
{$I C:\TURBO\PASLIB\PLOTDATA.PRO}
{Plotting Routine}
{$I C:\TURBO\PASLIB\TPDECL.PAS}
{Pascal-GPIB Interface}
{$I C:\TURBO\PASLIB\KEY.PRO}
{ClearKeyPressed; & GetKeyPressed;}
{$I C:\TURBO\PASLIB\DISKFREE.FNC}
{DiskFree;}
{$I C:\TURBO\PASLIB\DIRLIST.PRO}                        {For
Directory List}
{$I C:\EPW\DASH8\TDASH8.MOD}                            {Dash-8
I/O Board Software}

var
  IEEEbuffer    : iobuf;                 {type iobuf declared
in TPDECL.PAS}
  RawData       : iobuf;                 {to be
Array[1..MAXIBBUF] of Char}
{.PA}

procedure Error; {checks IEEE interface}
const
  K64 : Real = 65536.0;
begin
Beep;
WriteLn;
Write('IEEE Interface Error Detected:  ');
case iberr of
  0:  WriteLn('DOS error');
  1:  WriteLn('Function requires GPIB-PC to be CIC');
  2:  WriteLn('No Listener or write function');
  3:  WriteLn('GPIB-PC not addressed correctly');
  4:  WriteLn('Invalid argument to function call');
  5:  WriteLn('GPIB-PC not System Controller as required');
  6:  WriteLn('I/O operation aborted');
  7:  WriteLn('Non-Existent GPIB-PC board');
  10: WriteLn('I/O started before previous operation
completed');
  11: WriteLn('No capability for operation');
  12: WriteLn('File System Error');
  14: WriteLn('Command Error during device call');
  15: WriteLn('Serial Poll status byte lost');
  16: WriteLn('SRQ stuck in on position');
  end; {of case}
WriteLn;
WriteLn('Copy Status Codes And Refer To National Instruments
```

```
GPIB-PC Manual:');
WriteLn('ibsta = ',ibsta+K64:5:0,'    iberr = ',iberr,'
  ibcnt = ',ibcnt);
WriteLn;
WriteLn('Start Program Again Or Re-Boot System.');
IBCLR(Digitizer);
IBLOC(Digitizer);
Halt;
end;
{.PA}

procedure LineSave; {records line addresses}
begin
Assign(StartFile, StartFileName);
Rewrite(StartFile);
WriteLn(StartFile,NewFreq:5:2);
WriteLn(StartFile,StepNum);
Close(StartFile);
end;

procedure ExitProgram;
var
  Ch : Char;
begin
Write('Are You Sure? (Y/N)');
Read(Kbd,Ch);
if UpCase(Ch) <> 'Y' then Key := 0;
LineSave;
end;
{.PA}

procedure ReadRef(var NewPwr : Real); {reads laser power}
var
  Dataval : Integer;
begin
d8_ains(BoardNum,Chanlo,Dataval,ErrCode3);
if ErrCode3 <> 0 then
WriteLn('Error Code ',ErrCode3)
else
  NewPwr := Dataval / 409.5;
if (NewPwr > 4.9) or (NewPwr < -4.9) then
  begin
  WriteLn('Power exceeded range.');
  WriteLn('Program exited.');
  exit;
  end;
end;

procedure Trigger; {internal excimer trigger control}

const
  C2Div = 2000;
```

```
var
  C1div,p : Integer;
  Ok2 : Boolean;

begin
Ok2 := False;
Repeat
Write('Enter the repetition rate (Hz):  ');
ReadLn(RepRate);
if (RepRate > 2) and (RepRate < 70) then Ok2 := True
Else WriteLn('Rate out of range.');
Until Ok2;
C1div := Round(500*2.38/RepRate);
d8_cset(0,2,C2div,ErrCode);
d8_cset(0,1,C1Div,ErrCode);
end;

procedure Squirt(OnOff : Integer); {controls flow solenoid}
var
  on,off,xtra : Integer;
begin
xtra := 0;
if Sol2 = True then
  xtra := 8;
on := 4 + xtra;
off := 0 + xtra;
if OnOff = 0 then
  begin
  d8_bous(BoardNum,on,ErrCode3);
  Delay(10);
  d8_bous(BoardNum,off,ErrCode3);
  end
else
  begin
  d8_bous(BoardNum,off,ErrCode3);
  Delay(10);
  d8_bous(BoardNum,on,ErrCode3);
  end;
if Sol1 = True then
  Sol1 := False
else Sol1 := True;
end;

procedure Blast(OnOff : Integer); {controls shutter
solenoid}
var
  on,off,xtra : Integer;
begin
xtra := 0;
if Sol1 = True then
  xtra := 4;
```

```
on := 8 + xtra;
off := 0 + xtra;
if OnOff = 0 then
  begin
  d8_bous(BoardNum,on,ErrCode3);
  Delay(10);
  d8_bous(BoardNum,off,ErrCode3);
  end
else
  begin
  d8_bous(BoardNum,off,ErrCode3);
  Delay(10);
  d8_bous(BoardNum,on,ErrCode3);
  end;
if Sol2 = True then
  Sol2 := False
else Sol2 := True;
end;

procedure WriteIEEE(Message: IEEEString); {sends IEEE
messages}
var
  i,MessageLength : Integer;
begin
MessageLength := Length(Message);
for i := 1 to MessageLength do
  IEEEbuffer[i] := Message[i];
IBWRT(Digitizer,IEEEbuffer,MessageLength);
if ((ibsta and ERR) <> 0) then error;
end;

procedure ReadIEEE(var Message: IEEEstring); {reads IEEE
messages}
var
  i : Integer;
begin
IBRD(Digitizer,IEEEbuffer,IEEEStrLength);
if ((ibsta and ERR) <> 0) then error;
Message[0] := Chr(ibcnt);
for i := 1 to ibcnt do
  Message[i] := IEEEbuffer[i];
end;

procedure AverageNShots; {averages 1-64 traces}
var
  i : Integer;
begin
if (Ntr = 1) then
  WriteIEEE('DIG SA,1');
if (Ntr = 2) then
  WriteIEEE('DIG SA,2');
if (Ntr = 4) then
```

```
  WriteIEEE('DIG SA,4');
if (Ntr = 8) then
  WriteIEEE('DIG SA,8');
if (Ntr = 16) then
  WriteIEEE('DIG SA,16');
if (Ntr = 32) then
  WriteIEEE('DIG SA,32');
if (Ntr = 64) then
  WriteIEEE('DIG SA,64');
WriteIEEE('READ SA');
IBRD(Digitizer,IEEEbuffer,3);
if ((ibsta and ERR) <> 0) then error;
if IEEEbuffer[1] <> '%'
then
  begin
  Beep;
  WriteLn('Incorrect Data Format Error.  Please Start
Program Again.');
  Halt;
  end;
IBRD(Digitizer,RawData,$400);
if ((ibsta and ERR) <> 0) then error;
IBRD(Digitizer,IEEEbuffer,2);
if ((ibsta and ERR) <> 0) then error;
if IEEEbuffer[2] <> ';'
then
  begin
  Beep;
  WriteLn('Incorrect Data Format Error.  Please Start
Program Again.');
  Halt;
  end;
for i := 1 to 512 do
  AveragedData[i] := 256*Ord(RawData[2*i-1]) +
Ord(RawData[2*i]);
end;
{.PA}

procedure DisplaySummedData; {displays data}
var
  i : Integer;
  Title,
  Xlabel,
  Ylabel,
  TA,TS   : GraphicsString;
begin
Xdata := Ptr(Seg(TimeBase),Ofs(TimeBase));
Ydata := Ptr(Seg(SummedData),Ofs(SummedData));
Xlabel := HorizUnitStr;
Ylabel := 'Counts';
Str(TracesAdded:8:0,TA); Str(TracesSubtracted:8:0,TS);
Title := 'Traces Added:'+TA+'          Traces
```

```
Subtracted:'+TS;
for i := 0 to 511 do
  TimeBase[i+1] := i*HorizScale/51.1;
EnterGraphics;
PlotData(188.89,130,900,930,Title,Xlabel,Ylabel,Xdata,Yda-
ta,512,0,0,0,0,'/D');
MoveScreen(337.5,0);
Delay(3000);
ExitGraphics;
end;
{.PA}

procedure Initialize; {initializes both GPIB and Dash-8
boards}
begin
InitGraphics;
TracesAdded := 0;
TracesSubtracted := 0;
DefaultDrive := 'C';
DefaultDirectory := ':\7912\DATA\';
Digitizer := IBFIND('DEV0');
if Digitizer < 0
then
  begin
  WriteLn('Initialization Error for IEEE Bus.');
  halt;
  end;
Brd0 := IBFIND('GPIB0');
if ((ibsta and ERR) <> 0) then error;
IBSIC(Brd0);
if ((ibsta and ERR) <> 0) then error;
IBCLR(Digitizer);
if ((ibsta and ERR) <> 0) then error;
IBLOC(Digitizer);
if ((ibsta and ERR) <> 0) then error;
Drive := DefaultDrive + DefaultDirectory;
WriteLn('Drive = ',Drive);
Sol1 := False;
Sol2 := False;
RepRate := 10;
Intern := True;
Chanlo := 0;
Ntr := 8;
d8_init(BoardNum,BaseAddress,IntLev,ErrCode);
d8_set_cntr_config(0,2,1,ErrCode);
d8_set_cntr_config(0,3,2,ErrCode);
d8_cset(0,2,2000,ErrCode);
d8_cset(0,1,119,ErrCode);
end;
{.PA}

procedure DigitizeDefects;
```

```
begin
WriteLn('Digitizing Defects...256 Traces...Please Wait...');

WriteIEEE('DIG DEF,256');
WriteIEEE('MODE TV');
IBLOC(Digitizer);
if ((ibsta and ERR) <> 0) then error;
end;
{.PA}

procedure AcquireNewTrace; {environment for AverageNShots}
var
  N,i,j,
  ErrorCode    : Integer;

begin
InputString := '';
Write('Input Number of Traces ( x 8) to be Averaged: ');
Repeat
  Read(InputString);
  if InputString = '' then InputString := ' ';
  Val(InputString,N,ErrorCode);
  if ErrorCode <> 0
  then
    begin
    Beep;
    WriteLn;
    WriteLn;
    Write('Please Try Again: ');
    end;
Until ErrorCode = 0;
if N <= 0 then exit;
if N > 40 then
  begin
  WriteLn('Are you sure you want to take ',N,' X 8 shots?');

  ReadLn(InputString);
  if (InputString <> 'y') or (InputString <> 'Y') then exit;

  end;
for i := 1 to 512 do
  SummedData[i] := 0;
Write('     Traces Completed:  ');
CursorX := WhereX; CursorY := WhereY;
WriteIEEE('VS1?'); ReadIEEE(VerticalScaleStr);
WriteIEEE('VU1?'); ReadIEEE(VerticalUnitStr);
WriteIEEE('HS1?'); ReadIEEE(HorizScaleStr);
WriteIEEE('HU1?'); ReadIEEE(HorizUnitStr);
Delete(VerticalScaleStr,1,4);
Delete(VerticalScaleStr,Length(VerticalScaleStr),1);
Delete(VerticalUnitStr,1,4);
Delete(VerticalUnitStr,Length(VerticalUnitStr),1);
```

```
Delete(HorizScaleStr,1,4);
Delete(HorizScaleStr,Length(HorizScaleStr),1);
Delete(HorizUnitStr,1,4);
Delete(HorizUnitStr,Length(HorizUnitStr),1);
if Pos('+',VerticalScaleStr)=1 then
Delete(VerticalScaleStr,1,1);
if Pos('+',HorizScaleStr)=1 then Delete(HorizScaleStr,1,1);
Val(HorizScaleStr,HorizScale,i);
WriteLn;
WriteLn;
Write('VerticalScale = ',VerticalScaleStr,'
',VerticalUnitStr);
GotoXY(40,WhereY);
WriteLn('HorizontalScale = ',HorizScaleStr,'
',HorizUnitStr);
squirt(1);
Delay(500);
Blast(1);
for j := 1 to N do
  begin
  AverageNShots;
  ReadRef(PwrArray[j]);
  GotoXY(CursorX,CursorY); Write(j);
  for i := 1 to 512 do
    SummedData[i] := SummedData[i] + AveragedData[i];
  end;
squirt(0);
Blast(0);
PwrSum := 0;
for j := 1 to N do
  PwrSum := PwrSum + PwrArray[j];
SavPwr := PwrSum/N;
WriteIEEE('MODE TV');
IBLOC(Digitizer);
if ((ibsta and ERR) <> 0) then error;
TracesAdded := N*Ntr;
TracesSubtracted := 0;
DisplaySummedData;
end;
{.PA}

procedure AverageAddlShots;
var
  InputString : String[20];
  N,i,j,
  ErrorCode   : Integer;
begin
if TracesAdded = 0
then
  begin
  Beep;
  WriteLn('Cannot Average Additional Traces Until New Trace
```

```
Is Taken');
  WriteLn;
  Write('Strike Any Key To Continue...');
  ClearKeyPressed;
  Repeat Until Keypressed;
  exit;
  end;
InputString := '';
Write('Input Number of Traces ( x ',Ntr,') to be Added: ');
Repeat
  Read(InputString);
  if InputString = '' then InputString := ' ';
  Val(InputString,N,ErrorCode);
  if ErrorCode <> 0
  then
    begin
    Beep;
    WriteLn;
    WriteLn;
    Write('Please Try Again: ');
    end;
Until ErrorCode = 0;
if N <= 0 then exit;
if N > 40 then
  begin
  WriteLn('Are you sure you want to take ',N,' X ',Ntr,'
shots?');
  ReadLn(InputString);
  if (InputString <> 'y') or (InputString <> 'Y') then exit;

  end;
Write('     Traces Completed:  ');
CursorX := WhereX; CursorY := WhereY;
squirt(1);
Delay(500);
Blast(1);
for j := 1 to N do
  begin
  AverageNShots;
  if ((ibsta and ERR) <> 0) then exit;
  ReadRef(PwrArray[Round(j+(TracesAdded/Ntr))]);
  GotoXY(CursorX,CursorY); Write(j);
  for i := 1 to 512 do
    SummedData[i] := SummedData[i] + AveragedData[i];
  end;
squirt(0);
Blast(0);
WriteIEEE('MODE TV');
IBLOC(Digitizer);
for j := 1 to N do
PwrSum := PwrSum + PwrArray[Round(j + (TracesAdded/Ntr))];
SavPwr := PwrSum/(N + (TracesAdded/Ntr));
```

```
TracesAdded := TracesAdded+N*Ntr;
DisplaySummedData;
end;
{.PA}

procedure SubtractPickup;
var
  InputString : String[20];
  N,i,j,
  ErrorCode   : Integer;
begin
if TracesAdded = 0
then
  begin
  Beep;
  WriteLn('Cannot Subtract Pickup Until New Trace Is
Taken');
  WriteLn;
  Write('Strike Any Key To Continue...');
  ClearKeyPressed;
  Repeat Until Keypressed;
  exit;
  end;
InputString := '';
Write('Input Number of Traces ( x ',Ntr,') to be Subtracted:
');
Repeat
  Read(InputString);
  if InputString = '' then InputString := ' ';
  Val(InputString,N,ErrorCode);
  if ErrorCode <> 0
  then
    begin
    Beep;
    WriteLn;
    WriteLn;
    Write('Please Try Again: ');
    end;
Until ErrorCode = 0;
if N <= 0 then exit;
if N > 40 then
  begin
  WriteLn('Are you sure you want to take ',N,' X ',Ntr,'
shots?');
  ReadLn(InputString);
  if (InputString <> 'y') or (InputString <> 'Y') then exit;

  end;
Write('     Traces Completed:  ');
CursorX := WhereX; CursorY := WhereY;
for j := 1 to N do
  begin
```

```
  AverageNShots;
  GotoXY(CursorX,CursorY); Write(j);
  for i := 1 to 512 do
    SummedData[i] := SummedData[i] - AveragedData[i];
  end;
WriteIEEE('MODE TV');
IBLOC(Digitizer);
if ((ibsta and ERR) <> 0) then error;
TracesSubtracted := TracesSubtracted+N*Ntr;
DisplaySummedData;
end;
{.PA}

function FileExist(var FileName : string50) : boolean;
var
  Fil : file;
begin
  assign(Fil,FileName);
  {$I-} reset(Fil) {$I+};
  FileExist := (IOresult = 0);
end; {of FileExist}

procedure StoreOnDisk;
type
  String50 = String[50];
var
  OutFile     : Text;
  OutFileName : string50;
  TitleString : string[80];
  OK          : boolean;
  Ch          : char;
  i           : Integer;

begin {of StoreOnDisk}
if TracesAdded = 0
then
  begin
  Beep;
  WriteLn('Cannot Store on Disk Until New Trace is Taken');
  WriteLn;
  Write('Strike Any Key To Continue...');
  ClearKeyPressed;
  Repeat Until Keypressed;
  exit;
  end;
  (*
repeat                                  {Check for room on
data disk}
  OK := false;
  if DiskFree(Drive) < 6
  then
    begin
```

```
    Beep;
    WriteLn('Insufficient Space on Disk ',DefaultDrive,'.
Please Insert New Disk');
    Write('and Strike Any Key When Ready...');
    ClearKeyPressed;
    Read(Kbd,Ch);
    end
  else
    OK := true;
until OK = true;
  *)
repeat                                    {Check if file
already exists}
  OK := false;
  Str((10*NewFreq):5:0,outfilename);
  Outfilename:=outfilename+suffix;
  OutFileName := Drive+OutFileName;
  if FileExist(OutFileName)
  then
    begin
    Beep;
    WriteLn;
    Write('File "',OutFileName,'" Already Exists; OK to
Overwrite (DESTROY)? (y/n)');
    ClearKeyPressed;
    Read(Kbd,Ch);
    WriteLn;
    if upcase(Ch)='Y' then OK:=true else OK:=false;
    end
  else OK := true;
  if OK
  then
    begin
    Assign(OutFile,OutFileName);
    Rewrite(OutFile);
    end;
  if not OK then exit;
until OK;
WriteLn(OutFile,SavPwr:5:3);
WriteLn(OutFile,TracesAdded:8:0);
WriteLn(OutFile,TracesSubtracted:8:0);
WriteLn(OutFile,VerticalScaleStr);
WriteLn(OutFile,VerticalUnitStr);
WriteLn(OutFile,HorizScaleStr);
WriteLn(OutFile,HorizUnitStr);
for i := 1 to 512 do
  WriteLn(OutFile,SummedData[i]:8:0);
Close(OutFile);
end; {of StoreOnDisk}
{.PA}

procedure ChangeDefault;
```

```
var
  InputString : String[50];
begin
InputString := '';
WriteLn;
WriteLn;
WriteLn('To Keep Current Program Defaults, Strike Enter
Key');
WriteLn;
WriteLn('Current Default Drive for Data:  ',DefaultDrive);
Repeat
  WriteLn;
  Write('New Default Drive: ');
  ReadLn(InputString);
  if InputString <> '' then DefaultDrive := InputString[1];
  DefaultDrive := UpCase(DefaultDrive);
  if not (DefaultDrive in ['A','B','C'])
  then
    begin
    Beep;
    WriteLn;
    WriteLn('"',DefaultDrive,'" is Not a Valid Drive; Must
be "A", "B", or "C"');
    end;
  Until DefaultDrive in ['A','B','C'];
if DefaultDrive = 'C' then DefaultDirectory :=
':\7912\DATA\';
Drive := DefaultDrive + DefaultDirectory;
end;
{.PA}

procedure ViewTrace;

var
  ViewFileName    :  String[50];
  ExitFlag        :  Boolean;
  i               :  Integer;
  Title,
  Xlabel,
  Ylabel          :  GraphicsString;
  Timebase,
  Waveform        :  Array[1..512] of Real;
  Trace           :  Array[1..512] of Real;
  LetMeOut        :  Char;

procedure Translate; {turns file into plot data}

var
  i : Integer;
  InFile : text;

begin
```

```
Assign(InFile,ViewFileName);
Reset(InFile);
ReadLn(InFile);
ReadLn(InFile);
ReadLn(InFile);
ReadLn(InFile);
ReadLn(InFile);
ReadLn(InFile,HorizScale);
ReadLn(InFile);
for i := 1 to 512 do
  ReadLn(InFile,Trace[i]);
Close(InFile);
end;

begin                          {of ViewTrace}
ExitFlag := False;
Repeat
ClrScr;
Write('Filename:  ');
ReadLn(ViewFileName);
ChDir('C:\7912\DATA');
if (FileExist(ViewFileName) = True) then
  begin
  ExitFlag := True;
  Translate;
  for i := 1 to 512 do
    begin
    Waveform[i] := Trace[i];
    Timebase[i] := (i-1)*HorizScale/51.1;
    end;
  Xdata := Ptr(Seg(Timebase),Ofs(Timebase));
  Ydata := Ptr(Seg(Waveform),Ofs(Waveform));
  InitGraphics;
  EnterGraphics;
  SetColor(15);

PlotData(188.89,130,900,930,ViewFileName,'SECONDS','COUNTS'-
,Xdata,Ydata,512,0,0,0,0,'/D');
  MoveScreen(337.5,0);
  Delay(2000);
  ExitGraphics;
  end
Else
  begin
  WriteLn('File does not exist on ',Drive,'.');
  WriteLn('Strike any key to continue.');
  Writeln;
  Repeat until KeyPressed;
  Write('Do you wish to exit? (y/n)  ');
  ReadLn(LetMeOut);
  if (LetMeOut = 'y') or (LetMeOut = 'Y') then ExitFlag :=
True;
```

```
  end;
Until (ExitFlag = True);
ChDir('C:\7912');
end;

procedure Rectify1(InStep : Integer; var OutFreq : Real);
{turns step number into frequency}

const
  Wander = 35;

var
  i : Integer;
  Diff : Real;
  OutStep : Integer;

begin
Diff := abs(LineArray[2,1] - InStep);
TrialFreq := LineArray[1,1];
for i := 1 to LineNum do
  begin
  if (abs(LineArray[2,i] - InStep) < Diff) then
    begin
    OutFreq := LineArray[1,i];
    OutStep := Round(LineArray[2,i]);
    Diff := abs(LineArray[2,i] - InStep);
    end;
  end;
if (abs(OutStep - InStep) > Wander) then
  begin
  WriteLn('Cannot find true line freq. within ',Wander,'
steps.');
  write('Enter your guess for the frequency:  ');
  ReadLn(OutFreq);
  end;
end;

procedure Rectify2(InFreq : Real; var OutStep : Integer);
{reverse of rectify1}

var
  i : Integer;
  OutFreq : Real;
  Diff2 : Real;

begin
Diff2 := abs(LineArray[1,1] - InFreq);
for i := 1 to LineNum do
  begin
  if (abs(LineArray[1,i] - InFreq) < Diff2) then
    begin
    OutStep := Round(LineArray[2,i]);
```

```
    Diff2 := abs(LineArray[1,i] - InFreq);
    end;
  end;
end;

procedure MoveStep(Outputval : Integer); {moves laser
grating one step}

var
  ErrCode2 : Integer;
begin
d8_bous(BoardNum,0,ErrCode2);
if (ErrCode2 <> 0) then
  begin
  WriteLn('Error Code in MoveStep :  ',ErrCode2);
  end
else
  begin
  d8_bous(BoardNum,Outputval,ErrCode2);     {production of}
  Delay(10);                                {TTL pulse for}
  d8_bous(BoardNum,0,ErrCode2);             {StepperMike}
  Delay(10);
  If (outputval=1) then stepnum:=stepnum+1;   {increment or}

  If (outputval=2) then stepnum:=stepnum-1;   {decrement
stepnum}
  end;
end;

procedure tweak; {maximizes laser power by tweaking grating}
const
  Backtrack = 15;
  TweakScan = 30;

var
  i,j,jMax : Integer;
  TweakArray : Array[1..TweakScan] of Real;
  TweakDir : Integer;
  OutRef : Real;
  MaxTweak : Real;

begin
j := Backtrack;
for i := 1 to j do {go back past the beginning of the line}
  MoveStep(2);
MaxTweak := 0; {initialize maximization param}
for j := 1 to TweakScan do
  begin
  Delay(50);
  ReadRef(OutRef);            {create an array of powers
while}
  TweakArray[j] := OutRef;    {passing through the line
```

```
 }
  if (OutRef > MaxTweak) then
    begin
    jMax := j;              {record where in the array maximum
found and}
    MaxTweak := OutRef;     {update the maximization param.
         }
    end;
  MoveStep(1);
  end;
for i := 1 to Abs(jMax - TweakScan) do   {go back to maximum
 }
  MoveStep(2);
ReadRef(NewPwr);
Rectify1(StepNum,NewFreq);
LineSave;                   {save the line on disk}
end;

procedure BigMove(Input : Real); {moves from one freq. to
another}

var
  BigTrialStep,
  bigdir,i       : Integer;

begin
  BigDir := 1;
  OldStep := StepNum;
  if (Input<NewFreq) then BigDir := 2;
  rectify2(Input,BigTrialStep);
  for i := 1 to abs(StepNum-BigTrialStep) do begin
    MoveStep(BigDir);
  end;
  tweak;
end;

procedure LaserMenu(var StepNum : Integer; var NewFreq :
Real);
{all of the laser control procedures are nested within}
const
  Slope = 31.7;  {change this}
  Criterion = 0.05;

var
  KeyA,MoveVal,
  Dir2,i            :Integer;
  Freq2,Intercept   :Real;
  StepFlag,Okay     : Boolean;
  InputString       : String[20];

procedure Steptofreq;       {generates trialfreq}
begin
```

```
 TrialFreq:=Increment/slope + NewFreq;
end;

procedure ManuStep; {allows for step-by-step moving of
grating}
var
  Key          : Char;
  StepX,StepY  : Integer;

begin
ClearKeyPressed;
ClrScr;
OldStep := StepNum;
GotoXY(10,10);
WriteLn('Press "f" to go up, "r" to go down, and <ESC> to
exit.');
GotoXY(10,15);
WriteLn('Step number ',Stepnum:4);
ReadRef(NewPwr);
GotoXY(10,22);
StepToFreq;
WriteLn('Volts = ',NewPwr:5:2,'     Approx. Freq. =
',TrialFreq:5:2,' cm^-1');
Repeat
  Read(Kbd,Key);
    Case Key of
      #102 :  MoveStep(1);
      #114 :  MoveStep(2);
      #27  :  WriteLn('ManuStep exited.');
    end;
   Increment := StepNum - OldStep;
   GotoXY(10,15);
   WriteLn('Step number ',Stepnum:4);
   ReadRef(NewPwr);
   GotoXY(10,22);
   StepToFreq;
   WriteLn('Volts = ',NewPwr:5:2,'     Approx. Freq. =
',TrialFreq:5:2,' cm^-1');
  Until (Key = #27);
  rectify1(StepNum,NewFreq);
end;

procedure LineMove(MovDir : Integer); {moves up or down one
laser line}

const
  MoveOff=40;

var
  i : Integer;
  PrePwr,
  Power        : Real;
```

```
  oldmovdir : Integer;

begin
   OldStep:=StepNum;
   for i:=1 to MoveOff do begin
      MoveStep(movdir);
   end;
   repeat
     MoveStep(movdir);
     ReadRef(power);
   until (power>minimum) or (abs(oldstep-stepnum)>800);
{won't go further}
   if (abs(oldstep-stepnum)>800) then
     begin
     WriteLn('Cannot find next line.  Returning to previous
line.');
     oldmovdir := movdir;
     if oldmovdir = 1 then movdir := 2;
     if oldmovdir = 2 then movdir := 1;
     for i := 1 to 800 do
       MoveStep(movdir);
     end
   else
     begin
     tweak;
     end;
end;

procedure ChParam;
var
  Choice : Integer;
  oldsol1,oldsol2,oldintern : Boolean;
  solkey : Integer;

begin
Repeat
  ClearKeyPressed;
  ClrScr;
  WriteLn('                MENU FOR CHANGING PARAMETERS');
  WriteLn;
  WriteLn;
  WriteLn('1.)  Frequency: ',NewFreq:5:2,' cm^-1');
  WriteLn('2.)  Step Number: ',StepNum);
  if Sol1 = True then
    WriteLn('3.)  Solenoid 1 Status: Open')
  else
    WriteLn('3.)  Solenoid 1 Status: Closed');
  if Sol2 = True then
    WriteLn('4.)  Solenoid 2 Status: Open')
  else
    WriteLn('4.)  Solenoid 2 Status: Closed');
  WriteLn('5.)  Spectrum Suffix: ',Suffix);
```

```
  WriteLn('6.)  Change minimum voltage (Presently =
',minimum:4:2,').');
  if Intern then
    WriteLn('7.)  Triggering mode:  Internal.  Rep. Rate:
',RepRate:5:0)
  else
    WriteLn('7.)  Triggering mode:  External.');
  WriteLn('8.)  Reference Input Channel:  ',Chanlo+1);
  WriteLn('9.)  Number of shots per trace:  ',Ntr);
  WriteLn('a.)  Exit this menu.');
  GotoXY(10,22);
  Write('Enter your choice:  ');
  GetKeyPressed(Choice);
  GotoXY(10,22);
  Case Choice of
    49 : begin
         Write('Input frequency:  ');
         ReadLn(NewFreq);
         end;
    50 : begin
         Write('Input step number:  ');
         ReadLn(StepNum);
         end;
    51 : begin
         ClearKeyPressed;
         WriteLn('Strike <ENTER> to toggle solenoid status,
any other key to leave');
         WriteLn('in current status.');
         GetKeyPressed(solkey);
         if solkey = 13 then
           begin
           oldsol1 := sol1;
           if oldsol1 = False then sol1 := true;
           if oldsol1 = True then sol1 := false;
           end;
         end;
    52 : begin
         ClearKeyPressed;
         WriteLn('Strike <ENTER> to toggle solenoid status,
any other key to leave');
         WriteLn('in current status.');
         GetKeyPressed(solkey);
         if solkey = 13 then
           begin
           oldsol2 := sol2;
           if oldsol2 = False then sol2 := true;
           if oldsol2 = True then sol2 := false;
           end;
         end;
    53 : begin
         Write('Input suffix:  ');
         ReadLn(Suffix);
```

```
          end;
    54:   begin
          ClrScr;
          WriteLn('Enter the minimum power, in volts,');
          Write('that each laser line must have:  ');
          ReadLn(Minimum);
          end;
    55 : begin
          ClearKeyPressed;
          WriteLn('Strike <ENTER> to toggle trigger status,
any other key to leave');
          WriteLn('in current status.');
          GetKeyPressed(solkey);
          if solkey = 13 then
            begin
            oldintern := intern;
            if oldintern = False then intern := true;
            if oldintern = True then intern := false;
            end;
          if Intern then Trigger;
          end;
    56 : begin
          Repeat
          ClearKeyPressed;
          Write('Enter the new reference input channel (1,2,
or 3):  ');
          ReadLn(Chanlo);
          Chanlo := Chanlo - 1;
          Until Chanlo in [0,1,2];
          end;
    57 : begin
          Repeat
          ClearKeyPressed;
          Write('Enter the new number of shots per trace
(1,2,4,8,16,32, or 64):  ');
          ReadLn(Ntr);
          Until Ntr in [1,2,4,8,16,32,64];
          end;
    97 : exit;

    Else Beep;
  end;
Until (Choice = 97);
end;  {of menu for changing parameters}

begin     {main laser tuning program}
   Intercept:=stepnum-(slope*newfreq);
   Repeat
    ClrScr;
    GotoXY(20,5);
    WriteLn('                LASER MENU');
    WriteLn;
```

```
    WriteLn('1.)  Go up one line.');
    WriteLn('2.)  Go down one line.');
    WriteLn('3.)  Go to specific frequency.');
    WriteLn('4.)  Maximize power at this line.');
    WriteLn('5.)  Manually move the laser grating.');
    WriteLn('6.)  Change solution in cell.');
    WriteLn('7.)  Change parameters.');
    WriteLn('8.)  Go to a specific step number.');
    WriteLn('9.)  Open shutter.');
    WriteLn('a.)  View files in data directory.');
    WriteLn('b.)  View trace stored on disk.');
    WriteLn('c.)  Exit this menu.');
    ClearKeyPressed;
      GotoXY(10,22);
      ReadRef(NewPwr);
      Delay(100);
      WriteLn('Step number:  ',StepNum:4,'     Freq:
',NewFreq:6:2,' cm^-1    Power:  ',NewPwr:6:2);
    GetKeyPressed(KeyA);
    Case KeyA of
      49:  LineMove(1);
      50:  LineMove(2);
      51:  begin
           GotoXY(10,23);
           Okay := False;
           Repeat
           Write('Enter the frequency (in cm^-1) you wish to
go to:  ');
           ReadLn(TrialFreq);
           if (TrialFreq > 2100) or (TrialFreq < 1750) then
             begin;
             WriteLn('Target freq. out of range.');
             Exit;
             end;
           Okay := true;
           if (TrialFreq > 2055) or (TrialFreq < 1800) then
             begin
             WriteLn('Are you sure? (y/n) ');
             ReadLn(InputString);
             if (InputString <> 'y') or (InputString <> 'Y')
then Okay := true;
             end;
           Until Okay;
           BigMove(TrialFreq);
           end;
      52:  Tweak;
      53:  ManuStep;
      54:  begin
           squirt(1);
           GotoXY(10,23);
           WriteLn('Strike any key to stop flow.');
           repeat
```

```
            until KeyPressed;
            squirt(0);
            end;
      55:   ChParam;
      56:   begin
            Write('Enter the step number destination:  ');
            ReadLn(TrialStep);
            StepFlag := True;
            if (TrialStep < -7000) or (TrialStep > 6000) then

              begin
              StepFlag := False;
              WriteLn('Step number out of range.');
              Delay(500);
              end;
            if (StepFlag = True) then
              begin
              Dir2 := 1;
              if (StepNum > TrialFreq) then
                Dir2 := 2;
              for i := StepNum to TrialStep do
                MoveStep(Dir2);
              rectify1(StepNum,NewFreq);
              end;
            end;
      57:   begin
            Blast(1);
            GoToXY(10,23);
            WriteLn('Strike any key to close shutter.');
            Repeat
            until KeyPressed;
            Blast(0);
            end;
      97,65:  begin
              ClrScr;
              ChDir('C:\7912\DATA');
              DirectoryList('*.*');
              GotoXY(10,20);
              WriteLn('Strike any key to continue.');
              Repeat until keypressed;
              ChDir('C:\7912');
              end;
      98,66:  ViewTrace;
      99,67:  exit;
      Else  Beep;
    end;
   Until Key in [99,67];
   end;

procedure Scan; {automated laser scan.  Acquires N traces,
subtracts same number with shutter closed, stores data, for
all lines above threshold power in range specified.}
```

```
var
  BeginFreq,EndFreq : Real;
  Ans3 : Char;
  ScanShots : Integer;
  PreStep : Integer;
  ScanDir : Integer;
  i,k,l : Integer;
  Differ : Real;
  ErrorCode   : Integer;

begin
ClrScr;
GotoXY(10,10);
WriteLn('Automated laser scan:  Enter parameters below.');
GotoXY(15,12);
Okay2 := False;
Repeat
  Write('Starting frequency:  ');
  ReadLn(BeginFreq);
  if (BeginFreq > 2100) or (BeginFreq < 1800) then
    WriteLn('Invalid Starting Frequency!')
  else Okay2 := True;
Until Okay2;
Okay2 := False;
GotoXY(15,14);
Repeat
  Write('Ending frequency:  ');
  ReadLn(EndFreq);
  if (EndFreq > 2100) or (EndFreq < 1800) then
    WriteLn('Invalid Ending Frequency!')
  else Okay2 := True;
Until Okay2;
Okay2 := False;
GotoXY(15,16);
Write('Display traces? (y/n) ');
ReadLn(Ans3);
GotoXY(15,18);
InputString := '';
WriteLn('Enter the number of multiples of eight shots to be
acquired -- ');
GotoXY(15,19);
Write('an equal number will be subtracted:  ');
Repeat
  Read(InputString);
  if InputString = '' then InputString := ' ';
  Val(InputString,ScanShots,ErrorCode);
  if ErrorCode <> 0
  then
    begin
    Beep;
    WriteLn;
```

```
    WriteLn;
    Write('Please Try Again: ');
    end;
Until ErrorCode = 0;
if ScanShots <= 0 then exit;
GotoXY(15,22);
Repeat
  WriteLn('Enter the minimum power, in volts,');
  GotoXY(15,23);
  Write('that each laser line must have:  ');
  ReadLn(Minimum);
  if (Minimum > 5) or (Minimum < -5) then
    WriteLn('Invalid Minimum!')
else Okay2 := True;
Until Okay2;
ClrScr;
GotoXY(5,5);
WriteLn('Laser now being moved to starting line.');
BigMove(BeginFreq);
ClrScr;
ReadRef(NewPwr);
GotoXY(15,10);
ClearKeyPressed;
WriteLn('Strike any key to get out of the automated scan.');

GotoXY(10,22);
WriteLn('Step number:  ',StepNum:4,'     Wavelength:
',NewFreq:6:2,'    Power:  ',NewPwr:6:2);
k := 1;
Repeat
  begin
  Differ := NewFreq - LineArray[1,k];
  k := k + 1;
  end
Until Round(Differ) = 0;
k := k - 1;
if (BeginFreq < EndFreq) then
  ScanDir := 1
else ScanDir := 2;
Repeat
  begin
  PreStep := StepNum;
  GotoXY(10,22);
  WriteLn('Step number:  ',StepNum:4,'     Wavelength:
',NewFreq:6:2,'    Power:  ',NewPwr:6:2);
  ReadRef(NewPwr);
  if NewPwr > Minimum then
    begin
    for l := 1 to 512 do
      SummedData[l] := 0;
    WriteIEEE('VS1?'); ReadIEEE(VerticalScaleStr);
    WriteIEEE('VU1?'); ReadIEEE(VerticalUnitStr);
```

```
    WriteIEEE('HS1?'); ReadIEEE(HorizScaleStr);
    WriteIEEE('HU1?'); ReadIEEE(HorizUnitStr);
    Delete(VerticalScaleStr,1,4);
Delete(VerticalScaleStr,Length(VerticalScaleStr),1);
    Delete(VerticalUnitStr,1,4);
Delete(VerticalUnitStr,Length(VerticalUnitStr),1);
    Delete(HorizScaleStr,1,4);
Delete(HorizScaleStr,Length(HorizScaleStr),1);
    Delete(HorizUnitStr,1,4);
Delete(HorizUnitStr,Length(HorizUnitStr),1);
    if Pos('+',VerticalScaleStr)=1 then
Delete(VerticalScaleStr,1,1);
    if Pos('+',HorizScaleStr)=1 then
Delete(HorizScaleStr,1,1);
    Val(HorizScaleStr,HorizScale,1);
    squirt(1);
    Delay(500);
    Blast(1);
    GotoXY(10,5); Write('Adding Shots.');
    for j := 1 to ScanShots do
      begin
      AverageNShots;
      ReadRef(PwrArray[j]);
      GotoXY(CursorX,CursorY); Write(j);
      for l := 1 to 512 do
        SummedData[l] := SummedData[l] + AveragedData[l];
      end;
    squirt(0);
    Blast(0);
    PwrSum := 0;
    for j := 1 to ScanShots do
      PwrSum := PwrSum + PwrArray[j];
    SavPwr := PwrSum/ScanShots;
    WriteIEEE('MODE TV');
    IBLOC(Digitizer);
    if ((ibsta and ERR) <> 0) then error;
    TracesAdded := ScanShots*Ntr;
    GotoXY(10,5);ClrEol;Write('Subtracting Shots.');
    TracesSubtracted := 0;
    for j := 1 to ScanShots do
      begin
      AverageNShots;
      for l := 1 to 512 do
        SummedData[l] := SummedData[l] - AveragedData[l];
      end;
    WriteIEEE('MODE TV');
    IBLOC(Digitizer);
    if ((ibsta and ERR) <> 0) then error;
    TracesSubtracted := TracesSubtracted+ScanShots*Ntr;
    if (Ans3 = 'y') or (Ans3 = 'Y') then
      DisplaySummedData;
    WriteLn('Storing on diskette.');
```

```
    StoreOnDisk;
    end;
  if (ScanDir = 1) and (NewFreq > EndFreq) then exit;
  if (ScanDir = 2) and (NewFreq < EndFreq) then exit;
  if ScanDir = 1 then
    k := k + 1
  else k := k - 1;
  if (k < 1) then k := 1;
  if (k > LineNum) then k := LineNum;
  for i := 1 to Abs(PreStep - Round(LineArray[2,k])) do
begin
    MoveStep(ScanDir);
  end;
  tweak;
  end
Until KeyPressed;
end;

procedure Help;
var
  Ch : Char;
begin
WriteLn('Not available.');
end;

procedure DisplayMenu;
begin
ClrScr;
WriteLn('        CO SCANNING AND 7912AD DATA ACQUISITION
MENU');
WriteLn;
WriteLn('     F1  -  Digitize Defects');
WriteLn('     F2  -  Acquire New Trace');
WriteLn('     F3  -  Average Additional Traces');
WriteLn('     F4  -  Subtract Pickup');
WriteLn('     F5  -  Store on Disk');
WriteLn('     F6  -  Change Default Parameters');
WriteLn('     F7  -  Help');
WriteLn('     F8  -  Exit Program');
WriteLn('     F9  -  Change CO Laser Setting (menu)');
WriteLn('     F10 -  Initiate Automated Scan');
WriteLn;
WriteLn('Traces Added: ',TracesAdded:8:0,'
Traces Subtracted:',TracesSubtracted:8:0);
WriteLn;
Write('Please Enter Menu Choice: ');
end;

begin {of program coscan3}
Initialize;
if (ErrCode <> 0) then
  begin
```

```
  WriteLn('Initialization error code ',ErrCode,'.');
  ExitProgram;
  end
else
begin
ClrScr;
WriteLn('Welcome to coscan3.  In order to run this program,
LINEFILE.BNK');
WriteLn('and START.CFG must be on disk.');
WriteLn('Strike any key to continue.');
GetKeyPressed(Key);
Assign(LineBankFile,LineFileName);
Reset(LineBankFile);
ReadLn(LineBankFile);
j := 1;
while not Eof(LineBankFile) do
  begin
  ReadLn(LineBankFile,LineArray[1,j]);
  ReadLn(LineBankFile,LineArray[2,j]);
  j := j + 1;
  end;
LineNum := j;
Close(LineBankFile);
Write('Enter the suffix for this spectrum:  ');
ReadLn(suffix);
Assign(StartFile,StartFileName);
Reset(StartFile);
ReadLn(StartFile,NewFreq);
ReadLn(StartFile,StepNum);
Write('Internal or external triggering (i/e)?  ');
ReadLn(Answer2);
if (Answer2 = 'e') or (Answer2 = 'E') then Intern := False;
if Intern then Trigger;           {asks for rep. rate}
ChangeDefault;
Repeat
  DisplayMenu;
  ClearKeyPressed;
    GotoXY(10,22);
    ReadRef(NewPwr);
    Delay(100);
    WriteLn('Step number:  ',StepNum:4,'     Freq:
',NewFreq:6:2,' cm^-1    Power:  ',NewPwr:6:2);
  GetKeyPressed(Key);
  Case Key of
    49,187: {1 or F1}  DigitizeDefects;
    50,188: {2 or F2}  AcquireNewTrace;
    51,189: {3 or F3}  AverageAddlShots;
    52,190: {4 or F4}  SubtractPickup;
    53,191: {5 or F5}  StoreOnDisk;
    54,192: {6 or F6}  ChangeDefault;
    55,193: {7 or F7}  Help;
    56,194: {8 or F8}  ExitProgram;
```

```
    57,195: {9 or F9}  LaserMenu(Stepnum,NewFreq);
    48,196: {0 or F10} Scan;
    Else               Beep;
  end; {of case}
Until Key in [56,194];
IBSIC(Brd0);
IBONL(Brd0,0);
end;
end. {of program coscan3}
^Z
```

Appendix 2.

Turbo-Pascal 3.0 program for generation of transient absorption spectra from traces. Non-functional sections are in italics. Include files were written by Will Polik and are stored in the Moore group software archives.

```
program EPWspectra;

{This program will take a series of kinetic traces,
normalize them with
 respect to probe laser power, adjust the baseline of each
(assuming the first
 10 data points in each array to represent its baseline),
and turn them into
 another series of arrays at different times, stored as a
function of
 frequency.  It will also subtract a normalized null trace
as well.}

const
  TitleLength    = 11;
  NumOfKin       = 100;
  NumOfSpectra   = 20;

type
  KinTitle       = String[TitleLength];
  KinTrace       = Array[1..512] of Real;
  TitleList      = Array[1..NumOfKin] of KinTitle;
  RealList       = Array[1..NumOfKin] of Real;
  BigArray       = Array[1..NumOfKin,1..NumOfSpectra] of
Real;
  DataPointer     = ^KinTrace;
  String20       = String[20];
  String80       = String[80];
  char80arr      = Array[1..80] of Char;

var
  Trace,
  NullTrace              :  KinTrace;
  InFile,OutFile         :  Text;
  TitleNull              :  KinTitle;
  h,i,j,k,l,n,ii,z,jj,
  ZeroOut,cursorkey,
  MaxKin,MaxSpect,
  FileNum,
  BoxDelayPts,
  BoxWindowPts           :  Integer;
  Power,
  NullPower,
  IntervalOut,
```

```
  MaxAbs,MinAbs,
  MaxFreq,MinFreq,
  HorizScale,VertScale,
  AvgWdw                  :  Real;
  ShockAns,BoxAns,
  Answer,RunAvgAns,
  Answer3,LSIAnswer       :  Char;
  GlobalTitle,NewTitle,
  Mask,HorizUnits,
  VertUnits               :  String80;
  FileName                :  String20;
  AddIt                   :  String[1];
  AddOn                   :  String[2];
  AddString               :  String[4];
  SpectralArray           :  BigArray;
  FileArray               :  TitleList;
  FreqList,PwrList        :  RealList;
  AvgWdwPts,TraceAddr     :  Integer;

{$I C:\TURBO\GRAPHLIB\GRAPHLIB.TGT}
{$I C:\TURBO\PASLIB\PLOTDATA.PRO}
{$I C:\TURBO\PASLIB\KEY.PRO}
{$I C:\EPW\INFILEB.PRO}
{$I C:\EPW\DIRLISTC.PRO}
(*($I C:\EPW\HANDLER.PRO)*)

procedure Normalize;
var
  v              : Integer;

begin
for v := 1 to 512 do
  Trace[v] := Round(Trace[v]/Power);
end;

procedure Baseline;
var
  v             : Integer;
  Offset        : Real;

begin
Offset := Trace[ZeroOut];
for v := 1 to 512 do
  begin
  Trace[v] := Trace[v] - Offset;
  end;
end;

procedure ReadKin;

const
  MaxKin = 100;
```

```
type
  IntList          = Array[1..MaxKin] of Integer;
  SubPrefix        = String[5];
  Suffix           = String[6];


var
  i,Code,cursorkey      : Integer;
  MonoList              : IntList;
  MonoString            : SubPrefix;
  InFile,OutFile,
  BankFile,OldBankFile : Text;
  ParamName,
  OmitFile,AddFile,
  OldBank, BankTitle    : KinTitle;
  Answer2               : Char;

procedure Shuffle;

var
  x,y                   : Integer;
  TempFile              : KinTitle;
  TempFreq,TempPwr      : Real;

begin
x := FileNum;
for y := 1 to (x-1) do
  begin
  for i := (y + 1) to x do
    begin
    if (FreqList[y] <  FreqList[i]) then
      begin
      TempFile := FileArray[y];
      TempFreq := FreqList[y];
      TempPwr := PwrList[y];
      FileArray[y] := FileArray[i];
      FreqList[y] := FreqList[i];
      PwrList[y] := PwrList[i];
      FileArray[i] := TempFile;
      FreqList[i] := TempFreq;
      PwrList[i] := TempPwr;
      end;
    end;
  end;
end;

begin {of procedure ReadKin}
WriteLn('Does a parameter file exist for this set of traces?
(Y/N)');
ReadLn(Answer);
Case Answer of
```

```
      'Y','y' : begin
                WRiteln('Place the diskette with the
parameter file in A.');
                Write('Enter the filename of the databank:
');
                ChDir('A:\');
                ReadLn(OldBank);
                OpenInfileB(OldBank,OldBankFile);
                ReadLn(OldBankFile);
                ReadLn(OldBankFile,HorizScale);
                ReadLn(OldBankFile,VertScale);
                i := 1;
                while not Eof(OldBankFile) do
                  begin
                  ReadLn(OldBankFile,FileArray[i]);
                  ReadLn(OldBankFile,FreqList[i]);
                  ReadLn(OldBankFile,PwrList[i]);
                  i := i + 1;
                  end;
                Close(OldBankFile);
                FileNum := i-1;
                end;
      'N','n' : begin
Write('Enter the directory mask associated with the
spectrum:  ');
ReadLn(Mask);
WriteLn;
ChDir('B:');
Repeat
  DirectoryList(Mask);
  WriteLn('Do you want to omit (o) a file, add (a) a file,
or no change (n)?');
  ReadLn(Answer2);
  Case Answer2 of
    'o','O' :  begin
               Write('Enter the filename to be omitted:  ');

               ReadLn(OmitFile);
               for i := 1 to FileNum do
                 begin
                 if (FileArray[i] = OmitFile) then
                   begin
                   FileArray[i] := FileArray[FileNum];
                   FileNum := FileNum - 1;
                   exit;
                   end
                 else WriteLn('Cannot find ',Omitfile);
                 end;
               end;
    'a','A' :  begin
               Write('Enter the filename to be added:  ');
               ReadLn(AddFile);
```

```
                FileNum := FileNum + 1;
                FileArray[FileNum] := AddFile;
                end;
    end
  Until (Answer2 = 'n') or (Answer2 = 'N');
  for i := 1 to FileNum do
    begin
    MonoString := Copy(FileArray[i],1,5);
    Val(MonoString,MonoList[i],Code);
    FreqList[i] := MonoList[i]/10;
    OpenInFileB(FileArray[i],InFile);
    ReadLn(InFile,PwrList[i]);
    Close(InFile);
    end;
  Shuffle; {arranges the files to be in}
  OpenInFileB(FileArray[1],InFile);
  ReadLn(InFile);                    {reads off horiz, vert
  scales for storage}
  ReadLn(InFile);
  ReadLn(InFile);
  ReadLn(InFile,VertScale);
  ReadLn(InFile);
  ReadLn(InFile,HorizScale);
  Write('Enter the filename for the parameter file:  ');
  {ascend. freq. order}
  ReadLn(ParamName);
  WriteLn('Place target diskette in drive A and hit <RTN>.');
  Repeat
    ClearKeyPressed;
    GetKeyPressed(cursorkey);
    Case cursorkey of
      13 :
        WriteLn('Diskette has been accepted.');
      Else
        begin
        Sound(440);
        Delay(500);
        NoSound;
        end;
      end
    Until cursorkey = 13;
  ChDir('A:\');
  Assign(OutFile,ParamName);
  Rewrite(OutFile);
  WriteLn(OutFile,ParamName);
  WriteLn(OutFile,HorizScale);
  WriteLn(OutFile,VertScale);
  for i := 1 to FileNum do
    begin
    WriteLn(OutFile,FileArray[i]);
    WriteLn(OutFile,'     ',FreqList[i]:5:1);
    WriteLn(OutFile,'     ',PwrList[i]:5:3);
```

```
  end;
Close(OutFile);
end;
end; {of case}
ChDir('B:\');
end; {of procedure ReadKin}

procedure Translate;
  {This procedure turns the file into a simple 512X1 array.}

var
  i : Integer;
  InFile : Text;

begin {of procedure Translate}
OpenInFileB(FileName,InFile);
ReadLn(InFile,Power); {these are the title and heading lines
of the file}
ReadLn(InFile);
ReadLn(InFile);
ReadLn(InFile,VertScale);
ReadLn(InFile,VertUnits);
ReadLn(InFile,HorizScale);
if (LSIAnswer = 'y') or (LSIAnswer = 'Y') then
  HorizScale := 51.1 * HorizScale;
ReadLn(InFile,HorizUnits);
for i := 1 to 512 do
  ReadLn(InFile,Trace[i]);
Close(InFile);
end;

procedure GetTimes;
{See CURSOR.PRO in FITDATA1.PAS for details.}

var
  InFile              : Text;
  t,q,
  Interval,
  BoxDelay,BoxLength  : Real;
  i,j,k,Zero          : Integer;
  Waveform,Timebase   : KinTrace;
  XData,YData         : DataPointer;
  PlotTitle,
  XLabel,YLabel,
  DisplayString       : GraphicsString;

begin
WriteLn('Enter the filename of the trace from which the time
= 0 point');
Write('and the temporal interval between spectra are to be
taken:  ');
ReadLn(FileName);
```

```
Translate;
Waveform := Trace;

for i := 1 to 512 do
  TimeBase[i] := (i-1)*HorizScale/51.1;
XData := Ptr(Seg(TimeBase),Ofs(TimeBase));
YData := Ptr(Seg(Waveform),Ofs(Waveform));
XLabel := HorizUnits;
YLabel := VertUnits;
PlotTitle := FileName;
InitGraphics;
EnterGraphics;
SetColor(15);
PlotData(188.89,170,900,890,PlotTitle,XLabel,YLabel,XData,Y-
Data,512,0,0,0,0,'/D');
DisplayString := 'Enter t(0) by using cursor pad left, right
arrows, then <RTN>';
MoveScreen(0,0);
DrawText(DisplayString);
SetColor(XORColor);
Zero := 1;
MoveUser(TimeBase[Zero],Waveform[Zero]);
DrawSymbol(1);
Repeat
  ClearKeyPressed;
  GetKeyPressed(CursorKey);
  Case CursorKey of
    203 : {left arrow}
      begin
      DrawSymbol(1);
      If Zero > 1
      then Zero := Zero - 1
      else
        begin
        Sound(440);
        Delay(500);
        NoSound;
        end;
      MoveUser(TimeBase[Zero],Waveform[Zero]);
      DrawSymbol(1);
      end;
    205 : {right arrow}
      begin
      DrawSymbol(1);
      If Zero < 512
      then Zero := Zero + 1
      else
        begin
        Sound(440);
        Delay(500);
        NoSound;
        end;
```

```
      MoveUser(TimeBase[Zero],Waveform[Zero]);
      DrawSymbol(1);
      end;
    13 : {enter}
      DrawSymbol(1);
    Else
      begin
      Sound(440);
      Delay(500);
      NoSound;
      end;
    end {of case}
  Until CursorKey = 13;
SetColor(1);
SetTextBlockColor(-1);
ZeroOut := Zero;
ClrScr;
ExitGraphics;
MoveScreen(0,0);
WriteLn;
if (BoxAns = 'y') or (BoxAns = 'Y') then
  begin
  Repeat
    Write('Choose the boxcar delay for spectrum (in
microsec):  ');
    ReadLn(BoxDelay);
    BoxDelayPts := Round((BoxDelay/HorizScale)*51.1*1E-6);
    q := BoxDelayPts + ZeroOut;
    if (q > 511) then
      WriteLn('Delay too long!');
    if (q <= 0) then
      WriteLn('Improper delay!');
  Until (q <= 511) and (q > 0);
  Repeat
    write('Enter the length of the boxcar window (in
microsec):  ');
    ReadLn(BoxLength);
    BoxWindowPts := Round((BoxLength/HorizScale)*51.1*1E-6);

    q := BoxDelayPts + BoxWindowPts + ZeroOut;
    if (q > 511) then
      WriteLn('Window too large!');
    if (q <= 0) then
      WriteLn('Improper window!');
  Until (q <= 511) and (q > 0);
  end
else
  begin
  WriteLn('This program will make ',MaxSpect,' spectrum
files.');
  Repeat
    Write('Enter the time interval (in microsec) between
```

```
spectra:  ');
    ReadLn(Interval);
    IntervalOut := (Interval/HorizScale)*51.1*1E-6;
    q := Round((IntervalOut*(MaxSpect-1)) + ZeroOut);
    if (q > 511) then
      begin
      Sound(880);
      Delay(250);
      NoSound;
      WriteLn('Error:  Interval too long.');
      end
    else if (q <= 511) then WriteLn('Value has been
accepted.')
  Until (q <= 511);
  end;
end; {of procedure GetTimes}


procedure RunAvg;

var
  Pennant     : Boolean;

begin
Write('Enter the window of the running average (in
microseconds):  ');
  ReadLn(AvgWdw);
Pennant := False;
While (Pennant = False) do
  begin
  AvgWdwPts := Round(5.11E-5*AvgWdw/HorizScale);
  if (AvgWdwPts >= 512) or (AvgWdw < 0) then
    begin
    WriteLn('Illegal running average window.');
    Write('Enter window (microseconds):  ');
    ReadLn(AvgWdw);
    end
  else
    Pennant := True;
  end;
if not Odd(AvgWdwPts) then
  AvgWdwPts := AvgWdwPts + 1;
WriteLn('AvgWdwPts = ',AvgWdwPts);
end;

procedure Average;

var
Crit,Border,indx,sum,tempaddr : integer;

begin
```

```
Crit := Abs(TraceAddr-512);
border := trunc((avgwdwpts-1)/2);
if (Crit<Border) or (TraceAddr<border) then  {don't take
avg. if too close}
   exit;                                     {to an edge of
the trace     }
Sum := 0;
for indx := 1 to AvgWdwPts do
  begin
  tempaddr := traceaddr - border - 1 + indx;
  Sum := Sum + Round(Trace[tempaddr]);
  end;
Trace[traceaddr] := Round(sum/avgwdwpts);
end;

procedure MaxFind;

var
  i,j : Integer;

begin
MaxAbs := SpectralArray[1,1];
for i := 1 to Filenum do
  for j := 1 to MaxSpect do
    begin
    if MaxAbs < SpectralArray[i,j] then
      MaxAbs := SpectralArray[i,j];
    end;
end;

procedure MinFind;

var
  i,j : Integer;

begin
MinAbs := SpectralArray[1,1];
for i := 1 to Filenum do
  for j := 1 to MaxSpect do
    begin
    if MinAbs > SpectralArray[i,j] then
      MinAbs := SpectralArray[i,j];
    end;
end;

begin {of program EPWspectra}
ClrScr;
WriteLn('Welcome to the wacky world of EPWspectra, where
your blah kinetic');
WriteLn('traces become the spectra of your dreams.');
WriteLn;
WriteLn;
```

```
Write('Number of spectra (20 is max): ');
ReadLn(MaxSpect);
WriteLn('Enter the global title for the spectra.  They will
be stored together');
Write('under the filenames GlobalTitle1, GlobalTitle2, etc.:
');
ReadLn(GlobalTitle);
WriteLn;
WriteLn('Place source diskette in drive B, target diskette
in A.');
WriteLn('Strike any key when ready.');
Repeat until KeyPressed;
ChDir('B:\');
ReadKin;
Write('Was this data acquired on the LSI-11 computer? (y/n)
');
ReadLn(LSIAnswer);
Write('Do you wish to subtract a null trace? (Y/N)');
ReadLn(ShockAns);
if (ShockAns = 'Y') or (ShockAns = 'y') then
  begin
  Write('Enter the filename of the trace to be subtracted:
');
  ReadLn(FileName);
  Write('Will this null trace be subtracted before (b) or
after (a) normalization?  ');
  ReadLn(Answer3);
  Translate;
  Baseline;
  Normalize;
  NullTrace := Trace;
  NullPower := Power;
  end;
WriteLn;
Write('Do you want a running average of the data? (y/n) ');
ReadLn(RunAvgAns);
if (RunAvgAns = 'y') or (RunAvgAns = 'Y') then
  RunAvg;
WriteLn;
Write('Do you choose the boxcar function? (y/n)');
ReadLn(BoxAns);
if (BoxAns = 'y') or (BoxAns = 'Y') then
  MaxSpect := 1;
GetTimes;
WriteLn('ZeroOut = ',ZeroOut,' pts');
for i := 1 to filenum do
  begin
  FileName := FileArray[i];
  Power := pwrlist[i];
  Translate;
  Baseline;
  Normalize;
```

```
  if (ShockAns = 'Y') or (ShockAns = 'y') then
    begin
    if (Answer3 = 'b') or (Answer3 = 'B') then
      begin
      for z := 1 to 512 do
        NullTrace[z] := (NullPower/pwrlist[i])*NullTrace[z];

      end;
    for jj := 1 to 512 do
      Trace[jj] := Trace[jj] - NullTrace[jj];
    Baseline;
    end;
  for j := 1 to MaxSpect do
    begin
    TraceAddr := Round(ZeroOut + (IntervalOut*(j-1)));
    if (RunAvgAns = 'y') or (RunAvgAns = 'Y') then
      Average;
    SpectralArray[i,j] := Trace[TraceAddr];
    if (BoxAns = 'y') or (BoxAns = 'Y') then
      begin
      SpectralArray[i,j] := 0;
      for ii := 1 to BoxWindowPts do begin
        SpectralArray[i,j] := SpectralArray[i,j] +
Trace[(ZeroOut+BoxDelayPts+ii)];
        end;
      SpectralArray[i,j] := SpectralArray[i,j]/BoxWindowPts;

      end;
    end;
  end;
  MaxFind;
  MinFind;
  MaxFreq := freqlist[1];
  MinFreq := freqlist[filenum];
  ChDir('A:\');
  for k := 1 to MaxSpect do
    begin
    if (k <= 9) then
      begin
      Str(k:1,AddIt);
      AddOn := '0' + AddIt;
      end
    else if (k > 9) then
    Str(k:2,AddOn);
    AddString := '.0' + AddOn;
    NewTitle := GlobalTitle + AddString;
    Assign(OutFile,NewTitle);
    Rewrite(OutFile);
    WriteLn(OutFile,NewTitle);
    WriteLn(OutFile,'Frequency (cm**-1)');
    WriteLn(OutFile,'Absorption (Arb. Units)');
    Write(OutFile,'/L/C',MinFreq:6:2);
```

```
    Write(OutFile,',',MinAbs:6:2,',');
    WriteLn(Outfile,MaxFreq:6:2,',',MaxAbs:6:2);
    for l := 1 to filenum do
      begin
      WriteLn(OutFile,freqlist[l]:7:2,'
',SpectralArray[l,k]:9);
      end;
    Close(OutFile);
    end;
WriteLn('Have a nice day.');
ChDir('C:\EPW');
end.
```

LAWRENCE BERKELEY LABORATORY
TECHNICAL INFORMATION DEPARTMENT
1 CYCLOTRON ROAD
BERKELEY, CALIFORNIA 94720